Molecular Insight into Photocatalytic Reactions by TiO_2 Investigated by ATR-IR Spectroscopy

Thèse présentée à la Faculté des Sciences

Institut de Microtechnique

Université de Neuchâtel

Par

Igor DOLAMIC

Acceptée sur proposition du jury :

Prof. T. Bürgi, directeur de thèse

Prof. H. Stoeckli - Evans, rapporteur

Dr. L. Kiwi - Minsker, rapporteur

Dr. S.J. Hug, rapporteur

Soutenue le 29 mai 2008

Université de Neuchâtel

Université de Neuchâtel unine

FACULTE DES SCIENCES
Secrétariat-Décanat de la faculté
- Rue Emile-Argand 11
- CP 158
- CH-2009 Neuchâtel

IMPRIMATUR POUR LA THESE

Molecular insight into photocatalytic reactions by TiO_2 investigated by ATR-IR spectroscopy

Igor DOLAMIC

UNIVERSITE DE NEUCHATEL

FACULTE DES SCIENCES

La Faculté des sciences de l'Université de Neuchâtel,
sur le rapport des membres du jury

T. Bürgi (directeur de thèse), H. Stoeckli-Evans, L. Kiwi-Minsker,
et S. Hug (Eawag, Dübendorf)

autorise l'impression de la présente thèse.

Neuchâtel, le 23 juin 2008

Le doyen :
F. Kessler

UNIVERSITE DE NEUCHATEL
FACULTE DES SCIENCES
Secrétariat - décanat de la faculté
Rue Emile-Argand 11 - CP 158
CH-2009 Neuchâtel
felix Kessler

■ Téléphone : +41 32 718 21 00 ■ E-mail : secretariat.sciences@unine.ch ■ www.unine.ch/sciences

Keywords

Photocatalysis, Heterogeneous Catalysis, Attenuated Total Reflection Infrared Spectroscopy, Solid-Liquid Interface

Thesis Abstract

Today mankind faces several environmental pollution problems which are a result of our fossil fuels dependence. Water pollution, global warming, air pollution are just several tasks that rapt scientists today. The importance of the previous problems constrained people to find and use other sources of energy. The sun is one of the alternative energy sources that can be used. Continuously our planet is provided by a huge sun light energy of about $4.3x10^{20}$J per hour, which roughly corresponds to the energy consumed on the Earth in one year ($4.1x10^{20}$J).

So far solar energy was consumed for different purposes, from more primitive, drying cloths and foodstuff to very complex such as photovoltaic cell and photocatalysis. One of the materials which find huge application in solar energy conversion is titanium dioxide. TiO_2 was successfully applied as material in many fields and was extensively studied during the last three decades after A. Fujishima and K. Hondas discovery of photocatalytic activity of TiO_2.

In the last years photocatalytic reactions on TiO_2 nanoparticles have attracted much interest due to their application in solar energy conversion i.e. water splitting and environmental cleaning or decomposition of organic pollutants in gaseous effluents and wastewater. Despite the importance of photocatalysis, not too much molecular level information is available today on the processes occurring at the respective solid –liquid interfaces.

However, the reactions that take place at solid-liquid and gas-solid interface are of crucial importance for a better understanding these systems. A lot of studies have been carried out in the last years but most of them are based on analysis of stable reaction intermediates in the liquid or gas phase. Very few scientific insights were based on direct information of the reactions that take place at the interfaces.

Fourier-transform infrared spectroscopy (FT-IR) applied in the attenuated total reflection (ATR-IR) mode is a promising method to probe solid-liquid interfaces in order to give molecular insight of the reactions occurring. In combination with modulation excitation

(ME) spectroscopy the signal to noise ratio can be improved and separation of overlapping bands is possible.

In the first part of this thesis (Chapters 3 and 4) adsorption, photocatalytic decompositions and reaction routs of dicarboxylic acids were investigated using ATR-IR spectroscopy in combination with ME spectroscopy. For the first time dissolved CO_2 as the final product was detected in situ. Also other reaction products like oxalate, carbonate and carboxylate were detected on the TiO_2 surface and were reported in this thesis.

Chapter 5 deals with adsorption of monolayer protected gold nanoparticles (MPNs) on TiO_2 and their behavior upon UV illumination. ATR-IR spectroscopy in combination with UV-visible spectroscopy and transmission electron microscopy (TEM) gives detailed information on the fate of adsorbed gold MPNs on TiO_2 upon UV illumination. Furthermore, the combination of both in situ techniques reveals the importance of mass transport through the porous films prepared on internal reflection elements (IRE).

In the Chapters 6 and 7 adsorption and photocatalytic degradation of several amino acids over TiO_2 and Au-TiO_2 thin films was investigated. Also the preparation and tailoring of Au-TiO_2 catalyst was reported. Using ATR-IR combined with MES the main intermediate species could be detected on the catalytic surfaces in situ. For the first time CN^- species were reported during photocatalytic mineralization of amino acids over TiO_2 and Au-TiO_2. The CN^- promotes leaching of the gold. These findings are relevant for the application of photocatalysis by TiO_2-based materials for the cleaning of drinking water.

1

Introduction

1.1 Probing Solid-Liquid Interfaces

Solid-liquid interface play a fundamental role in nature and technology. During the last years metal oxide-aqueous solution interfaces have attracted great attention because of their importance in several fields ranging from heterogeneous catalysis, atmospheric chemistry, corrosion, implants and adhesion to metal oxide crystal growth. Despite great importance in science and industry, solid-liquid interfaces were always less studied than vacuum-solid interfaces. The choice between these two was very often explained by limitation of tools suitable for exploring solid-liquid interfaces and not so much by scientific arguments that solid-liquid interface are more complex and therefore more difficult to understand. The fundamental understanding of such processes requires information from different physical and chemical points of view and application of a wide variety of techniques[1, 2].

Different motivations and principles exist regarding the techniques that should be applied for understanding interfaces and one can generally make the distinction between *ex situ* versus *in situ* techniques. There is truth in both approaches and both are important for a better understanding of surface science. Several techniques are available to examine surfaces *ex situ* such as Electron Energy Loss Spectroscopy (EELS), X-ray (XPS) and Ultra Violet Photoelectron Spectroscopy (UPS).

To probe solid-liquid interfaces *in situ* the following techniques have found application: Infrared spectroscopy (IR), X-ray absorption spectroscopy (XAS), sum frequency generation (SFG) and surface enhanced Raman spectroscopy (SERS).

The most important motivation to use in situ techniques is the fact that the properties of an interface during the process of interest may be drastically different from the properties determined during analysis beforehand or afterwards. Therefore, information that can be obtained *in situ* is precious. Infrared spectroscopic methods are difficult to apply to solid – liquid and in particular solid – water interfaces due to the strong absorption of the solvent. A promising method to identify species at the interfaces *in situ* during reactions and to unravel their fate is attenuated total reflection infrared (ATR-IR) spectroscopy. [3-6]

ATR-IR spectroscopy is perfectly suitable to investigate interfaces. The vibrational spectrum contains detailed information about interaction modes between surface and adsorbate, orientation of the molecules and intermolecular interactions within the adsorbate layer. Metal oxide surfaces in contact with a liquid phase play an important role in heterogeneous catalysis and in particular also in photocatalysis and they were considered in this thesis.

1.2 Attenuated Total Reflection Infrared Spectroscopy

The phenomenon of internal reflection was already known in the seventeenth century and electromagnetic theory has been studied intensively by Newton. It needed two centuries until this phenomenon finds application in science. Finally N.J. Harrick from the Philips Laboratories in New York proposed measuring samples in the close contact with an internal reflection element by making use of this phenomenon.[7-9]

Internal reflection can only occur when the angle of the refracted beam θt is larger than the angle of incidence θi. According to Snell's law the refractive index of the medium two must be smaller than that of medium 1 see Figure 1-1. Total internal reflection occurs when the θi of the beam exceeds the critical angle θc. Equation 1-1

$$\sin\theta_c = {}^{n_2}\!/_{n_1} = n_{21} \qquad \text{Equation 1-1}$$

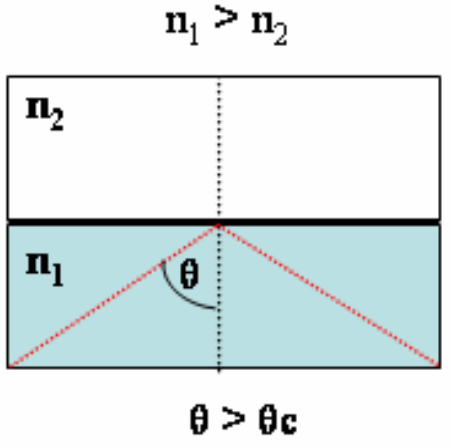

Figure 1-1: Schematic representation of the path of a ray of light for total internal reflection where n_1 and n_2 represent refractive index of dense and rare medium respectively, θ_i is the angle of incidence and θ_c the critical angle

When the light is totally reflected $\theta > \theta_c$, an electric field is formed at the reflection points that penetrate into the rare medium. This electric field is referred to as evanescent field. The amplitude of the evanescent electric field decays exponentially with the distance z from the interface, according to Equation 1-2

$$E = E_0 e^{-z/dp} \qquad \text{Equation 1-2}$$

Where, E_0 is the electric field amplitude at the interface which depends on the angle of incidence, polarization of the field and refractive index. The depth of penetration d_p is defined as the distance required for the electric field amplitude to fall to e^{-1} of its value at the surface.

$$dp = \frac{\lambda_1}{2\pi\sqrt{\sin^2\theta - n^2{}_{21}}} \qquad \text{Equation 1-3}$$

$\lambda_1 = \lambda/n_1$ wavelength in the optical denser medium, θ angle of incidence and refractive index $n_{21} = n_2 / n_1$. Depending on the refractive index of the IRE and medium 2 and the angle of incidence the values of d_p is in the range of 0.1 – 1.3 μm for infrared radiation.

For attenuated total reflection (ATR) -IR spectroscopy internal reflection elements (IREs) are used as the denser medium. The IRE is an infrared transparent optical element with high refractive index. Depending on the geometry the infrared light undergoes multiple

internal reflections. Most common materials used as IRE's in ATR-IR spectroscopy are: ZnSe (n_1 = 2.4), Ge (n_1 = 4.0), diamond, C (n_1 = 2.4), KRS-5, (n_1 = 2.37), authentic mixtures of thallium bromide / iodide).

The light propagates through the IRE striking the element at θ_i. The evanescent electromagnetic field is generated that penetrates into the sample at the point of the reflection. If the medium adjacent to the IRE (the sample) is absorbing the reflection is not total anymore, since the reflected beam is attenuated. Therefore a spectrum can be obtained when the light is attenuated by the sample.

The principle of this phenomenon is depicted in the Figure 1-2 : where a powder thin film catalyst was deposited on Ge internal reflection element in contact with liquid phase.

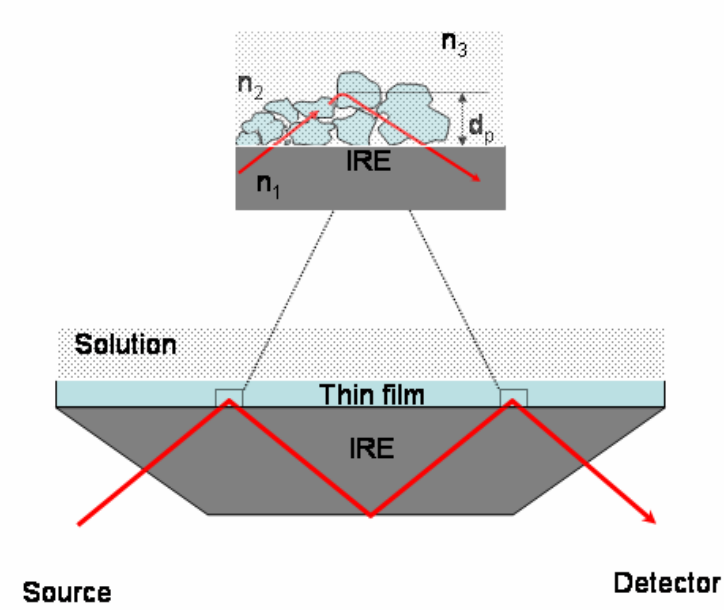

Figure 1-2 : Pictorial of a thin film coated Ge IRE in contact with liquid phase. A beam from the source is coupled into IRE at $\theta_i = 45^\circ$ and is totally reflected at the thin-film liquid interface, where an evanescent electromagnetic field penetrates into rare medium.

The processes that take places at the catalytic interfaces are the primary key in heterogeneous catalysis and therefore attenuated total reflection infrared (ATR-IR) spectroscopy is an ideal tool to study these processes. ATR-IR is suitable for studying thick or highly absorbing solid and liquid materials, including films, coatings, powders, threads, adhesives, polymers and aqueous samples. The technique requires little or no sample preparation for most samples and is one of the most versatile sampling techniques. High sensitivity of the ATR technique can be achieved by increasing the number of reflections.

ATR-IR has been used in the past to study solid-liquid and gas-solid interfaces, even at high pressures and temperatures, in the fields of catalysis[10, 11], polymers, environmental science[12, 13] biology and pharmacy.[14, 15]

1.3 Modulation Excitation Spectroscopy

1.3.1 Introduction

Studying complex systems with many species present simultaneously is a challenge for IR spectroscopy, because the method is not intrinsically selective. All species that absorb IR radiation will give rise to signals in the spectrum. This problem is particularly pronounced in heterogeneous catalysis and photocatalysis where many intermediate species are present during reaction. The problem is not only the number of species that are present in the system during reaction. It is important to be able to distinguish between species that are involved in the catalytic cycle and spectators, which may lead to static signals. A promising method to solve these problems and to improve sensitivity and selectivity is modulation excitation spectroscopy. In this technique a reversible system is periodically stimulated by modulating an external parameter.

1.3.2 The Theory of Phase Sensitive Detection

The change of any external parameter exerts a specific influence on the state of a chemical system. As a consequence the system will relax to a new state. This is the basis of relaxation techniques such as temperature or pressure jump techniques that give information about the relaxation kinetics of the system under investigation. Besides the well-known discrete parameter changes (jumps) it is also possible to apply periodic parameter changes, which has some advantages. Parameters that can be used for the stimulation of such systems are various: temperature (T), pressure (p), radiant power (Φ)[16], concentration (c), electric field (E), electric potential (ψ). If the disturbance (stimulation) is periodic the disturbed system will also respond periodically at the same frequency as the stimulation or harmonics therefore.[17] Modulation excitation (ME) helps to separate the signals affected by the stimulation from the stationary response, i.e. from the part of the system that is not affected by the stimulation. A phase lag ϕ between stimulation end responses occurs if the time constant of the process

giving rise to some signal is on the order of the time constant $2\pi/\omega$ of the stimulation (excitation).

Modulation excitation spectroscopy in combination with ATR-IR spectroscopy is a powerful tool for the investigation of photocatalytic reactions in situ. The combination of these techniques allows one to separate overlapping bands with considerable enhancement of the signal to noise ratio. Species with different time behavior can easily be separated and detected. More detailed information on the technique is available elsewhere[18, 19]. The principle of the ME is depicted in the Figure 1-3.

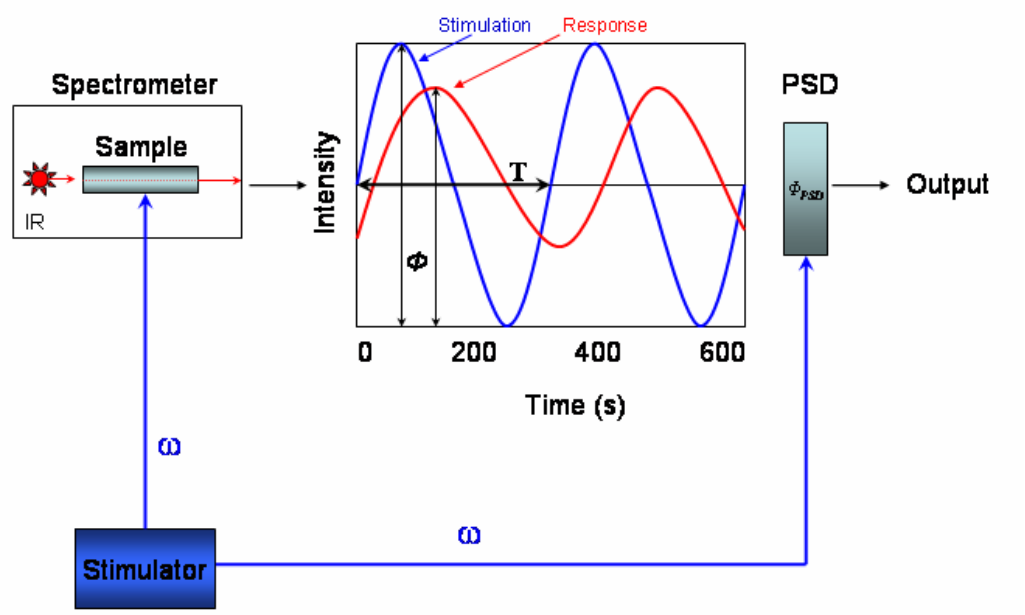

Figure 1-3: Schematic representation for modulated excitation (ME) spectroscopy.

After several periods of stimulation the system reaches a new quasi-stationary state, about which it oscillates at frequency ω. In this state the absorbance signals $A(\tilde{\nu},t)$ are measured as a function of time t for all wavenumbers. The measured time-resolved absorbance spectra are then converted into phase-resolved absorbance spectra according to Equation 1-4

$$A_k^{\phi_k^{PSD}}(\tilde{\nu}) = \frac{2}{T}\int_0^T A(\tilde{\nu},t)\ \sin\left(k\omega t + \phi_k^{PSD}\right)\ dt \qquad \text{Equation 1-4}$$

Where k determines the demodulation frequency $k = 1,2,3...$ (fundamental, first harmonic and so on), T is the duration of the modulation period, $\omega(=2\pi/T)$ denotes modulation frequencies, $A(\tilde{\nu},t)$ is the time dependent absorbance at wavenumber ν, ϕ_k^{PSD} is the demodulation phase angle.

1.4 Photocatalysis

1.4.1 Introduction

The chemical effects of light have a crucial influence for all mankind. One of the most important photo processes that occur on Earth is photosynthesis induced by sun-light. In recent years many attempts have been made to make sunlight an important source of energy in order to reduce the dependency of mankind on fossil fuels. Stimulated by the drastic consequences of global warming new technologies to make use of sunlight are searched for. Additionally, water, a necessary source of life on earth, becomes more and more polluted by human activity. This also calls for new technologies for water purification and the use of sunlight is a very attractive route.

A material that received great attention from scientists and engineers for solar energy conversion is TiO_2, a semiconductor. A. Fujishima and K. Honda discovered UV light-induced water splitting using TiO_2 photoanode in combination with a (Pt) counter electrode immersed in an aqueous electrolyte solution[20]. Upon irradiation of a semiconductor an electron-hole pair is generated, creating conditions for a solar energy conversion by semiconductors. Solar energy conversion in photovoltaic solar cells in one example for making use of this principle and photocatalysis is another. Under irradiation TiO_2 can be used for the photodegradation of organic compounds. An important disadvantage of TiO_2 is its

wide band gap. As a consequence only a small fraction of the sunlight can excite the semiconductor. Also, methods are searched for to increase the efficiency of the material. One way to do so is the combination with metal nanoparticles which act as sink for the excited electrons and as redox catalyst.[21]

1.4.2 Titanium dioxide TiO_2

The titanium was discovered by the German chemist Heinrich Klaporth in *rutile* ore who named it after Titans, mythological first son of goddess Ge (Earth in Greek mythology). The main titanium ores are *ilmenite*, $FeTiO_3$ and *rutile* TiO_2. There are several methods for manufacturing TiO_2 from ores. Today most frequently used methods are sulfate and chlorine processes. Titan (IV) - oxide exist in three crystalline forms as *rutile, brookite* and *anatase*. It has found a great application in different fields like photocatalysis, pigments, antimicrobial coatings and oxygen sensors.[22] TiO_2 is one of the most used semiconductors in photocatalysis because of several advantages. It is inert, non toxic and cheap material. A disadvantage is that it dose not absorb the visible light. It was reported that *anatase* shows the better photocatalytic properties.[23] Also there are researches that classify *rutile* as the most active photocatalyst. In the present investigation commercial type P25 TiO_2 was used, which contains two crystallite forms *anatase* 80% and *rutile* 20%. This material is very well characterized and is a standard material for many applications. Figure 1-4 shows wide range of application of photoactivated TiO_2.

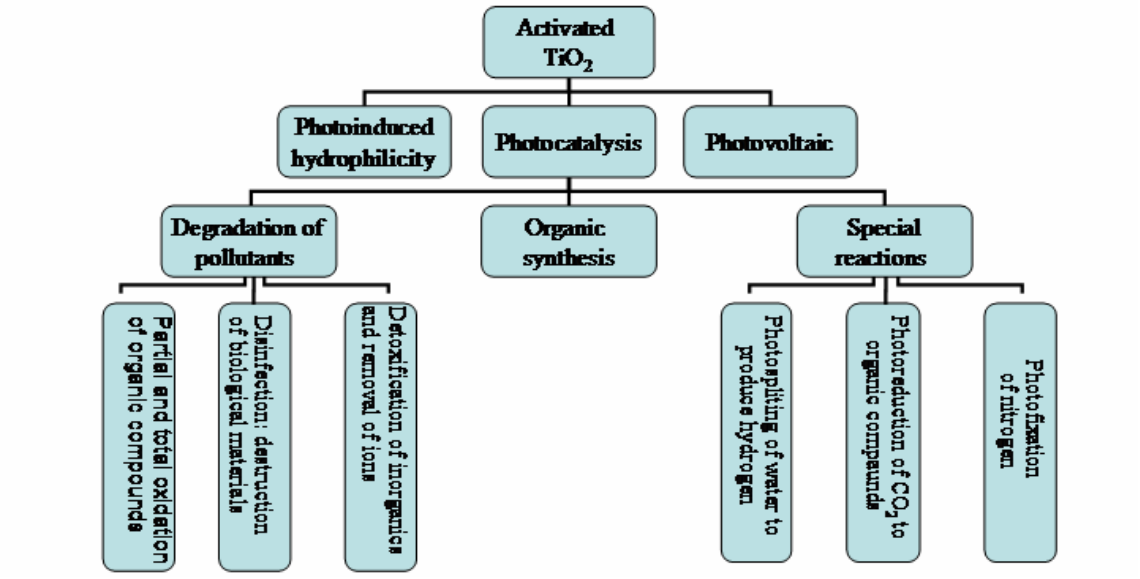

Figure 1-4 Light-induced processes on TiO_2

1.4.3 Photocatalysis by TiO_2

Photocatalysis can be defined as acceleration of a photoreaction in the presence of a catalyst[24]. When materials like TiO_2 are illuminated by light that has greater energy than its band gap (band gap of TiO_2 = 3.2 eV) an electron hole pair is generated.[22, 23, 25, 26] Figure 1-5 shows light-excited TiO_2 particle in which one electron is excited by light adsorption. Located now in the conduction band it is capable of reducing species A, for example dissolved oxygen from the air. The excited electron leaves behind a hole in the valence band i.e. a positive charge capable of oxidizing species D on the surface.

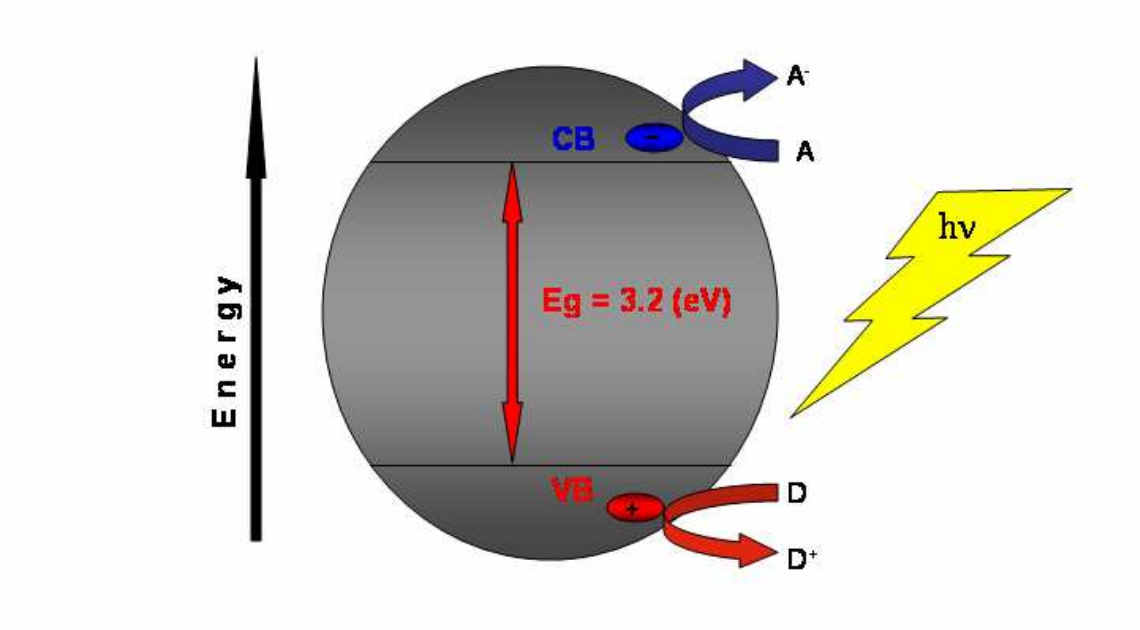

Figure 1-5 Energy scheme of TiO_2 nanoparticle where an electron is excited from the valence band (VB) to the conduction band (CB) by adsorbing photons of grater energy than its band gap energy.

Photogenerated electrons and holes diffuse to the surface of the TiO_2 nanoparticles and exhibit the following reactions on the surface[27], Equation 1-5.

These reactions result in cation and anion radicals which can undergo further reactions. They may react chemically with themselves or surface-adsorbed compounds. Also these species may diffuse from the semiconductor surface to the solution and take part in further reactions.

$$(a)\quad TiO_2 + h\nu \rightarrow TiO_2\,(e^-,\ h^+)$$
$$(b)\quad TiO_2\,(h^+) + RX_{ads} \rightarrow TiO_2 + RX_{ads}^{\bullet+}$$
$$(c)\quad TiO_2\,(h^+) + H_2O_{ads} \rightarrow TiO_2 + OH^{\bullet}_{ads} + H^+$$
$$(d)\quad TiO_2\,(h^+) + OH^-_{ads} \rightarrow TiO_2 + OH^{\bullet}_{ads}$$
$$(e)\quad TiO_2\,(e^-) + O_{2,ads} \rightarrow TiO_2 + O_2^{\bullet-}$$
$$(f)\quad TiO_2\,(e^-) + H_2O_{2,ads} \rightarrow TiO_2 + OH^- + OH^{\bullet}_{ads}$$

Equation 1-5

The redox potential for photogenerated holes of TiO_2 is +2.56 eV.[24] When holes react with water they can produce hydroxyl radicals $OH\bullet$, which have still very high oxidation power. The redox potential for conduction band electrons is (–0.52) eV[24]. These excited electrons can be trapped at $Ti(IV)O-H$ surface sites leading to $Ti(III)O-H^-$ and lose some of their reducing power. Excited electrons can also reacts with oxygen on the surface and produce superoxide O_2^{2-} [7]

One of the critical processes in photocatalysis, which directly affects the efficiency of the process, is electron hole recombination. When electron hole recombination occurs on the surface heat is released. This process usually occurs due to slow down diffusion. Especially hydrophobic TiO_2 surfaces show fast recombination. Many attempts have been made to prevent electron hole recombination. In order to extend the lifetime of the electron – hole pair and to increase the efficiency of the process metal nanoparticles can be used, which act as an electron acceptor [21]. This strategy was also applied in this work where monolayer-protected gold particles (MPNs) were used to prepare active gold titania catalyst Au-TiO_2[28]. The preparation and application of such catalyst was described in more details in the Chapter 7.

One of the most important tasks in photocatalysis and catalysis in general is their application in industry. Today several reports are available[29, 30]. One of the most encountered problems in application of photocatalysis in industry is the use of TiO_2 powder and its subsequent separation from the water. To avoid this problem TiO_2 powder nanoparticle can be immobilized on different supports in thin film forms. [31, 32]

1.5 Scope of the Thesis

Heterogeneous photocatalysis is an important strategy for environmental cleanup and in particular water purification. Despite its importance, not enough is known about reactions occurring at the catalytic solid-liquid interface. Shortage of information on the molecular level hinders a more rational design of the catalyst and process. Most of the numerous studies on photocatalysis focus on dissolved reactants and products, which has in most cases to do with the available analytical tools. The aim of this thesis is to shed some light on the important processes occurring at the catalytic solid-liquid interface by using in situ spectroscopy. This has to go hand in hand with the further development of the tools that allow us to give the desired information from the interface at work with the necessary sensitivity. We furthermore want to draw attention to the fact that reactions occurring on the catalytic surfaces are the primary key for understanding heterogeneous catalysis.

An important part of the study in this thesis was devoted to the photocatalysis by TiO_2. Catalytic solid-liquid interfaces were probed in situ unraveling intermediate species that only occur at the solid liquid interfaces. Some of these species were never reported before because their life-cycle is restricted to the interface.

References

1. Metal Oxide Surfaces and Their Interactions with Aqueous Solutions and Microbial Organisms. *Chemical reviews* **1999,** 99, (1), 77-174.
2. Somorjai, G. A., Introduction to Surface Chemisry and Catalysis
3. Kesselman-Truttmann, J. M.; Hug, S. J.; Rotzinger, F. P.; Gratzel, M., ATR-FTIR investigation of adsorption and photodegradation reactions on titanium dioxide and iron oxide surfaces. *Abstracts of Papers of the American Chemical Society* **2001,** 221, U470-U470.
4. Urakawa, A.; Wirz, R.; Burgi, T.; Baiker, A., ATR-IR flow-through cell for concentration modulation excitation spectroscopy: Diffusion experiments and simulations. *Journal of Physical Chemistry B* **2003,** 107, (47), 13061-13068.
5. Burgi, T.; Wirz, R.; Baiker, A., In situ attenuated total reflection infrared spectroscopy: A sensitive tool for the investigation of reduction-oxidation processes on heterogeneous Pd metal catalysts. *Journal of Physical Chemistry B* **2003,** 107, (28), 6774-6781.
6. Bürgi, T. Baiker., A., Attenuate Total Reflection Infrared Spectroscopy of Solid Catalysts Functioning in the Presance of Liquid-Phase Reactants *Advanced Catalysis* **2006,** 50, 227-283.
7. Surface Chemistry from Spectral Analysis of Totally Internally Reflected Radiation. *The Journal of physical chemistry* **1960,** 64, (9), 1110-1114.
8. Harrick, N. J., Study of Physics and Chemistry of Surfaces from Frustrated Total Internal Reflections. *Physical Review Letters* **1960,** 4, (5), 224.
9. Harrick, N. J., Internal reflection spectroscopy. *Innterscience Publishers New York* **1967**.

10. Bürgi, T., Combined in situ attenuated total reflection infrared and UV-Vis spectroscopic study of alcohol oxidation over Pd/Al_2O_3. *J. Catal.* **2005,** 229, 55-63.

11. Burgi, T., Time-resolved in situ ATR Spectroscopy of 2-propanol oxidation over Pd/Al2O3: Evidence for 2-propoxide intermediate. *The journal of physical chemistry. B, Condensed matter, materials, surfaces, interfaces & biophysical* 108, (35), 13364-13369.

12. Hug, S., In situ Fourier transform infrared measurements of sulfate adsorption on hematite in aqueous solutions. *Journal of colloid and interface science* **1997,** 188, (2), 415-422.

13. Hug, S., Infrared spectra of oxalate, malonate and succinate adsorbed on the aqueous surface of rutile, anatase and lepidocrocite measured with in situ ATR-FTIR. *Journal of Electron Spectroscopy and Related Phenomena* **2006,** 150, (2-3), 208-219.

14. Applications of Attenuated Total Reflection Infrared Spectroscopic Imaging to Pharmaceutical Formulations. *Analytical chemistry* **2003,** 75, (9), 2140-2146.

15. Schopflin, M., A Study on the Interaction of Local-Anesthetics with Phospholipid Model Membranes by Infrared Atr Spectroscopy. *Journal of the American Chemical Society* **1987,** 109, (8), 2375-2380.

16. Dolamic, I.; Burgi, T., Photocatalysis of dicarboxylic acids over TiO_2: An in situ ATR-IR study. *Journal Of Catalysis* **2007,** 248, (2), 268-276.

17. Baurecht, D., Quantitative modulated excitation Fourier transform infrared spectroscopy. *Review of scientific instruments* **2001,** 72, (10), 3782-3792.

18. Burgi, T.; Baiker, A., In situ infrared spectroscopy of catalytic solid-liquid interfaces using phase-sensitive detection: Enantioselective hydrogenation of a pyrone over Pd/TiO_2. *Journal of Physical Chemistry B* **2002,** 106, (41), 10649-10658.

19. Urakawa, A., Kinetic analysis using square-wave stimulation in modulation excitation spectroscopy: Mixing property of a flow-through PM-IRRAS cell. *Chemical Physics* **2006,** 324, (2-3), 653-658.

20. Fujishim.A, Electrochemical Photolysis of Water at a Semiconductor Electrode. *Nature* **1972,** 238, (5358), 37.

21. Dawson, A., Semiconductor-metal nanocomposites. Photoinduced fusion and photocatalysis of gold-capped TiO_2 (TiO_2/Gold) nanoparticles. *Journal of Physical Chemistry B* **2001,** 105, (5), 960-966.

22. Diebold, U., The surface science of titanium dioxide. *Surface Science Reports* **2003,** 48, (5-8), 53-229.

23. Amy L. Linsebigler, Guangquan Lu, and John T. YatesPhotocatalysis on TiO_2 Surfaces: Principles, Mechanisms, and Selected Results. Chemical reviews 1995, 95, (3), 735-758.

24. Masao Kaneko, I. O., Photocatlysis Science and Technology *Springer* **1999**.

25. Carp, O.; Huisman, C. L.; Reller, A., Photoinduced reactivity of titanium dioxide. *Progress in Solid State Chemistry* **2004,** 32, (1-2), 33-177.

26. Szczepankiewicz, S. H.; Colussi, A. J.; Hoffmann, M. R., Infrared spectra of photoinduced species on hydroxylated titania surfaces. *J. Chem. Phys. B* **2000,** 104, 9842 - 9850.

27. Infrared Spectra of Photoinduced Species on Hydroxylated Titania Surfaces. *The journal of physical chemistry. B, Condensed matter, materials, surfaces, interfaces & biophysical* **2000,** 104, (42), 9842-9850.

28. Adsorption of Thiol-Protected Gold Nanoparticles on TiO_2 and Their Behavior under UV Light Irradiation. *Journal of physical chemistry. C* **2008,** 112, (15), 5816-5824.

29. Kiwi-Minsker, L., Microstructured reactors for catalytic reactions. *Catalysis today* 110, (1-2), 2-14.

30. Luther, A., Novel design of a microstructured reactor allowing fast temperature oscillations. *Chemical engineering journal* 135, S254-S258.

31. Photooxidation of organic impurities in water using thin films of titanium dioxide. *The Journal of physical chemistry* **1987,** 91, (12), 3328-3333.

32. An Improved Photocatalyst of TiO_2/SiO_2 Prepared by a Sol-Gel Synthesis. *The Journal of physical chemistry* **1995,** 99, (24), 9882-9885.

2

Experimental

2.1 Introduction

For studies of photocatalytic reactions and solid liquid interfaces in situ a home built flow through cell was designed and applied in ATR-IR spectroscopy measurements and in combination with modulation excitation (MS) spectroscopy[1-3]. The design of the cell used in these experiments is an appropriate solution, allowing different types of the measurements in photocalysis.

2.2 ATR-IR Setup and Application of Modulation Excitation Spectroscopy

Infrared spectra were recorded on a Bruker Equinox-55 FTIR spectrometer, equipped with a narrow band MCT detector and attachment for ATR measurements (Wilks Scientific). All spectra were measured at room temperature at a resolution of 4 cm^{-1}. The sample was placed on a Ge IRE (52mm X 20mm X 1mm; KOMLAS) and fixed inside the home built flow-through cell and number of internal reflection was 52. The cell was made from a Teflon piece, a fused silica plate (45mm X 35mm X 3mm) with holes for the outlet and inlet 36 mm apart and a flat seal (1mm). The fluid compartment had a volume of 0.5mL. The solution was

passed through the cell at a flow rate of 2 mL/min by means of a peristaltic pump (Ismatec, Reglo 100).

A scheme of the experimental setup is shown in the Figure 2-1

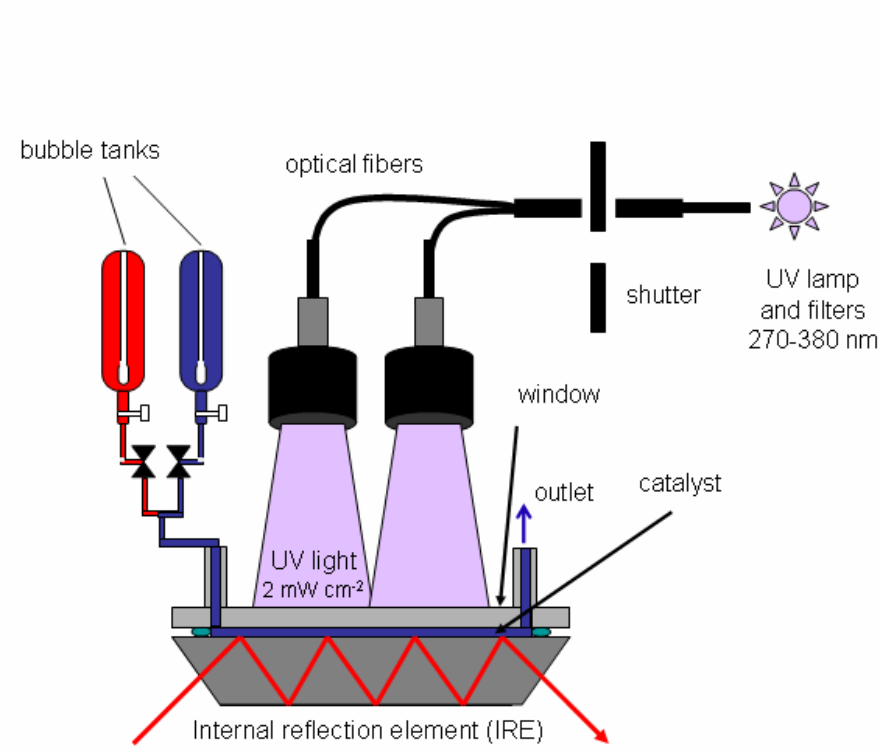

Figure 2-1:Schematic setup for in situ ATR-IR spectroscopy of photocatalytic reactions in a small volume flow-through cell.

Such cell model allowed different types of modulation excitation experiments: light modulation, concentration modulation or gas modulation experiments. In light modulation experiments irradiation of the sample was carried out by a 75 W Xenon arc lamp. Schott UG 11 and BG 42 (50mm X 50mm X 1mm) broadband filters from ITOS were used to remove visible light. An electronic shutter (Newport model 71445) was used to achieve UV light modulation. The UV light from the source was guided to the cell via two fiber bundles. For concentration modulation experiments two glass bubble tanks were used. When the gas modulation experiments were performed the solvents in the bubble thanks were saturated with oxygen and nitrogen gases. The electrical signals for switching the valves (concentration or gases modulation) or shutter (light modulation) were generated by the FTIR spectrometer. This ensures the synchronization of modulation and data acquisition.

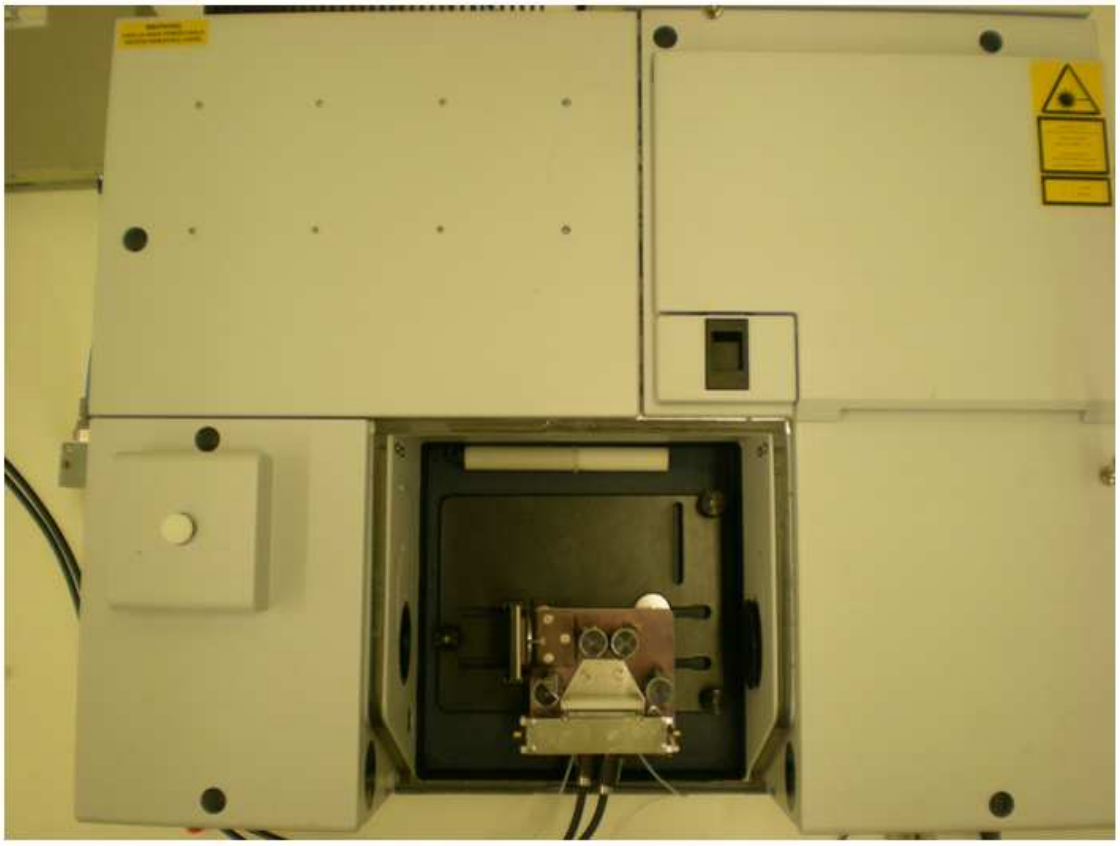

Figure 2-2: The Bruker Equinox 55 ATR-IR spectrometer equipped with ATR-IR attachment and flow-through cell for in situ photocatalytic measurements.

The Equinox 55 is a compact, rugged FT-IR spectrometer designed for demanding analytical laboratory applications. OPUS/IR software is used to control the spectrometer and for spectra manipulation. The physical dimensions (depth x width x height) of the Equinox 55 and sample compartment are as follows:

61 x 70 x 27 cm	physical dimensions of the EQUINOX 55
25.5 x 26 x 19 cm	sample compartment of the spectrometer

The frequency range of the spectrometer is 7500-370 cm^{-1}. Figure 2-3 shows sample compartment of the Equinox 55 spectrometer equipped with ATR-IR attachment and flow-through cell for in situ photocatalytic measurements.

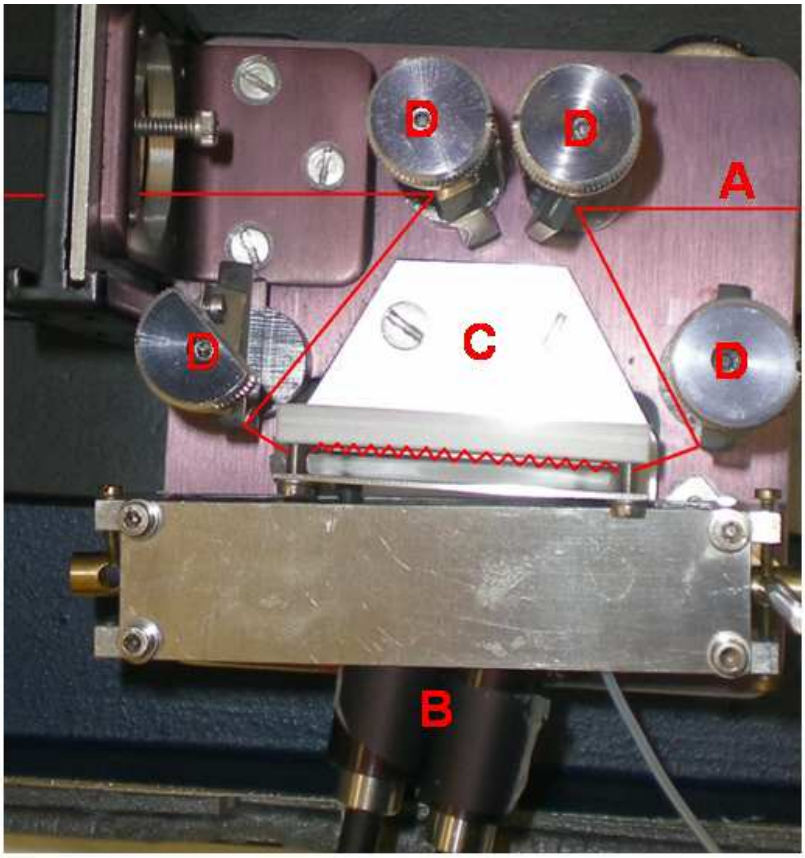

Figure 2-3: Setup for photocatalytic measurements in situ: (A) IR beam, (B) optical fibers from UV source, (C) flow-through cell with Ge internal reflection element (IRE) and fused silica window, (D) mirrors

References

1. Dolamic, I.; Burgi, T., Photoassisted decomposition of malonic acid on TiO_2 studied by in situ attenuated total reflection infrared spectroscopy. Journal Of Physical Chemistry B 2006, 110, (30), 14898-14904.

2. Dolamic, I.; Burgi, T., Photocatalysis of dicarboxylic acids over TiO_2: An in situ ATR-IR study. Journal Of Catalysis 2007, 248, (2), 268-276.

3. Dolamic I., Gautier C., Boudon J. Shalkevich N., Bürgi T., Adsorption of Thiol-Protected Gold Nanoparticles on TiO_2 and Their Behavior under UV Light Irradiation. Journal Of Physical Chemistry C 2008, 112, (15), 5816-5824.

3

Photoassisted Decomposition of Malonic Acid on TiO_2 Studied by in Situ ATR-IR Spectroscopy

3.1 Abstract

The photo-assisted mineralization, i.e. conversion to CO_2 and water, of malonic acid over P25 TiO_2 was investigated by in situ attenuated total reflection infrared (ATR-IR) spectroscopy in a small-volume flow-through cell. Re-assignment of the vibrational bands of adsorbed malonic acid, assisted by deuterium labeling, reveals two dissimilar carboxylate groups within the molecule. This indicates adsorption via both carboxylate groups, one in a bridging or bidentate and the other in monodentate coordination. During irradiation the coverage of malonic acid strongly decreases and oxalate is observed on the surface in at least two different adsorption modes. The major oxalate species observed during irradiation is characterized by monodentate coordination of both carboxylate groups. In the dark, however, part of these species adopts another adsorption mode, possibly interacting only with one carboxylate group. During band-gap illumination a large fraction of the surface is not covered by acid. Oxalate is a major intermediate in the mineralization of malonic acid. However, the observed transient kinetics of adsorbed malonic and oxalic acid indicates additional pathways not involving oxalate. The rate constant for oxalate decomposition is slightly larger than the one for oxalate formation from malonic acid. As the oxalate is desorbing slowly from the surface its concentration in the liquid phase is small, despite the fact that it is a major intermediate in the mineralization of malonic acid.

3.2 Introduction

Photo-assisted reactions on TiO_2 particles has attracted much interest due to promising applications in solar energy conversion (water splitting)[1, 2] and environmental cleaning, i.e. decomposition of organic pollutants in gaseous effluents and wastewater[3-5]. The latter two processes may largely contribute to future sustainable technologies. Upon excitation of TiO_2 across the band gap an electron hole pair is generated[6]. It is believed that these electrons and holes can be trapped at $Ti(IV)O-H$ surface sites, leading to $Ti(III)O-H^-$ and $Ti(IV)O\bullet -H^+$, respectively[7]. The photo-assisted degradation of organic molecules adsorbed on Ti sites can be initiated by their direct reaction with photogenerated holes, i.e. electron vacancies in the valence band of the semiconductor,[8] which leads to highly reactive species. This is likely the predominant mechanism for organic anions that strongly adsorb on the TiO_2 surface [9]. Alternatively, O-H radicals generated by the trapped holes may initiate reaction.

The trapped electrons are believed to react with adsorbed oxygen, leading to O^{2-} and O_2^{2-} species that may also contribute to the oxidation of organic compounds.

As most studies have focused on the analysis of stable reaction intermediates (in the gas or liquid phase) the fate of the organic reactants on the TiO_2 surface remains unclear. In fact, only a few studies were reported that give direct spectroscopic information on the composition of the adsorbate layer during or after photoreaction. Attenuated total reflection infrared (ATR-IR) spectroscopy[10] is a powerful tool to study the solid-liquid interface of powders[11-13]. and it has also been applied to study catalytic reactions[14-24]. ATR-IR spectroscopy has recently also been used to study band gap irradiation of TiO_2 particle films in contact with water. Vibrational bands below 1000 cm^{-1} that appeared upon irradiation were assigned to surface peroxo and hydroperoxo species[25, 26]. In another ATR-IR study the influence of adsorbed water on TiO_2 was investigated [27]. When removing water several bands below 1000 cm^{-1} appeared under near-UV irradiation.

Studies that directly address the fate of molecules adsorbed on the TiO_2 surface upon UV-exposure are rare. The photodegradation of 4,4'-bis(2-sulfostyryl)biphenyl was followed by ATR-IR [28]. The adsorption and photo-assisted reaction of glyoxylic acid on TiO_2 was studied[29]. Glyoxylic acid $(HCO-COOH)$ exists in aqueous solutions as the hydrated gem-diol and most likely adsorbs on TiO_2 through bidentate chelation to Ti via carboxylate and hydroxylate[29]. Upon band gap irradiation this species is transformed to oxalate. The photo-assisted reaction of oxalic acid [30, 31] and catechol [30] on TiO_2 was also probed by ATR-IR spectroscopy. Upon irradiation the adsorbed catechol is depleted and evidence was given for carbonate formation. Oxalic acid adsorbs in three different modes on TiO_2 surfaces.[11] Based on kinetic analysis it was concluded that upon irradiation the two less stable adsorption modes transform into the most stable adsorbed species, which is the most photo-labile and reacts to CO_2.[31]

Here we report the photo-assisted degradation of malonic acid on TiO_2 as studied by in situ ATR-IR spectroscopy. In contrast to oxalic acid $(HOOC-COOH)$, which is easily oxidized to two CO_2 molecules, the photoreaction of malonic acid is expected to proceed in several consecutive steps. This opens up the possibility to detect intermediate adsorbed species and therefore to shed light on the reaction pathway.

3.3 Experimental Section

3.3.1 Catalyst and Chemicals

Degussa P25 TiO_2, containing 80% anatase and 20% rutile with a surface area of 51 $m^2\ g^{-1}$ and average primary particle size of 21 nm was used in the photo-assisted reactions. Malonic acid (Sigma-Aldrich, 99%), d_4-malonic acid (Aldrich, 99+ atom % D), sodium hydroxide (Sigma-Aldrich, 97%), deuterium oxide (Aldrich, D-99, 9%) were used as received.

3.3.2 Thin Film Preparation

Slurry of the catalysts powder was prepared from about 20 mg catalyst and 25ml water (Milli-Q, 18 MΩcm). After sonication (Ultrasonic cleaner, Branson 200) for 30 min TiO_2 thin-films were formed by dropping the slurry onto a Ge internal reflection element (IRE) (52 x 20 x 1 mm; KOMLAS). The amount of slurry for one coating was 0.5 ml. The solvent was allowed to evaporate, and the procedure was repeated two times. After drying for several minutes at 40°C in air, loose catalyst particles were removed by flowing water over the IRE. After drying in air the film was ready for use. From the amount of deposited TiO_2 and its density an average film thickness of 4 μm was estimated. ZnSe internal reflection elements were also used for this type of experiments. However, upon irradiation some degradation of the ZnSe crystal was observed, resulting in a precipitate, likely Se^0, on the ZnSe crystal and a pH increase in reactant solution.[31]

3.3.3 ATR-IR Spectroscopy

ATR spectra were recorded with a dedicated flow-through cell, made from a Teflon piece, a fused silica plate (45 x 35 x 3 mm) with holes for in- and outlet (36 mm apart), and a flat (1mm) viton seal. The cell was mounted on an attachment for ATR measurements within the sample compartment of a Bruker Equinox-55 FTIR spectrometer equipped with narrow-band MCT detector. Spectra were recorded at 4 cm^{-1}. The reactant was passed through the cell and over the catalyst at a flow rate of 0.2 ml/min by means of a peristaltic pump (Ismatec, Reglo 100) located in front of the cell. Solutions of malonic acid (10^{-4}mol/l, pH about 3.5) were flown over the TiO_2 film in the dark for 30 min in order to reach equilibrium. The pKa values of malonic acid are 2.84 and 5.79[32]. Irradiation of the sample with UV light was

carried out using a 75 W Xe arc lamp. The UV light from the source is guided to the cell via two fiber bundles. The light was passed through a 5 cm water filter to remove any infrared radiation. A Schott UG 11 (50 x 50 x 1mm) broadband filter from ITOS was used to remove visible light (transmission between 270 and 380 nm). An estimate based on the supplier specifications gave a power at the sample of slightly less than 10 mW/cm^2. All experiments were performed at room temperature. A schematic of the experimental setup is given in Figure 3-1

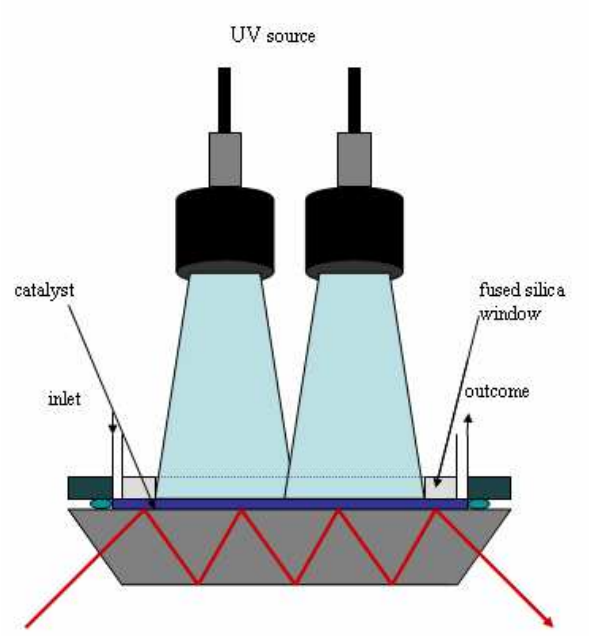

Figure 3-1: Schematic set-up for in situ ATR-IR spectroscopy of photo-assisted reactions in a small volume flow-through cell.

3.4 Results

3.4.1 ATR-IR spectra of dissolved and adsorbed malonic acid on TiO_2.

Figure 3-2 shows ATR-IR spectra of dissolved malonic acid, both in its protonated (b) and deprotonated state (a), and of malonic acid adsorbed from a dilute solution on a TiO_2 film (c).

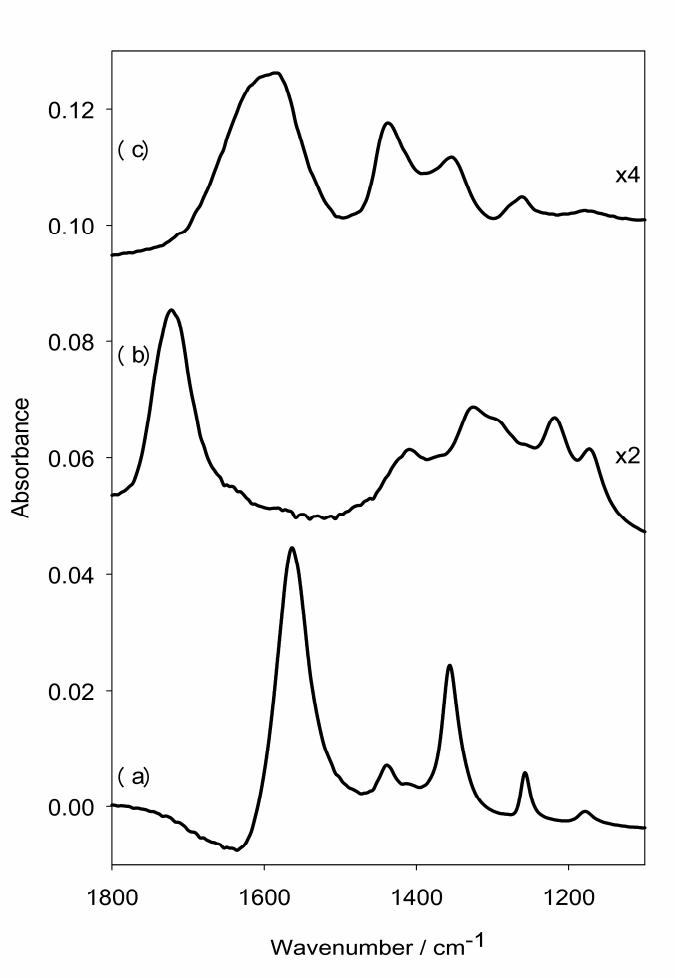

Figure 3-2: ATR-IR spectra of dissolved malonic acid and malonic acid adsorbed on TiO_2. (a) Malonic acid 0.1 mol/l in water at pH 8.6. The pH was adjusted with NaOH. As reference served water at the same pH. (b) Malonic acid 0.1 mol/l in water (pH=1.5, no addition of NaOH). As reference served pure water. (c) Malonic acid adsorbed on a TiO_2 film. The spectrum was recorded while flowing a solution of 10^{-4} mol/l malonic acid over the film and represents the equilibrium state reached after about 30 min of contact. As reference served the TiO_2 film in contact with pure water. The spectra were shifted for clarity. The negative band in spectrum (a) slightly above 1600 cm^{-1} is due to an incompensation of bulk water.

The spectra are in good agreement with previous reports[33]. The most prominent band of protonated malonic acid is associated with the $\nu(C=O)$ vibration at 1718 cm^{-1}. In the spectrum of the dissolved deprotonated acid the $\nu_{as}(COO^-)$ and $\nu_s(COO^-)$ modes at 1564 and 1355 cm^{-1} are the most intense. Weaker modes at 1437 and 1258 cm^{-1} were previously assigned to $\nu(CH_2)$ vibrations[33]. Upon adsorption from solution ((c)) the molecule is deprotonated as evidenced by the broad $\nu_{as}(COO^-)$ band at 1600 cm^{-1}.

Figure 3-3 shows infrared spectra of malonic acid adsorbed on the TiO_2 film measured under different conditions.

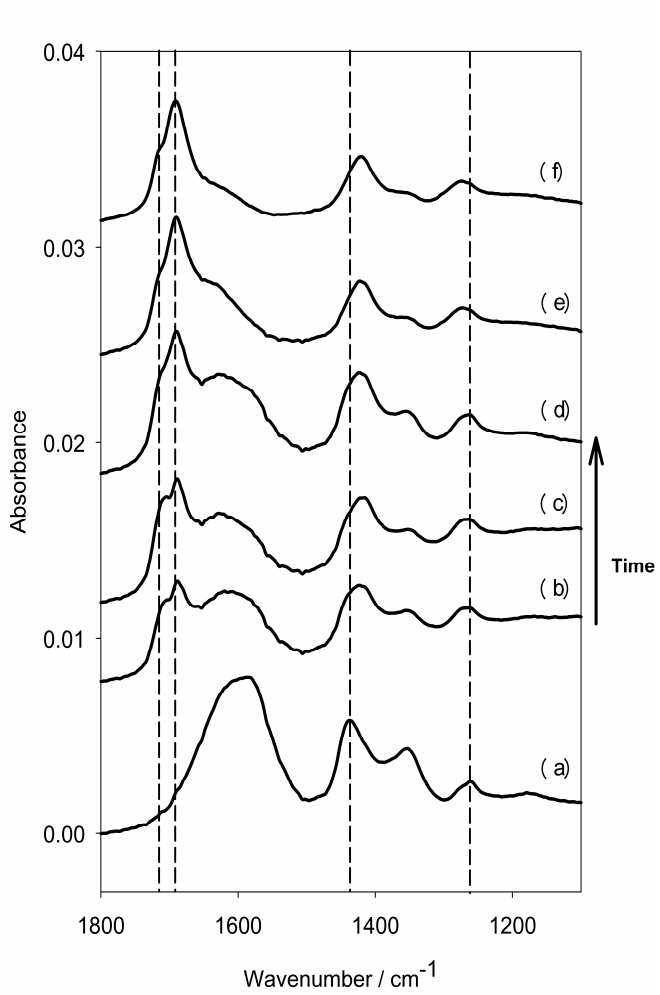

Figure 3-3: Series of ATR-IR spectra of malonic acid on TiO_2. The reference spectrum was recorded while flowing pure water over the TiO_2 film. Spectrum (a) was recorded in the dark while a solution of malonic acid (10^{-4} mol/l) was flowing over the TiO_2 film. Spectra (b) and (c) were recorded while illuminating the TiO_2 film and simultaneously flowing malonic acid solution (10^{-4} mol/l). Spectra (b) and (c) respectively, were recorded 7 min and 20 min, respectively, after switching on the UV-light. Spectra (d) - (f) were subsequently recorded in the dark while flowing pure water over the TiO_2 film. Spectra are offset for clarity. The vertical lines are just to guide the eye.

Spectrum (a) refers to adsorbed malonic acid in the dark. Spectra (b) and (c) were recorded under UV irradiation and while flowing a solution of malonic acid (10^{-4} mol/l) over the TiO_2 film. Under irradiation the bands of adsorbed malonic acid decrease. Concomitantly other bands increase, notably at 1708, 1690, 1421 and 1275 cm^{-1}. After about 20 min the spectrum hardly changes anymore. It should be noted that under illumination a broad absorption was observed, extending from above 2000 to below 900 cm^{-1} and exponentially

increasing at lower wavenumbers. Part of the intensity of this absorption increased/decreased abruptly upon turning the light on/off. Part of the absorbance showed slower response. A similar broad absorption was reported when irradiating dry TiO_2 films and ascribed to an excitation of electrons from shallow traps to the conduction band of the TiO_2 semiconductor[27]. Alternatively the broad band could be due to a scattering effect. Spectra (d) - (f) were recorded in the dark and while flowing neat water over the TiO_2 film. This leads to desorption of the adsorbed malonic acid, leaving behind on the TiO_2 surface the species that were formed during illumination. Figure 3-4 shows spectra for an analogous experiment as the one in Figure 3-3 but with deuterated malonic acid (d_4-malonic acid) in D_2O.

The CH_2 vibrations in malonic acid strongly shift to lower wavenumbers in d_4-malonic acid. This is evident for the vibration at 1260 cm^{-1}, for the normal malonic acid (spectrum (b) in Figure 3-4), which was assigned to a CH_2 wagging mode[33, 34]. In the corresponding spectrum of deuterated malonic acid (spectrum (a) in Figure 3-4) no band is observed at 1260 cm^{-1}. However, the species that is formed during illumination is not affected by deuteration (compare spectra (c) and (d) in Figure 3-4).

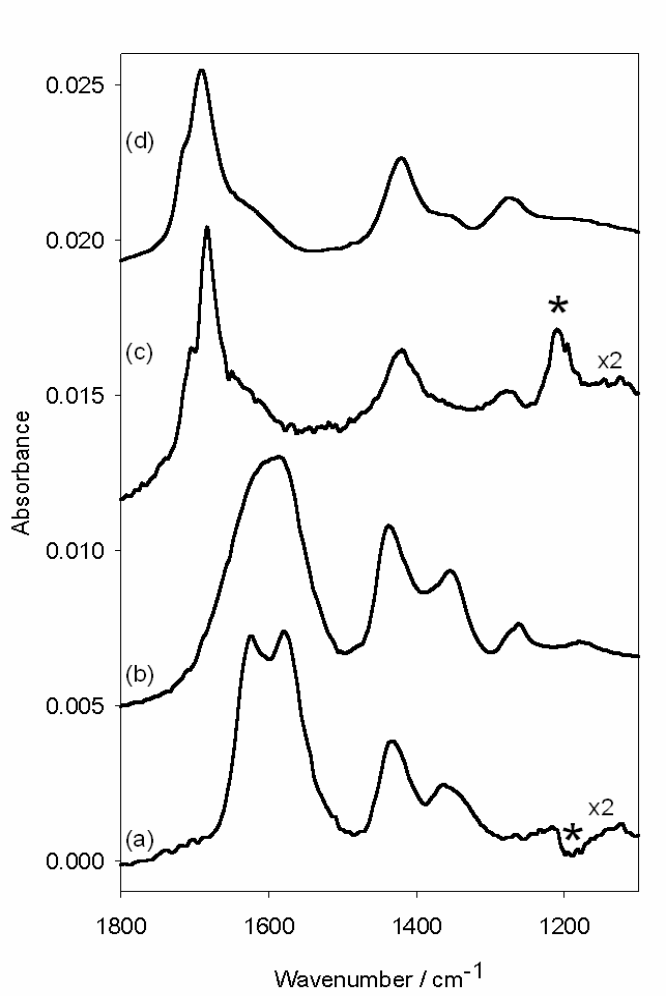

Figure 3-4: ATR-IR spectra of (a) d_4-malonic acid on TiO_2 adsorbed from D_2O, (b) malonic acid on TiO_2 adsorbed from H_2O, (c) d_4-malonic acid on TiO_2 after illumination and washing with D_2O, (d) malonic acid on TiO_2 after illumination and washing with H_2O. Asterisks (*) mark signals from uncompensated D_2O solvent.

Figure 3-5 shows the time-dependence of two signals at 1350 and 1708 cm^{-1} in the ATR-IR spectra. The former signal is associated with the $\nu_s(COO^-)$ mode of malonic acid adsorbed on TiO_2, whereas the latter can be assigned to $\nu_s(C=O)$ vibrations of the species that are formed under irradiation. The lines at the top of the figure indicate the state of the two parameters that were changed during the course of the experiment, namely the UV-light (on or off) and the concentration of malonic acid in solution (zero or 1.5×10^{-4} mol/l). First malonic acid is adsorbed in the dark (regime 1 in Figure 3-5). After reaching equilibrium the light is switched on (2), which leads to a fast decrease of the amount of adsorbed malonic acid (signal at 1350 cm^{-1}). The latter reached a new stable level after about 5 minutes. Upon illumination the species associated with the 1708 cm^{-1} band appears. Figure 3-5 reveals that

the disappearance of the 1350 cm^{-1} band is faster than the appearance of the 1708 cm^{-1} signal. Upon switching off the light again (3 in Figure 3-5) malonic acid re-adsorbs fast. At the same time a slight increase of the absorbance at 1708 cm^{-1} is also observed. The subsequent flow of neat water in the dark (4 in Figure 3-5) removes almost all malonic acid within about 15 minutes. The absorbance at 1708 cm^{-1} initially decreases fast and keeps decreasing further but at a much slower rate after about 5 minutes. When switching on the light again (5 in Figure 3-5) the species associated with the 1708 cm^{-1} band vanishes initially very fast and later disappears completely, however at a considerably slower rate. Illumination after re-adsorption (7 in Figure 3-5) again leads to depletion of malonic acid on the surface and formation of the 1708 cm^{-1} signal (, analogous as observed for treatment 2 in Figure 3-5). The small increase of the absorbance at 1708 cm^{-1} observed upon re-adsorption of malonic acid in the dark (6 in Figure 3-5) can be attributed to the broad band of malonic acid centered around 1600 cm^{-1}, which has a tail above 1700 cm^{-1} (see also difference spectra in Figure 3-6).

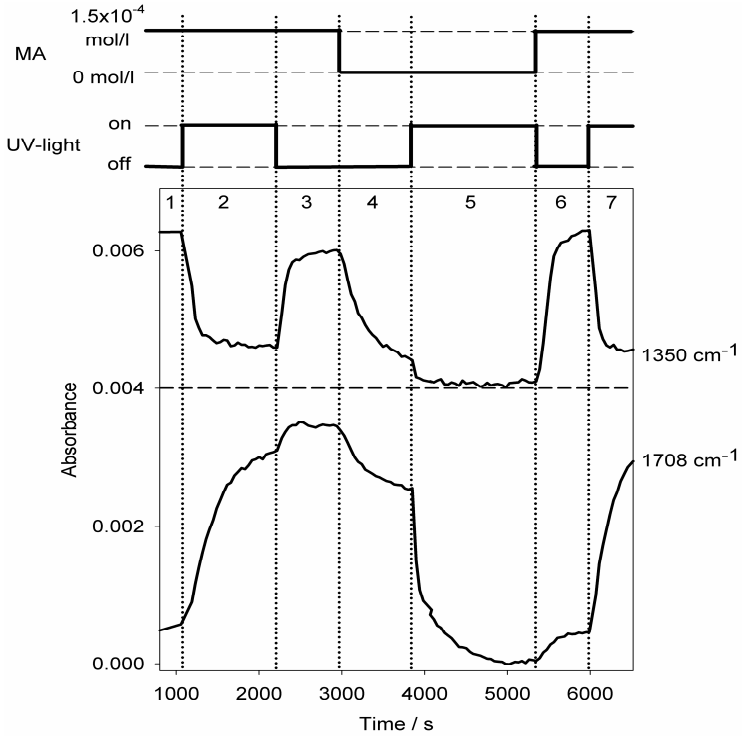

Figure 3-5: Absorbance at 1350 cm^{-1} and at 1708 cm^{-1} as a function of time as followed by ATR-IR spectroscopy during different treatments of a TiO_2 film with UV-light and malonic acid solution. The state of the two parameters that were changed during the experiment, the UV-light and the concentration of the malonic acid in solution are given in the upper part of the Figure. Regimes that correspond to a certain state of the two parameters are numbered consecutively. In order to get rid of drifts during the long experiment the two absorption signals were baseline corrected by subtracting the signal from a nearby spectral region with no absorption bands (1742 and 1315 cm^{-1}). The 1350 cm^{-1} signal was shifted by 0.004 for clarity.

Figure 3-6 shows difference spectra for the same experiment as shown in Figure 3-5. The difference spectra reveal the spectral changes observed upon changing conditions. For example, upon illumination (difference spectrum 1 → 2) the bands of adsorbed malonic acid appear negative, because the malonic acid coverage is decreasing. At the same time two positive bands at 1708 and 1690 cm^{-1} indicate the appearance of a new species containing C=O groups.

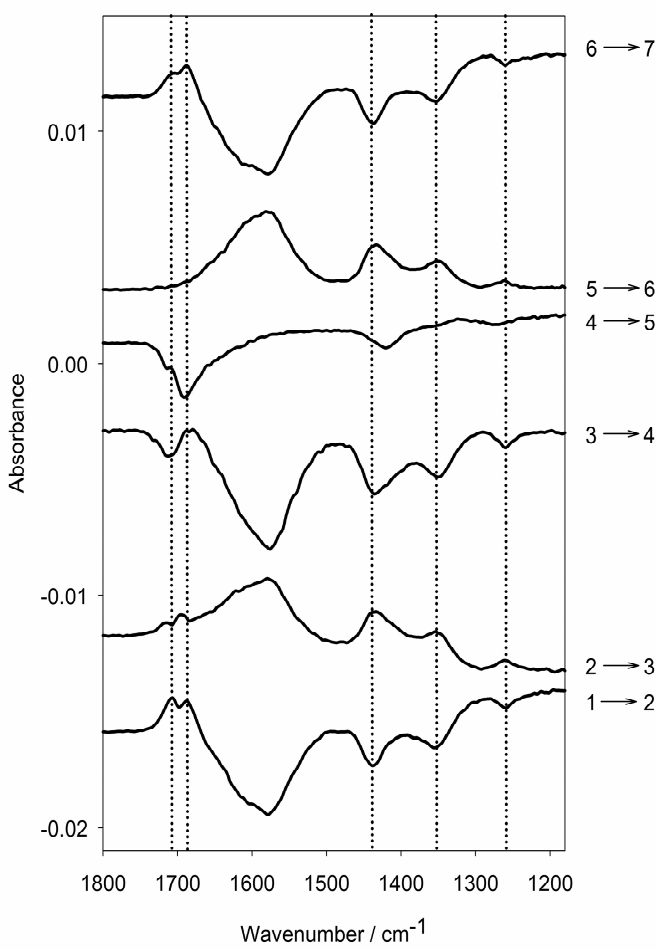

Figure 3-6: ATR-IR difference spectra for the same experiment as described in Figure 3-5 The numbers and arrows on the right side of the figure denote the two regimes, as described in Figure 3-5 that were used to calculate the difference spectrum. For example 1 → 2 refers to a difference spectrum between the last spectrum recorded in regime 1 (flowing malonic acid over the surface in the dark) and one of the first spectra recorded in regime 2 (flowing malonic acid and turning on the UV-light). Vertical lines are just to guide the eye.

Figure 3-7 shows difference spectra recorded during illumination of the adsorbed species that is formed upon illumination of malonic acid, i.e. after illumination and desorption of unreacted malonic acid (corresponding to regime 5 in Figure 3-5). Spectrum (a) refers to the spectral changes during the first two minutes (steep initial decrease in Figure 3-5, regime

(5), spectrum (b) corresponds to the spectral changes of the subsequent five minutes and spectrum (c) during the subsequent 20 min. The spectra change qualitatively with time, which reveals that more than one species are involved in the process.

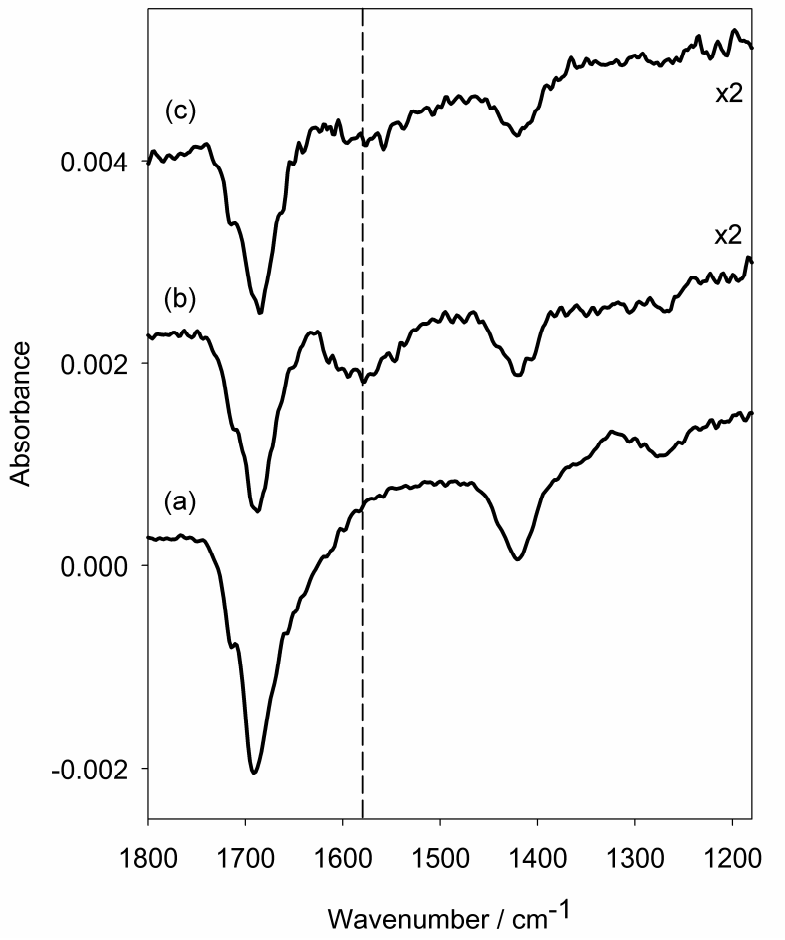

Figure 3-7: ATR-IR difference spectra for the same experiment as described in Figure 3-5 and Figure 3-6. The spectra were recorded during illumination in water of a TiO_2 film that contained mainly adsorbed oxalic acid (regime 5 in Figure 3-5). Difference spectrum (a) reveals the changes during the first two minutes of illumination; difference spectrum (b) reveals the changes during the subsequent five minutes of illumination; and difference spectrum (c) reveals the changes during the subsequent twenty minutes of illumination.

3.5 Discussion

3.5.1 Identification of the species absorbing at 1708 cm^{-1}

Figure 3-4 clearly shows that the spectrum of the species formed during irradiation does not change upon deuteration. It is therefore concluded that the new species does not

contain hydrogen (deuterium) and consequently is composed of oxygen and carbon atoms only. Adsorbed oxalic acid, more precisely oxalate $^{-}OOC-COO^{-}$ is a feasible possibility.

Adsorption of oxalic acid from aqueous solutions on TiO_2 surfaces was investigated before by ATR-IR spectroscopy[11, 31]. From the coverage-dependent spectral changes it was shown that several surface oxalate complexes coexist. Using singular value decomposition the spectra of three different components could be determined. The spectrum of the most strongly adsorbed species (with a Langmuir adsorption constant $\log(K_L)$ of 6.1 – 6.6)[11] showed a band at 1690 cm^{-1} and a shoulder slightly above 1700 cm^{-1}. Furthermore the same species exhibited a band at 1421 cm^{-1} and a weaker one at 1275 cm^{-1}. The reported spectrum[11] matches perfectly the one shown in Figure 3-3 (f) and 6 (4 → 5) and the species that is formed upon irradiation of malonic acid adsorbed on TiO_2 can be attributed to adsorbed oxalate. The bands at 1421 cm^{-1} and 1275 cm^{-1} are therefore assigned to $\nu(C-O)+\nu(C-C)$ and $\nu(C-O)+\nu(O-C=O)$ vibrations[33]. The appearance of two bands around 1700 cm^{-1} reveals two groups with C=O character, which suggests an adsorption geometry as shown in (Scheme 1 a). In this form of the oxalate the two C=O groups may be equivalent (depending on the surrounding) and the two distinct vibrational bands in the spectrum correspond to the symmetric and antisymmetric C=O stretching vibration.

Figure 3-6 shows that more than one species absorbing above 1700 cm^{-1} are present on the TiO_2 surface after illumination (compare 3 → 4 with 4 → 5 in Figure 3-6). Once formed under band-gap illumination of TiO_2 from adsorbed malonic acid these species disappear at different rates from the surface in the dark, which allows distinguishing between them. The faster disappearing species has one absorption band above 1700 cm^{-1} (Figure 3-6, 3 → 4), whereas the slower disappearing species has two bands (Figure 3-6, 4 → 5). As discussed above the latter species is assigned to oxalate adsorbed as shown in Scheme 1 a). The species associated with the band at 1711 cm^{-1} (Figure 3-6, 3 → 4) is assigned to oxalate in a different adsorption mode. The exact nature of this species is less clear but likely only one carboxylate group is interacting with the surface in this case (see Scheme 1 b), c)). The band above 1700 cm^{-1} is then ascribed to the $\nu(C=O)$ vibration of the protonated acid group. The analysis of ATR-IR spectra of oxalate adsorbed on TiO_2 by singular value decomposition resulted, in addition to the strongly adsorbed oxalate species, in two different species with only one absorption band above 1700 cm^{-1} (with Langmuir constants $\log(K_L)$ of (4.4 – 5.6 and 3 – 3.5, respectively)[31, 33]. The observed band in Figure 3-6 (3 → 4) is compatible with the reported spectra for the more strongly bound of these two species, which

has a band slightly above 1710 cm^{-1}. For this species an adsorption geometry as shown in (Scheme 3-1 b) or c)) has been proposed[31]. Note that this assignment implies that the acid group which is not bound to the surface is protonated.

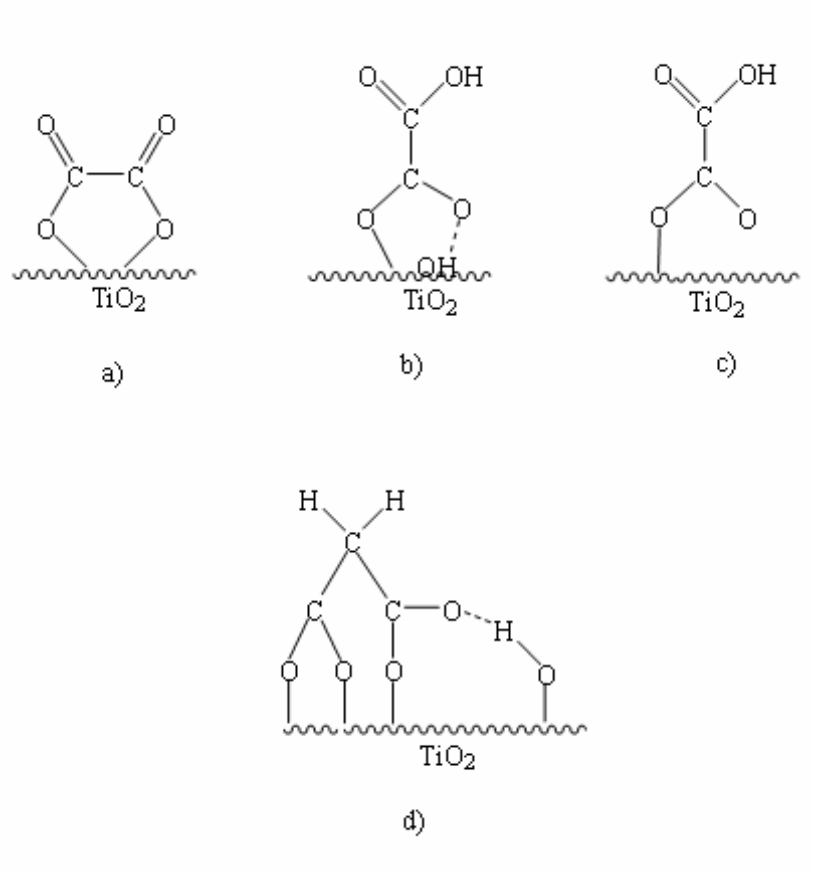

Scheme 3-1: Different adsorption modes of oxalate on TiO_2 and proposed adsorption mode of malonate on TiO_2.

3.5.2 Adsorption mode of malonic acid

Previously the vibrational band at 1430 cm^{-1} of adsorbed malonic acid was ascribed to a $\nu(CH_2)$ mode[33, 34]. This mode may indeed bear some $\nu(CH_2)$ character, but the observation of the same band in the spectrum of deuterated malonate (Figure 3-4) clearly shows that it has to be assigned primarily to a $\nu_s(COO^-)$ mode. The four bands observed at 1625, 1575, 1430 and 1362 cm^{-1} for deuterated malonate on TiO_2 (Figure 3-4 (a)) are assigned to $\nu_{as}(COO^-)$ (former two bands) and $\nu_s(COO^-)$ (latter two bands) vibrations. This is evidence for quite different carbocylate groups, which may have several origins. First of all P25 is a mixture of anatase (80 – 90%) and rutile (10 – 20%) and the two sets of carboxylate bands could

originate from adsorption on the two crystal phases. We can exclude this possibility as the spectrum of malonic acid adsorbed on P25 strongly resembles the spectrum of malonic acid on anatase[35]. Another possibility which could lead to two sets of carboxylate bands would be the presence of two distinctly different adsorbed species. From ATR-IR spectra at different pH and based on a singular value decomposition it was concluded that the adsorption of malonic acid on TiO_2 can very well be described by only one adsorbed species.35 All the bands observed in Figure 3-4 (a) therefore belong to the same adsorbed species, which shows that the two carboxylate groups within the adsorbed molecule are largely different.

The wavenumber difference Δ between the $\nu_{as}(COO^-)$ and $\nu_s(COO^-)$ modes is diagnostic for the coordination mode of the carboxylate.[33, 36-38] If this difference for the adsorbed carboxylate is larger than for the dissolved carboxylate then the coordination mode is monodentate[36]. If Δ is smaller for the adsorbed species than for the dissolved one then chelating and/or bridging coordination is indicated. Obviously, for the two pairs of carboxylate vibrations in the spectrum of adsorbed malonic acid two different combinations are possible with Δ values of either 263 and 145 cm^{-1} or 213 and 195 cm^{-1}, whereas for dissolved malonic acid Δ = 209 cm^{-1} (Figure 3-2). We prefer the former of the two possibilities, as the spectrum indicates largely different coordination for the two carboxylate groups and propose an adsorption mode with one monodentate (large Δ) and one bidentate/chelating carboxylate as shown in Scheme 3-1 (d).

3.5.3 Qualitative Consideration

From Figure 3-5 some qualitative considerations on relative reaction rates and coverage can be made. Under our conditions the coverage of malonic acid under irradiation is only about 25% of its value in the dark (Figure 3-5, regimes 1 and 2). Upon irradiation malonic acid reaches almost steady state coverage after about 5 minutes, whereas it takes at least 20 minutes for oxalic acid to reach steady state. This indicates that the transformation of malonic acid into oxalic acid is not the only surface reaction that is occurring. Oxalic acid is reacting further under illumination and malonic acid is constantly desorbing from the surface. Furthermore reaction pathways that do not involve oxalic acid may be possible (see later).

Figure 3-5 shows that the photo-assisted degradation of oxalic acid is very fast (regime 5, 50% depletion of adsorbed oxalic acid in about 1 min). The fact that during continuous illumination and flow of malonic acid the intermediate oxalic acid is observed on

the TiO_2 surface means that the formation of oxalic acid (and therefore the photo-assisted reaction of malonic acid) is also fast. An estimate for the relative rates can be made as follows. Figure 3-5 shows that re-adsorption of malonic acid after illumination results in coverage of only about 85% of its value before illumination (regime 3 in Figure 3-5). The remaining 15% of surface sites are occupied by oxalic acid at this point (regime 3), which can not be displaced by malonic acid. As most of the oxalic acid is desorbing very slowly, this coverage corresponds approximately to the steady state oxalic acid coverage under illumination (regime 2). Under illumination in the steady state malonic acid reaches only 25% of full coverage (first adsorption in the dark). From the steady state condition for oxalic acid under illumination one can estimate the relative rate constants for photo-assisted reaction of oxalic acid (k_{OA}) and of malonic acid for the pathway leading to oxalic acid (k_{MA}): $k_{OA}/ k_{MA} = \theta_{MA}/\theta_{OA} \approx 0.25/0.15 = 1.67$, where θ_{MA} and θ_{OA} respectively, is the steady state coverage of malonic acid and oxalic acid, respectively. The rate constant for oxalic acid is slightly larger than the one for malonic acid. It should be pointed out that the overall reaction rate for malonic acid photo-assisted degradation may be larger due to other possible pathways that do not go through oxalic acid.

Another important conclusion emerging from the analysis of Figure 3-5 is that under illumination the surface is largely depleted from adsorbed acid (malonic and oxalic acid). As no other species are observed in significant amount it is concluded that under illumination a large fraction of the surface (about 60%) is not covered with adsorbate. Difference spectrum $2 \rightarrow 3$ in Figure 3-6 reveals the spectral changes upon switching off the light in the presence of dissolved malonic acid. Two weak positive features around 1700 cm^{-1} can be observed. The increase of these bands in the dark is somehow surprising because significant bands around 1700 cm^{-1} were never observed to grow in the dark under any other condition. Close inspection reveals that the maxima of the two bands are not identical to the maxima of the bands associated with strongly adsorbed oxalic acid (see difference spectrum $1 \rightarrow 2$ in (Figure 3-6). In fact, at the position of the latter bands, as indicated by the vertical lines in Figure 3-6, minima are observed in the difference spectrum $2 \rightarrow 3$. The observed features can be explained by a restructuring of the adsorbed oxalic acid, from structure (a) in Scheme 3-1, responsible for the negative bands at 1708 and 1690 cm^{-1}, into structure (b) or (c) in Scheme 3-1, responsible for the broad band at 1711 cm^{-1}. This observation furthermore shows that the steady state distribution of adsorption modes of oxalic acid under irradiation does not correspond to the equilibrium distribution in the dark.

After illumination and in the presence of dissolved malonic acid the ATR-IR spectrum stabilizes after some time (Figure 3-5, regime 3). Under these conditions oxalic acid remains on the surface. However, the change from dissolved malonic acid towards water flow leads to a decrease of the signal at 1711 cm^{-1} (see Figure 3-6, 3 → 4) that we assign to weakly adsorbing oxalic acid (Scheme 3-1, b), c)). This could be explained either by desorption of this species from the TiO_2 surface or by a deprotonation of the free (not surface bound) acid group. We prefer the latter interpretation. At pH 3.5 the free acid group of adsorbed oxalic acid (Scheme 3-1, b), c)) is expected to be protonated, whereas at neutral pH in pure water it is expected to be deprotonated. Note that the pKa values of dissolved oxalic acid are 1.23 and 4.19.32 This view is corroborated by Figure 3-7 (corresponding to regime 5 in Figure 3-5), where a surface that mainly contains adsorbed oxalic acid is illuminated in water. Spectrum (b) in Figure 3-7, and to a minor extent spectrum (c), reveals a broad band centered at 1580 cm^{-1}, which we assign to the deprotonated form of weakly adsorbed oxalic acid (Scheme 1, b), c)). Dissolved deprotonated oxalic acid in solution is characterized by a broad $\nu_{as}\left(COO^{-}\right)$ band at 1570 cm^{-1}[33]. It has been proposed before that under band gap illumination the weakly adsorbed oxalate species (Scheme 3-1, b), c)) are transformed to strongly adsorbed oxalate (Structure a) in (Scheme 3-1), which is then undergoing photo-assisted degradation[31]. In the latter study, however, the experiments were performed at pH values, at which the weakly bound oxalic acid (Scheme 3-1, b), c)) was protonated.

3.5.4 Mechanism of Photoassisted Mineralization of Malonic Acid on TiO_2

The primary initial reaction mechanism for strongly adsorbed carboxylic acid is a photo-Kolbe reaction, initiated by a photogenerated hole. This leads to CO_2 and a carbon centered radical. The fate of this radical may be more complex. The radical can abstract a hydrogen atom from any other suitable molecule, which would lead to acetic acid. Acetic acid only weakly adsorbs on TiO_2 (Langmuir constant of $\log(K_L)=2.2$[39]) and is therefore expected to desorbs readily from the surface. There is no sign in the ATR-IR spectra of adsorbed acetic acid, which is characterized by a strong band slightly above 1500 cm^{-1} [39]. The carbon centered radical can also react with oxygen to the corresponding peroxyl radical, which may then ultimately be transformed to a carboxylic acid,[40] in our case oxalic acid, which is observed in the ATR-IR spectra. Adsorbed oxalate ($^{-}OOC\text{-}COO^{-}$) can further react with a photogenerated hole (photo-Kolbe reaction) to form CO_2 and a $CO_2^{\cdot -}$ radical. The latter ultimately also leads

to CO_2, possibly via the formation of formic acid[41]. Scheme 3-2 summarized the discussed reaction mechanism.

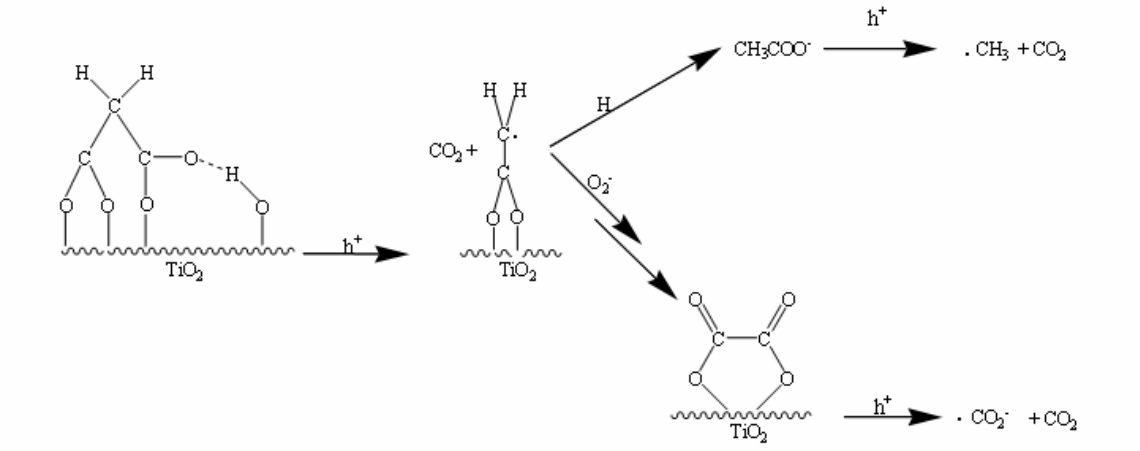

Scheme 3-2: Proposed reaction mechanism for photo-assisted mineralization of malonic acid over TiO_2.

ATR-IR technique as applied here is sensitive to the processes taking place at the solid-liquid interface and the investigation shows that oxalic acid is an intermediate during the photo-assisted mineralization of malonic acid. Oxalic acid is desorbing slowly and mineralized fast, which implies that the concentration of oxalic acid in solution is small, despite the fact that it is a major intermediate in the mineralization of malonic acid. Indeed, in the photo-assisted degradation of fumaric and maleic acid oxalic acid was observed only in very small amount in solution[41]. These considerations indicate that care must be taken when reaction mechanisms are derived from dissolved intermediates, because intermediates on the catalytic surface may not be observed in large quantities in solution but still play a major role.

3.6 Conclusion

The photo-assisted mineralization of malonic acid on P25 TiO_2 can be followed in situ by attenuated total reflection infrared spectroscopy. Upon illumination the coverage of adsorbed malonic acid is decreasing and oxalic acid is observed on the TiO_2 surface. Under illumination a large fraction of the surface is free from adsorbed acid. The transient behavior of malonic and oxalic acid observed on the catalyst surface upon illumination indicates other reaction pathways for malonic acid decomposition not involving oxalic acid. Because oxalic acid desorption from the TiO_2 surface is slow, its concentration in solution is low despite the

fact that it is a major intermediate in the decomposition of malonic acid. This indicates that care must be taken when deriving reaction mechanisms and pathways based only on stable intermediate species observed in solution.

References

1. Fujishima, A.; Honda, K., Electrochemical photolysis of water at a semiconductor electrods. Nature 1972, 238, 37.
2. Khan, S. U. M.; Al-Shahry, M.; Ingler, W. B., Efficient photochemical water splitting by a chemically modified n-TiO2. Science 2002, 297, 2243-2245.
3. Wang, R.; Hashimoto, K.; Chikuni, M.; Kojima, E.; Kitamura, A.; Shimohigashi, M.; Watanabe, T., Nature 1997, 388, 431.
4. Asahi, R.; Morikawa, T.; Ohwaki, T.; Aoki, K.; Taga, Y., Visible-light photocatalysis in nitrogen-doped titanium oxides. Science 2001, 293, 269-271.
5. Hoffmann, M. R.; Martin, S. T.; Choi, W. Y.; Bahnemann, D. W., Environmental applications of smiconductor photocatalysis. Chem. Rev. 1995, 95, 69-96.
6. Linsebigler, A. L.; Lu, G.; Yates, J. T., Photocatalysis on TiO2 surfaces: Principles, mechanisms, and selectrd results. Chem. Rev. 1995, 95, 735 -758.
7. Szczepankiewicz, S. H.; Colussi, A. J.; Hoffmann, M. R., Infrared spectra of photoinduced species on hydroxylated titania surfaces. J. Chem. Phys. B 2000, 104, 9842 - 9850.
8. Draper, R. B.; Fox, M. A., Titanium dioxide photosensitized reactions studied by diffuse reflectance flash photolysis in aqueous suspensions of TiO2 powder. Langmuir 1990, 6, 1396 - 1402.
9. Kesselman, J. M.; Weres, O.; Lewis, N. S.; Hoffmann, M. R., Electrochemical production of hydroxyl radical at polycrystalline Nb-doped TiO2 electrodes and estimation of the partitioning between hydroxyl radical and direct Hole oxidation pathways. J. Phys. Chem. B 1997, 101, (14), 2637 - 2643.
10. Harrick, N. J., Internal reflection spectroscopy. Interscience Publishers: New York, 1967.
11. Hug, S. J.; Sulzberger, B., In situ Fourier transform infrared spectroscopic evidence for the formation of several different surface complexes of oxalate on TiO2 in the aqueous phase. Langmuir 1994, 10, 3587.
12. Tejedor-Tejedor, M. I.; Yost, E. C.; Anderson, M. A., Characterization of benzoic and phenolic complexes at the goethite/aqueous interface using cylindrical internal reflection Fourier transform infrared spectroscopy. Part 1. Methodology. Langmuir 1990, 6, 979.
13. Connor, P. A.; Dobson, K. D.; McQuillan, A. J., New sol-gel attenuated total reflection infrared spectroscopic method for analysis of adsorption at metal oxide surfaces in aqueous solutions. Chelation of TiO2, ZrO2, and Al2O3 surfaces by catechol, 8-quinolinol, and acetylacetone. Langmuir 1995, 11, 4193.

14. Bürgi, T.; Baiker, A., In situ infrared spectroscopy of catalytic solid-liquid interfaces using phase-sensitive detection: Enantioselective Hydrogenation of a pyrone over Pd/TiO2. J. Phys. Chem. B 2002, 106, 10649-10658.

15. Ferri, D.; Bürgi, T., An in situ attenuated total reflection infrared study of a chiral catalytic solid-liquid interface: cinchonidine adsorption on Pt. J. Am. Chem. Soc. 2001, 23, 12074-12084.

16. Bürgi, T., Combined in situ attenuated total reflection infrared and UV-Vis spectroscopic study of alcohol oxidation over Pd/Al_2O_3. J. Catal. 2005, 229, 55-63.

17. Bürgi, T.; Bieri, M., Time-resolved in-situ ATR spectroscopy of 2-propanol oxidation over Pd/Al_2O_3: Evidence for 2-propoxide intermediate. J. Phys. Chem. B 2004, 108, (35), 13364-13369.

18. Bürgi, T.; Wirz, R.; Baiker, A., In situ attenuated total reflection infrared spectroscopy: A sensitive tool for the investigation of reduction-oxidation processes on heterogeneous Pd metal catalysts. J. Phys. Chem. B 2003, 107, 6774-6781.

19. Keresszegi, C.; Ferri, D.; Mallat, T.; Baiker, A., On the role of CO formation during the aerobic oxidation of alcohols on Pd/Al2O3: an in situ ATR-IR study. J. Catal. 2005, 234, 65-75.

20. Ortiz-Hernandez, I.; Williams, C., In situ investigation of solid-liquid catalytic interfaces by attenuated total reflection infrared spectroscopy. Langmuir 2003, 19, 2956-2962.

21. Ortiz-Hernandez, I.; Owens, D. J.; Strunk, M. R.; Williams, C. T., Multivariate analysis of ATR-IR spectroscopic data: Applications to the solid-liquid catalytic interface. Langmuir 2006, in press, published on the web.

22. Hamminga, G. M.; Mul, G.; Moulijn, J. A., Real-time in situ ATR-FTIR analysis of he liquid phase hydrogenation of gamma-butyrolactone over Cu-ZnO catalysts: A mechanistic study by varying lactone ring size. Chem. Eng. Sci. 2004, 59, 5479 - 5485.

23. He, R.; Davafa, R. R.; Dumesic, J. A., In situ ATR-IR spectroscopic and reaction kinetics studies of water-gas shift and methanol reforming on Pt/Al2O3 catalysts in vapor and liquid phases. J. Phys. Chem. B 2005, 109, (7), 2810 - 2820.

24. Ebbesen, S. D.; Mojet, B. L.; Lefferts, L., CO Adsorption and Oxidation at the Catalyst-Water Interface: An Investigation by Attenuated Total Reflection Infrared Spectroscopy. Langmuir 2006, 22, (3), 1079 - 1085.

25. Nakamura, R.; Imanishi, A.; Murakoshi, K.; Nakato, Y., In situ FTIR studies of primary intermediates of photocatalytic reactions on nanocrystalline TiO2 films in contact with aqueous solutions. J. Am. Chem. Soc. 2003, 125, 7443 - 7450.

26. Nakamura, R.; Nakato, Y., Primary Intermediates of oxygen photoevolution reaction on TiO_2 (rutile) particles, revealed by in situ FTIR absorptionn and photoluminescence measurements. J. Am. Chem. Soc. 2004, 126, 1290 - 1298.

27. Warren, D. S.; McQuillan, A. J., Influence of water on phonon and UV-induced IR absorptions of TiO_2 photocatalytic particles films. J. Phys. Chem. B 2004, 108, 19373 - 19379.

28. Kesselman-Truttmann, J. M.; Hug, S. J., Photodegradation of 4,4 '-bis(2-sulfostyryl)biphenyl (DSBP) on metal glides followed by in situ ATR-FTIR spectroscopy. Environ. Sci. Technol. 1999, 33, (18), 3171 - 3176.

29. Ekström, G. N.; McQuillan, A. J., In situ infrared spectroscopy of glyoxylic acid adsorptiopn and photocatalysis on TiO_2 in aqueous solution. J. Phys. Chem. B 1999, 103, 10562.

30. Araujo, P. Z.; Mendive, C. B.; Rodenas, L. A. G.; Morando, P. J.; Regazzoni, A. E.; Blesa, M. A.; Bahnemann, D., FT-IR-ATR as a tool to probe photocatalytic interfaces. Colloids and Surf. A Physicochem. Eng. Aspects 2005, 265, 73 - 80.

31. Mendive, C. B.; Bahnemann, D. W.; Blesa, M. A., Microscopic characterization of the photocatalytic oxidation of oxalic acid adsorbed on TiO_2 by FTIR-ATR. Catal. Today 2005, 101, 237 - 244.

32. Smith, R. M.; Martell, A. E., Critical Stability Constants. Plenum Press: New York, 1979.

33. Dobson, K. D.; McQuillan, A. J., In situ infrared spectroscopic analysis of the adsorption of aliphatic carboxylic acids to TiO2, ZrO2, Al2O3, and Ta2O5 from aqueous solutions. Spectrochim. Acta 1999, A 55, 1395.

34. Schmelz, M. J.; Nakagawa, I.; Mizushima, S.-I.; Quagliano, J. V., Infrared absorption spectra of inorganic Coordination complexes. XVIII Infrared Studies of malonato metal complexes. J. Am. Chem. Soc. 1959, 81, 287 - 290.

35. Hug, S.; Bahnemann, D., Infrared spectra of oxalate, malonate and succinate adsorbed on the aqueous surface of rutile, anantase and lepidocrocite measured with in sotu ATR-FTIR. J. El. Spectr. Rel. Phenom. 2006, 150, 208 - 219.

36. Deacon, G. B.; Phillips, R. J., Relationships between the carbon-oxygen stretching frequencies of carboxylato complexes and the type of carboxylate coordination. Coord. Chem. Rev. 1980, 33, 227.

37. Mehrota, R. C.; Bohra, R., Vibrational spectra. In Metal carboxylates, Academic Press: New York, 1983; pp 48-60.

38. Ferri, D.; Bürgi, T.; Baiker, A., Probing catalytic solid-liquid interfaces by attenuated total reflection infrared spectroscopy: Adsorption of carboxylic acids on alumina and titania. Helv. Chim. Acta 2002, 85, 3639-3656.

39. Rotzinger, F. P.; Kesselman-Truttmann, J. M.; Hug, S.; Shklover, V.; Grätzel, M., Structure and Vibrational Spectrum of Formate and Acetate Adsorbed from Aqueous Solution onto the TiO2 Rutile (110) Surface. J. Phys. Chem. B 2004, 108, (16), 5004 - 5017.

40. von Sonntag, C.; Schuchmann, H. P., The elucidation of peroxyl radical reactions in aqueous solution with the help of radiation-chemical methods. Angew. Chem, Int. Ed. 1991, 30, 1229 - 1253.

41. Franch, M. I.; Ayllon, J. A.; Domènech, X., Photocatalytic degradation of short-chain organic diacids. Catal. Today 2002, 76, 221 - 233.

4

Photocatalysis of Dicarboxylic Acids over TiO_2: An in Situ ATR-IR Study

4.1 Abstract

Attenuated total reflection infrared (ATR-IR) spectroscopy in a flow-through cell was used to study the photocatalytic mineralization of malonic and succinic acid over P25 TiO_2 in situ. The experiments were performed in water at concentrations of 1.5 x 10^{-4} mol/l and pH 3.5 at room temperature. Changes on the catalyst surface were observed in the time frame of a few minutes. The first step in the mineralization of malonic acid is a photo-Kolbe reaction of adsorbed malonate. Part of the resulting C_2 species is converted into oxalate and finally into carbon dioxide and part is desorbing from the surface. The branching ratio for the two pathways is 50%:50%. The mineralization reaction was also observed in the absence of dissolved oxygen however, at a slower rate. In the presence of dissolved $^{18}O_2$, labeled oxygen was incorporated into the adsorbed oxalate. A dominant pathway in the mineralization of succinic acid involves the transformation to oxalate via malonate. It is therefore proposed that a favored pathway for dicarboxylic acid mineralization is a photo-Kolbe reaction followed by the oxidation of the carbon-centered radical to a carboxylate, which corresponds to the overall formal shortening of the alkyl chain by one CH_2 unit.

4.2 Introduction

The ecologically and economically driven demand for sustainable technologies has fostered the interest in methods for abatement of pollutants in wastewater. Photocatalysis over TiO_2 has great advantages in this important field [1-3].TiO_2 is non-toxic, inert and sunlight can be used for the excitation of the semiconductor across its band-gap. The latter process generates an electron-hole pair. Oxidation is assumed to proceed via direct attack of adsorbed species on the catalytic surface by photogenerated holes or is indirectly mediated by radicals, for example $OH\bullet$, which are generated from adsorbed water, oxygen and hydroxyl groups on the catalyst surface. In this way hazardous organic compounds can completely be mineralized, i.e. converted into water and carbon dioxide.

A tremendous amount of data is available in literature on the disappearance of organic molecules from the liquid phase during illumination of the photocatalyst and on the evolution of dissolved intermediate species on the way towards complete mineralization [3-5]. The nature of the catalytic interface during illumination is much less explored. However, the analysis of the processes taking place at the catalytic interface is perhaps the most direct way to unravel the mechanism of heterogeneous catalytic reactions. Attenuated total reflection infrared

(ATR-IR) spectroscopy [6] is an ideal tool for the investigation of solid-liquid interfaces of powders [7, 8] and it has recently been applied to study heterogeneous catalytic reactions taking place at solid-liquid interfaces [9-16]. Applications of ATR-IR to phototcatalysis are still limited [17-25], but the potential of this technique has been demonstrated.

Modulation excitation spectroscopy [26] was recently combined with ATR-IR in order to study heterogeneous catalytic reactions. By periodically modulating an external parameter the catalytic system is perturbed [10]. A subsequent phase-sensitive detection selectively highlights the species that are affected by the modulated parameter and in addition leads to a significant increase in sensitivity. Up to now concentration modulation experiments in a flow-through cell were used, i.e. the periodic variation of the concentration of one reactant at the inlet of the flow-through ATR-IR reactor, to disturb the catalytic system [10, 27 28].

Here we also use light modulation to turn the photocatalytic reactions on and off and we apply this strategy to study the photocatalytic mineralization of malonic and succinic acid over TiO_2 (P25). We have recently shown that oxalic acid is an important reaction intermediate on the TiO_2 surface in the mineralization of malonic acid [24]. The modulation technique furthermore allows one to detect the final reaction product, dissolved CO_2, near the interface. Selective ^{13}C labeling of malonic acid and ^{18}O labeling of dissolved oxygen gas gives additional information about the fate of malonic acid during mineralization. The phase-sensitive detection furthermore provides evidence for the presence of carbonates on the TiO_2 surface during the photocatalysis.

4.3 Experimental Section

4.3.1 Catalyst and Chemicals

Degussa P25 TiO_2, containing 80% anatase and 20% rutile with a surface area of 51 m^2g^{-1} and average primary particle size of 21 nm, was used in the photocatalysis experiments. Malonic acid (Sigma-Aldrich, 99%), malonic-2-^{13}C acid (Aldrich, 99% ^{13}C) and succinic acid (Sigma-Aldrich, 99%) were used as received. Nitrogen (N_2, 99.995%), oxygen (O_2, 99.995%) and carbon dioxide (CO_2, 99.995%) were applied to saturate the liquids and were received from CarbaGas. Labeled oxygen $^{18}O_2$ was received from Isotec (99%).

4.3.2 Thin-film Preparation

A slurry of the catalyst powder was prepared from about 20 mg of catalysts and 25mL of water (Milli-Q, 18 MΩ cm). After sonication (ultrasonic cleaner, Branson 200) for 30 min TiO_2 thin films were formed by dropping the slurry onto a Ge internal reflection element (IRE) (52 mm x 20 mm x 1 mm; KOMLAS). Ge was found to be inert under the applied experimental conditions in contrast to ZnSe. The amount of the slurry for one coating was 0.5 mL. The solvent was allowed to evaporate, and the procedure was repeated two times. After drying for several minutes at $40^0 C$ in air, loose catalyst particles were removed by flowing water over the IRE. After drying in air the film was ready for use. From the amount of deposited TiO_2 and its density an average film thickness of $4\mu m$ was estimated. Fresh films were prepared every day and results were reproducible on different catalyst films. It should also be noted that in the absence of TiO_2 film no adsorption and no reaction was observed.

4.3.3 In situ Spectroscopy

ATR spectra were recorded with a dedicated flow-through cell, made from a Teflon piece and a fused silica plate (45 mm x 35 mm x 3 mm). The cell inlet is connected to two bubble tanks, which allows fast exchange between two different fluids. The distance between inlet and outlet is 36 mm. A flat (1 mm) viton seal defines the thickness of the fluid compartment, which has a volume of about 0.5 ml. The cell was mounted on an attachment for ATR measurements (Wilks Scientific) within the sample compartment of a Bruker Equinox-55 FTIR spectrometer equipped with a narrow-band MTC detector. Spectra were recorded at room temperature with a resolution of 4 cm^{-1}.

The solvent was saturated with gases in the two separate glass bubble tanks and was passed through the cell and over the sample by means of a peristaltic pump (Ismatec, Reglo 100) located after the cell. A flow rate of 0.2 mL/min was used. If not otherwise stated the solvent was saturated with air.

For irradiation of the sample UV light was provided by a 75W Xenon arc lamp. The UV light from the source was guided to the ATR-IR cell via two fiber bundles. The light was passed through a 5 cm water filter to remove any infrared radiation. A Schott UG 11 (50mm x 50mm x 1 mm) broadband filter from ITOS was used to remove visible light (transmission between 270 and 380 nm). An estimate based on the supplier specifications gave a power at

the sample of slightly less than 10 mW/cm^2. The experimental setup is schematically shown in Figure 4-1.

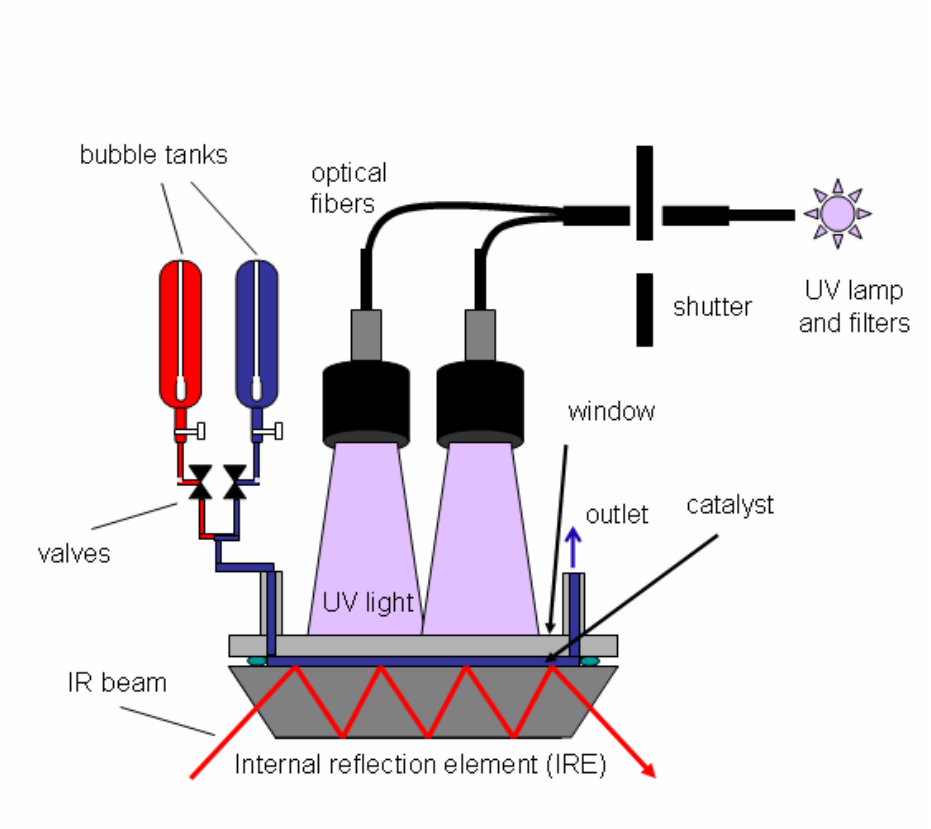

Figure 4-1: Schematic setup for in situ ATR-IR spectroscopy of photocatalytic reactions in a small volume flow-through cell.

4.3.4 Modulation Experiments and Data Acquisition

The periodic variation of an external parameter has a specific influence on the catalytic system. The concentration of all the species in the system affected by this external parameter will also change periodically at the same frequency as the stimulation. The following parameters were used for the modulation: the UV light flux, the reactant concentration (malonic acid) and the nature of the dissolved gas, oxygen – nitrogen. During one modulation period (typically 150 – 235 s) 60 infrared spectra were recorded at a sampling rate of 40 kHz or 80 kHz (4-8 scans per second), with the use of the rapid scan function of the FTIR spectrometer. Per spectrum recorded in one period typically 20 scans were averaged. Two modulation periods were performed before data acquisition was started. Infrared spectra were than averaged over five modulation periods.

Modulation experiments were performed as follows: UV light modulation was achieved using an electronic shutter (Newport model 71445). The light flux was modulated (on-off) in the presence of dissolved carboxylic acid or neat water over the TiO_2 catalyst.

For gas modulation experiments carboxylic acid solutions were saturated by nitrogen and oxygen in two separate glass bubble tanks. Nitrogen or oxygen saturated solution of the acid was than passed over the TiO_2 catalyst for 15 minutes. The modulation experiments were performed by switching two pneumatically actuated valves (see Figure 4-1).

During concentration modulation experiments two glass tanks were used, one contained neat water (pH 5.5) and the other one 1.5×10^{-4} mol/l carboxylic acid (pH 3.5), respectively. Note that at this concentration the dissolved acid is not observed in the ATR-IR spectra. Before the modulation experiment the carboxylic acid solution was flowed over the sample for 30 minutes in the dark. At this point the signals did not change anymore, indicating equilibrium. At higher solution concentrations the signals of the adsorbed species did not increase significantly, which indicates that the surface is saturated.

In all kinds of modulation experiments data acquisition and modulation were synchronized. Electrical signals generated by the FTIR spectrometer within the data acquisition loop were used to switch the valves (concentration or gas modulation) or the shutter (light modulation). Note that the modulation experiments performed here are square wave modulations. Under certain conditions the demodulated spectra can be viewed as (high quality) difference spectra between two states of the system, e.g. during light exposure and in the dark. However, if different species in the system have different kinetics then the spectra change qualitatively with demodulation phase angle. Modulation experiments are applicable only when the system response is reversible, which was verified by performing two or several identical modulation experiments one after the other. The time-resolved absorbance spectra $A(\tilde{\nu},t)$ were transformed into phase-resolved spectra using a digital phase sensitive detection (PSD) according to:

$$A_k^{\phi_k^{PSD}}(\tilde{\nu}) = \frac{2}{T}\int_0^T A(\tilde{\nu},t)\sin(k\omega t + \phi_k^{PSD})dt \qquad \text{Equation 4-1}$$

where k = 1,2,3,…determines the demodulation frequency, i.e. fundamental, first harmonic, and so on, T is the modulation period, $\tilde{\nu}$ denotes the wavenumber, ω the

stimulation frequency and ϕ_k^{PSD} the demodulation phase angle. With a set of time-resolved spectra $A(\tilde{\nu},t)$, the above equation can be evaluated for different demodulation phase angles ϕ_k^{PSD} resulting in a series of phase-resolved spectra $A_k^{\phi_k^{PSD}}$. Only spectra demodulated at the fundamental frequency (k = 1) are reported here. More detailed information on the technique can be found elsewhere [10, 29]

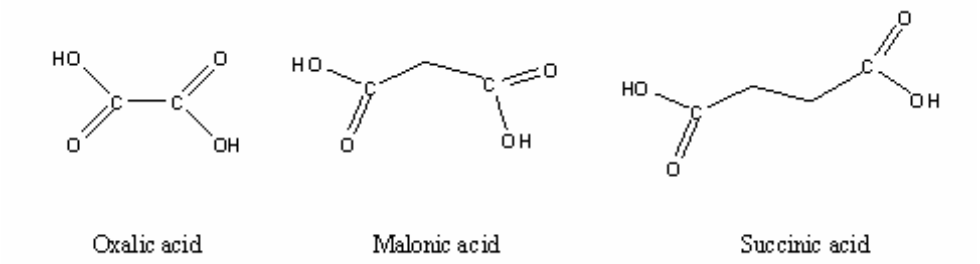

Scheme 4-1: Structure of oxalic, malonic and succinic acid

4.4 Result and Discussion

4.4.1 Major Adsorbed Species during Illumination of Adsorbed Malonate

Figure 4-2 shows ATR-IR spectra of (a) normal and (b) ^{13}C-labeled malonic adsorbed on the TiO_2 from aqueous air-saturated solution in the dark. Note that only the central carbon atom (C-2, Scheme 1) was ^{13}C-labeled. The most intense bands are assigned to carboxylate vibrations $\nu_{as}\left(COO^{-}\right)$ at 1625 and 1575 cm^{-1} and $\nu_{s}\left(COO^{-}\right)$ at 1436 and 1353 cm^{-1} [24]. As is evident from Figure 4-2 ^{13}C labeling of the central carbon atom of malonic acid has no influence on these bands, which corroborates their assignment to the two terminal carboxylate groups.

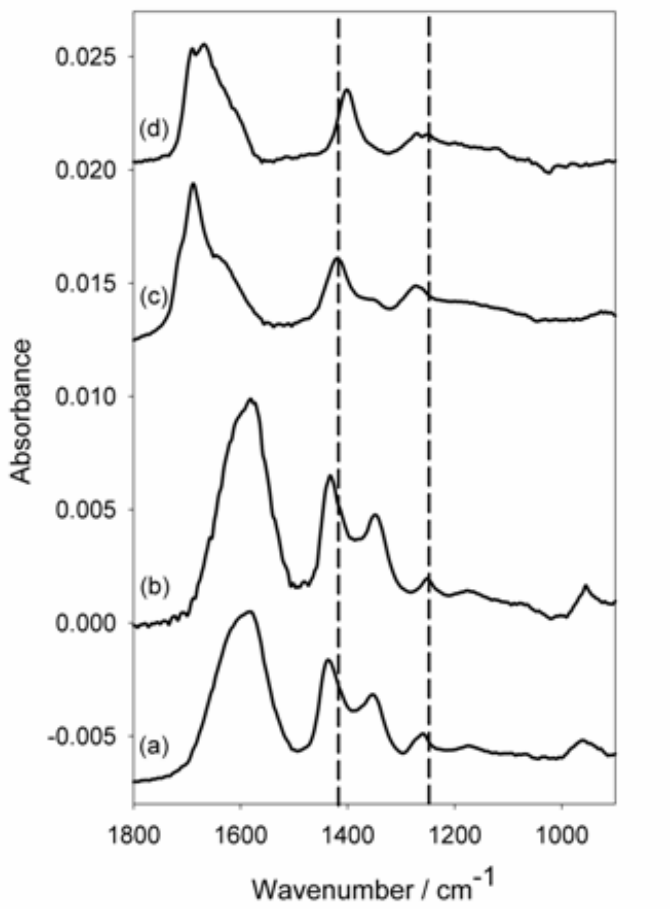

Figure 4-2: ATR-IR spectra of (a) malonic acid and (b) ^{13}C-labeled malonic acid adsorbed from aqueous solution (1.5×10^{-4} mol/l) on TiO_2 in the dark and of the corresponding adsorbed reaction product ((c), unlabeled and (d) ^{13}C-labeled) after illumination for 7 min and flowing neat water for 4 min. Malonic acid was allowed to adsorb for 30 min before recording the spectra. Note that only the central C atom of malonic acid was labeled.

In contrast the (CH_2) band at 1259 cm^{-1} shifts down to 1250 cm^{-1} upon ^{13}C labeling. The spectra provide evidence for two largely different carboxylate groups consistent with one monodentate and one bidentate/chelating adsorption geometry [24].

Spectra (c) and (d) in Figure 4-2 were obtained after illuminating adsorbed malonate and ^{13}C-labeled malonate, respectively, on TiO_2 in the presence of dissolved (labeled) malonic acid and oxygen and subsequent washing with water.

The latter procedure removes adsorbed malonic acid within 4 minutes and leaves behind oxalate species that are formed upon illumination 24. The two spectra are clearly different, in particular several bands associated with the COO vibrations shift to lower wavenumbers for oxalate formed from the ^{13}C-labeled malonate. The two bands at 1689 cm^{-1} and 1669 cm^{-1} of partly labeled oxalate are the antisymmetric and symmetric combination of two C=O stretching vibrations $\nu s(C=O)$ and $\nu as(C=O)$, respectively . The bands at 1401 cm^{-1} and 1272 cm^{-1} are associated with $\nu(C-O)$ + $\nu(C-C)$ modes [30], whereas the band at 1249 cm^{-1} can be assigned to $\nu(O-^{13}C=O)$. This clearly shows that the central (labeled) carbon atom of the malonate ends up in the oxalate, as expected. Strongly adsorbed carboxylic acids are thought to undergo a photo-Kolbe reaction, initiated by a photogenerated hole, leading to CO_2 and a carbon-centered radical [31, 32]. The latter ultimately leads to the oxalate. We have shown previously that oxalate adsorbed on TiO_2 is fast decomposed upon illumination leading to CO_2 [24].

4.4.2 Dissolved Carbon Dioxide

The enhanced sensitivity achieved by the phase-sensitive detection made the observation of dissolved CO_2 reaction product possible. Figure 4-3 shows a demodulated spectrum of a light modulation experiment. During that experiment a solution of ^{13}C-labeled malonic acid was flowed through the ATR-IR cell. The two bands at 2343 and 2277 cm^{-1} belong to dissolved CO_2 and $^{13}CO_2$, respectively, in water. The band positions are in good agreement with previous reports [33]. Note that gas-phase CO_2, due to the rotational envelope, has a distinctly different band shape from that observed in Figure 4-3.

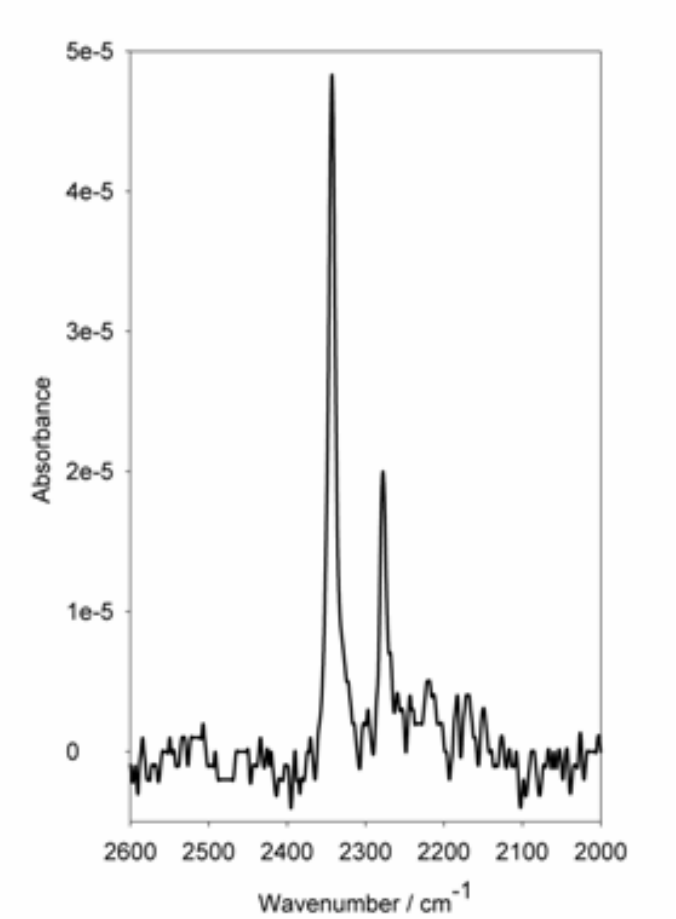

Figure 4-3: Demodulated ATR-IR spectrum of light modulation experiment where selectively ^{13}C-labeled malonic acid ($1.5x10^{-4}$ mol/l) was flowed over the TiO_2 film. During one half of the modulation period (T=155 seconds) the sample was illuminated and during the other half the sample was in the dark.

The first CO_2 molecule resulting from the photo-Kolbe reaction of selectively ^{13}C-labeled malonate, according to Scheme 4-2, is not labeled. Only in the further decomposition of the resulting C_2 compounds one of the two CO_2 molecules is ^{13}C-labeled. Complete mineralization of the selectively ^{13}C-labeled malonic acid leads to three CO_2 molecules, one of which is labeled, and hence to a $CO_2/^{13}CO_2$ ratio of 2.0. The intensity of the observed signals in Figure 4-3 is clearly different from 2.0. In fact, the ratio of the corresponding integrated signals is 3.2. One has to consider that the absorption coefficient of the asymmetric stretching vibration is affected by the isotopic labeling. A density functional theory (DFT) calculation revealed that the molar absorption coefficient ε is 5% lower for labeled $^{13}CO_2$. According to $C_{CO_2} / C_{^{13}CO_2} = A_{CO_2} / A_{^{13}CO_2} x\varepsilon^{13}CO_2 / \varepsilon\ CO_2$, where C stands for

the concentration and A for the integrated absorbance, a relative observed concentration of 3.2 * 0.95=3.04 is obtained. This shows that part of the C_2 intermediate species that are formed during the initial photo-Kolbe reaction are desorbing from the surface and are washed away in the flow through reactor before being further converted to CO_2.

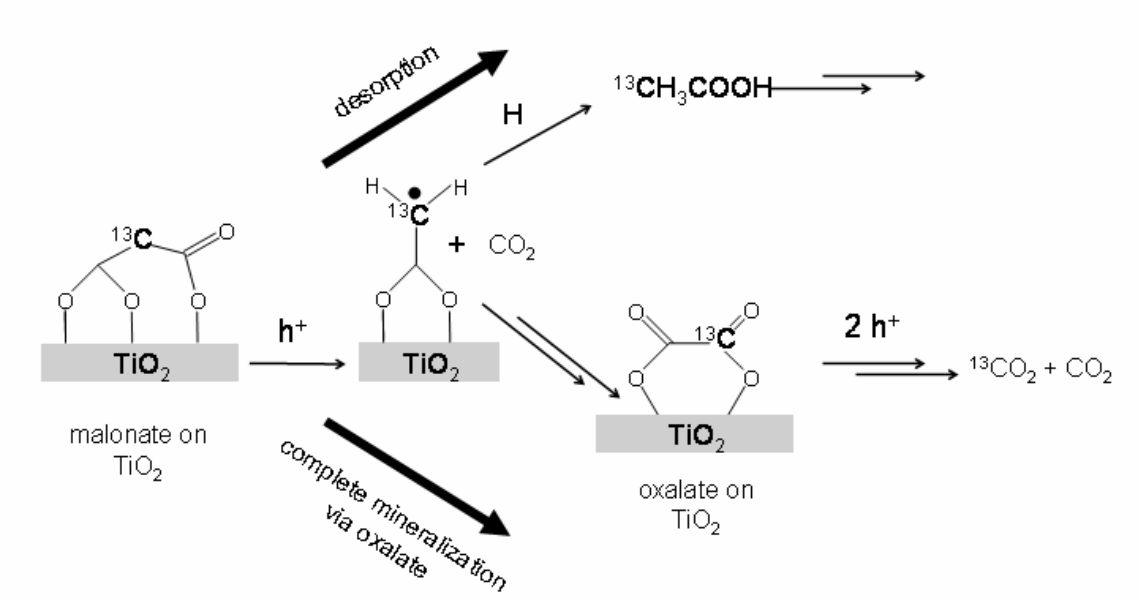

Scheme 4-2: Mechanism of photocatalytic mineralization of malonic acid over TiO_2.

The intermediates from the first photo-Kolbe reaction of malonic acid derive from a carbon centered radical (Scheme 4-2). Oxalate is one of these intermediates and it is observed by ATR-IR. It has been shown before that the oxalate does hardly desorb from the TiO_2 (P25) surface and that it mineralizes fast under the present conditions 24, which results in one labeled and one unlabeled CO_2 according to Scheme 4-2. Other intermediate species deriving from the carbon centered radical may be acetic acid (by abstraction of a hydrogen) and glycolic acid (hydroxyacetic acid), which are not observed on the TiO_2 surface by ATR-IR. Acetic acid is known to adsorb only weakly [34] and therefore desorbs from the catalyst surface before being further mineralized. Glycolic acid adsorbs more strongly on TiO_2 than acetic acid. There is no sign of it in the spectra [21], which indicates that it is not formed. From the observed relative concentration of labeled and unlabeled CO_2 one can determine the branching ratio of C_2 intermediates that are converted into oxalic acid (and completely mineralized) and acetic acid or other C_2 species that are desorbing from the surface. The limiting cases result in $CO_2/^{13}CO_2$ ratios of 2.0 for a complete mineralization (via oxalate) and of infinity for the case where no C_2 intermediates are further mineralized. The observed

$CO_2/^{13}CO_2$ ratio of 3.0 corresponds to a fraction of 50% that is completely mineralized (mainly via oxalate, yielding one labeled and two unlabeled CO_2 molecules) and 50% that is desorbing and washed away as C_2 species before being mineralized (yielding one unlabeled CO_2 molecule). In this context it is illustrative to mention the residence time in the flow-through reactor which is about 2.5 min.

The concentration of dissolved CO_2 observed while flowing a solution of 1.5×10^{-4} mol/l malonic acid over the TiO_2 film and during illumination can be quantified. In order to do so the observed absorbance (5×10^{-5} at 2343 cm^{-1}) was compared to the one measured while a solution saturated with CO_2 was flowed over the TiO_2 film (0.0136 at 2343 cm^{-1}). At 25° C about 0.035 mol/l CO_2 can be dissolved in water [35]. Only a small fraction of the dissolved CO_2, less than 1%, is converted to carbonic acid. Most of the CO_2 remains as solvated molecular CO_2 giving rise to the signal at 2343 cm^{-1}. The observed absorbance signal of 0.0136 for a saturated CO_2 solution therefore corresponds to a concentration of 0.035 mol/l and the signal (5×10^{-5}) observed during the photocatalytic mineralization to 0.035 mol/l x ($5 \times 10^{-5}/0.0136$) = 1.29×10^{-4} mol/l, which has to be compared to 1.5×10^{-4} mol/l malonic acid in solution.

Figure 4-4 shows the signal at 2343 cm^{-1} of CO_2 as a function of time during a light modulation experiment. Obviously the time-dependent signal is quite noisy. Still, useful information on mass transport out of the volume probed by the evanescent field can be obtained from this signal, assuming that CO_2 is produced only during illumination. When shutting off the light the CO_2 concentration decreases due to diffusion out of the evanescent field. The penetration depth of the latter is estimated to be 0.31 μm at 2343 cm^{-1}, as calculated from the refractive index of Ge (4.0) and the estimated effective refractive index (1.82) of the TiO_2 film in water. The latter is estimated from the refractive indices of water (1.33) and TiO_2 (2.2) by assuming a porosity of 0.5 according to $n_{eff} = (0.5(nH_2O)^2 + 0.5(nTiO_2)^2)^{1/2}$. Since the penetration depth is considerably smaller than the film thickness the observed decrease of the CO_2 signal in the dark is dominated by internal diffusion within the TiO_2 film. During illumination in the steady state the diffusion of CO_2 is compensated by photocatalytic mineralization,

$$\frac{dc}{dt} = 0 = -\left(\frac{dc}{dt}\right)_{diff} + \left(\frac{dc}{dt}\right)_{reaction} \qquad \text{Equation 4-2}$$

In the dark the term due to reaction vanishes and the observed decrease of the signal corresponds to the diffusion. A rough estimate from Figure 4-4 yields $(dc/dt)_{diff} = 3.4 \times 10^{-6}$ mol/ls, which therefore also corresponds to the estimated rate of production of CO_2 within the film during illumination. The reaction rate with respect to malonic acid is about half this value, i.e. 1.7×10^{-6} mol/ls, taking into account the branching ratio discussed above and hence the observation that on average each reacting malonic acid molecule leads to two CO_2 molecules under our conditions.

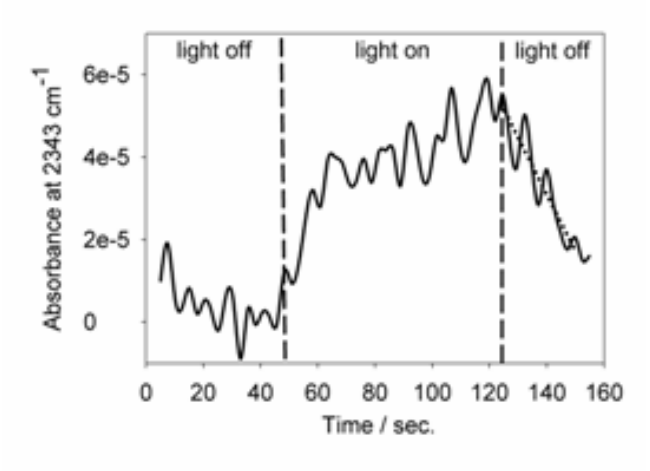

Figure 4-4 Absorbance at 2343 cm^{-1} associated with CO_2 as a function of time during a light modulation experiment (T=155 seconds, concentration of malonic acid: 1.5×10^{-4} mol/l). The dashed line was used for the calculation of the diffusion rate of CO_2 out of the catalyst film (see text).

4.4.3 Minor Adsorbed Species on TiO_2 during Illumination

Carbonate species might be expected on the TiO_2 surface during the mineralization of malonic and oxalic acid, due to the presence dissolved CO_2 and the observation that carbonate ions (HCO_3^-, CO_3^{2-}) strongly adsorb on metal oxides [36]. Furthermore, during malonic acid mineralization oxygen-rich compounds are adsorbed on the surface, which could directly convert into carbonates. No carbonates could be observed by ATR-IR during the photocatalytic mineralization of oxalic acid [25] and glyoxylic acid [21]. In fact the spectra in Figure 4-2 reveal no obvious sign of such species. However, the presence of carbonates becomes obvious from modulation experiments. Figure 4-5 (bottom) shows a demodulated spectrum for a malonic acid concentration modulation experiment.

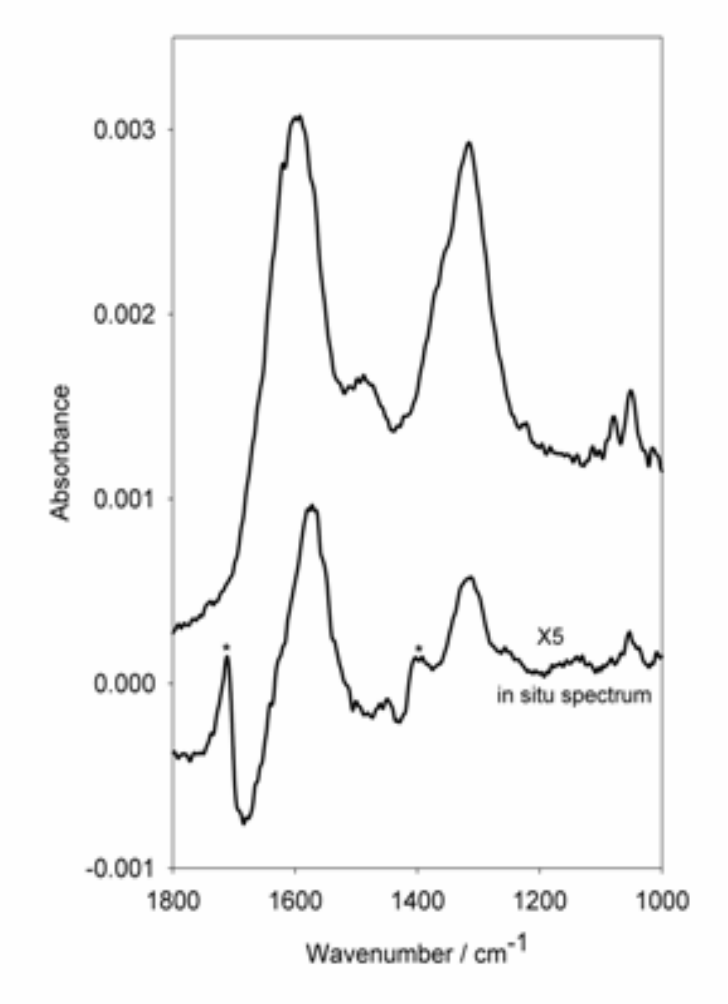

Figure 4-5: Bottom: Demodulated ATR-IR spectrum of a concentration modulation experiment (T=155 seconds, concentration of malonic acid: 1.5 x 10^{-4} mol/l). The demodulation phase angle was chosen such that the signals of adsorbed malonate vanish. Bands marked with an asterisk are associated with oxalate. Top: ATR-IR spectrum of carbonate species on the TiO_2 surface. The spectrum was measured after flowing a saturated aqueous CO_2 solution over the sample followed by flowing water.

One advantage of the digital phase-sensitive detection is that the demodulation phase angle can be chosen such that the dominant species is completely removed from the spectrum. In the present case the demodulation phase angle ϕ_k^{PSD} was adjusted to 90 degrees to get rid of the strong signals of adsorbed malonate, uncovering weaker signals of other species with different time (and therefore also phase) behavior. For comparison Figure 4-5 (top) shows an ATR-IR spectrum obtained after flowing a saturated aqueous solution of CO_2 over the TiO_2 sample and after washing with water. This leads to the formation of carbonate species on the TiO_2 surface such as monodentate and bidentate carbonates, bicarbonate and also carboxylate 37. Most importantly, the comparison in Figure 4-5 clearly shows the presence of carbonates

on the catalyst surface during the mineralization of malonic acid. The most prominent bands observed at 1598 cm^{-1} and 1317 cm^{-1} can be assigned to bidentate carbonate and monodentate carbonate, respectively [37].The positive bands in the demodulated spectrum marked with an asterisk belong to oxalate, which has a time behavior different from that of malonate. Therefore the oxalate signals do not vanish at the same demodulation phase angle as those of malonate. The sharp band at 1053 cm^{-1} is assigned to a C-O stretching vibration of a carbonate species. The negative band at 1680 cm^{-1} in the demodulated spectrum (partly overlapping with the carbonate band at 1598 cm^{-1}) may be assigned to bicarbonate species, which would mean that these bicarbonate species have different time (and phase) behavior compared to the other carbonates.

The carbonate species are stable in a flow of water at neutral pH in the dark. However, their concentration on the surface decreases upon illumination in water. Desorption or decomposition may be initiated by capturing a photo-generated hole.

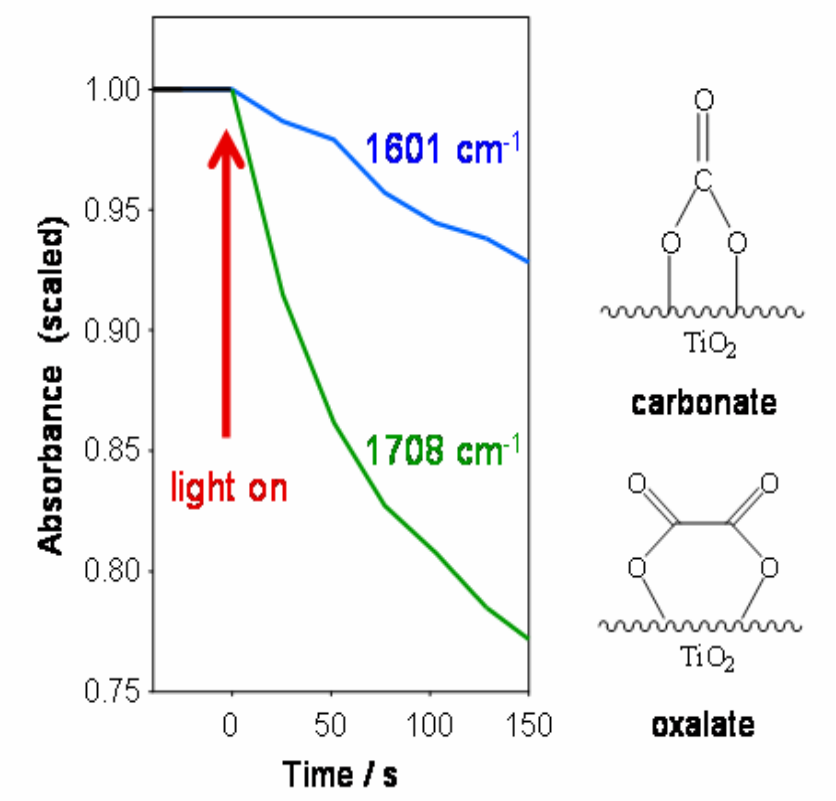

Figure 4-6: ATR-IR signals of carbonate (1601 cm^{-1}) and oxalate (1708 cm^{-1}) as a function of time during illumination. The signals were obtained from two different experiments and the signal before starting illumination was scaled to one. The surface covered by the carbonates was obtained by flowing a saturated solution of CO_2 over the sample followed by a flow of water. The surface covered by the oxalate was obtained by flowing a malonic acid solution saturated with oxygen over the sample during illumination followed by a flow of water in the dark.

Figure 4-6 shows the decrease of the signals at 1601 cm^{-1} and 1708 cm^{-1} associated with carbonate ions and oxalate species, respectively. The two signals measured before illumination were normalized to one. Note that the two curves were obtained from two separate experiments where the two species, carbonates and oxalate, were selectively prepared on the surface before illumination. Clearly carbonate species disappear considerably slower than oxalate.

The concentration of carbonate species on the TiO_2 surface is not large during illumination and it is therefore not observed in "normal" time-resolved experiments.

In the demodulated spectrum shown in Figure 4-5 the carbonate signals are about ten times smaller than in the upper spectrum in Figure 4-5, the latter corresponding to a surface saturated with carbonates. Hence, the coverage of carbonates during illumination under our conditions is on the order of 10% of a full coverage. Still, the carbonates slow down the mineralization process due to competition for adsorption sites and for photo-generated holes. The comparison in Figure 4-5 also shows that the relative intensity of the signals associated with mono- and bidentate carbonate is different for the two experiments, which indicates that the relative ratio of monodentate and bidentate carbonates is not the same when formed by adsorption of CO_2 on a clean TiO_2 surface and when formed during the photocatalysis. This may be due to the blocking of specific sites by the malonate and oxalate species in the latter case.

4.4.4 The Role of Oxygen

For the total mineralization of malonic acid according to oxygen has to be provided. In the above equation this corresponds formally to two oxygen molecules, but the source of oxygen remains to be determined.

$$C_3H_4O_4 + 2O_2 \xrightarrow[TiO_2]{h\nu} 3CO_2 + 2H_2O$$

Several possibilities are conceivable: The oxygen may directly come from dissolved O_2 molecules. In fact, previous reports on photocatalysis over TiO_2 propose reactive oxygen species deriving from O_2 as important intermediates responsible for the oxidation of organic pollutants [3, 38]. In aqueous environment the incorporated oxygen may also originate from water. For example the carbon centered radical may pick up OH from water. Finally, the TiO_2 surface may serve as an oxygen source. In this case, the oxygen consumed needs to be

regenerated either from water or dissolved O_2. In order to shed some light on the role of oxygen labeled $^{18}O_2$ was used and furthermore modulation experiments were performed where the dissolved gas, O_2 and N_2, served as the stimulation.

Figure 4-7 shows ATR-IR spectra of oxalate. In these experiments the TiO_2 sample was illuminated while flowing solutions of malonic acid saturated with oxygen through the cell. Afterwards neat water was flowed over the sample in order to remove remaining malonic acid thus leaving oxalate on the surface. The difference between the two spectra shown in Figure 4-7 is the type of oxygen used in the corresponding experiment. For the top (bottom) spectrum labeled $^{18}O_2$ (unlabeled O_2) was used. Clearly in the upper spectrum some bands are shifted to lower wavenumbers. The band of normal oxalate at 1421 cm^{-1} shifts down to 1400 cm^{-1} and the broad band at 1633 cm^{-1} shifts down to 1590 cm^{-1}. These bands are associated with C-O vibrations [25] and the shifts therefore show that ^{18}O from dissolved oxygen is incorporated in the adsorbed oxalate.

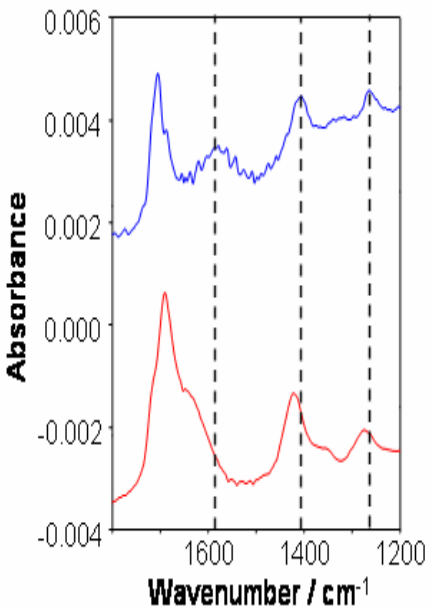

Figure 4-7: ATR-IR spectra of oxalate on TiO_2. The spectra were obtained by flowing a malonic acid solution saturated with oxygen over the sample during illumination followed by a flow of water in the dark. For the bottom spectrum normal oxygen (O_2) was used. For the top spectrum labeled oxygen ($^{18}O_2$) was used. Vertical lines are used to guide the eye.

Figure 4-7 indicates that reactive species formed from oxygen (electron acceptor) can directly react with the adsorbed C_2 species, i.e. the carbon centered radical or the species resulting from it. Interestingly, there was no clear sign in the spectra of ^{18}O labeled CO_2 (data not shown). We attribute this only partly to a low signal to noise ratio. More

importantly, oxygen exchange between CO_2 and the TiO_2 surface is possible [39]. Sato showed that oxygen isotope exchange among water, CO_2 and surface hydroxyls occurs easily on TiO_2 even in the dark[40]. This means that the labeled oxygen found in the oxalate (Figure 4-7) can be exchanged with normal oxygen once adsorbed CO_2 is formed and therefore the dissolved CO_2 is mostly unlabeled due to the large excess of normal oxygen in the system.

Figure 4-8 shows an ATR-IR spectrum recorded while flowing a solution of malonic acid saturated with nitrogen over the TiO_2 sample during illumination. Figure 4-8 reveals that oxalate can also be formed from malonate upon illumination in the absence of oxygen. This finding shows that oxygen from a different source than dissolved oxygen, i.e. from water or the TiO_2 surface, can also be incorporated into the oxalate.

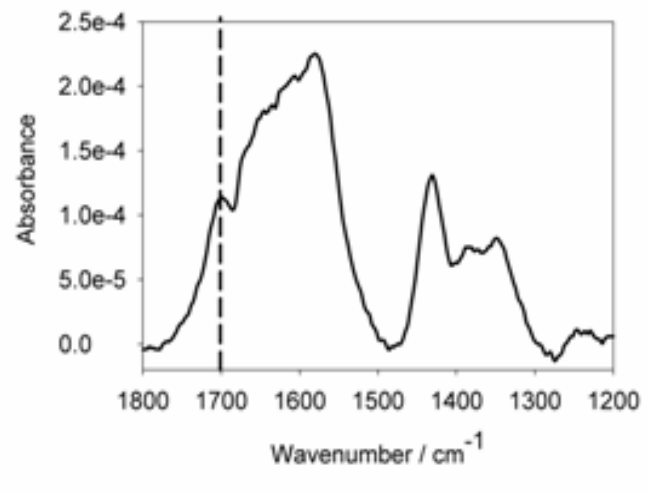

Figure 4-8 ATR-IR spectrum obtained while flowing a solution of malonic acid saturated with nitrogen over the TiO_2 sample during illumination. The vertical line indicates the strongest oxalate band.

Dissolved oxygen not only acts as one possible source of oxygen atoms but also has a pronounced influence on the reaction rate. Figure 4-9 shows the signal at 1700 cm^{-1} associated with the oxalate on the TiO_2 surface as a function of time during one modulation period.

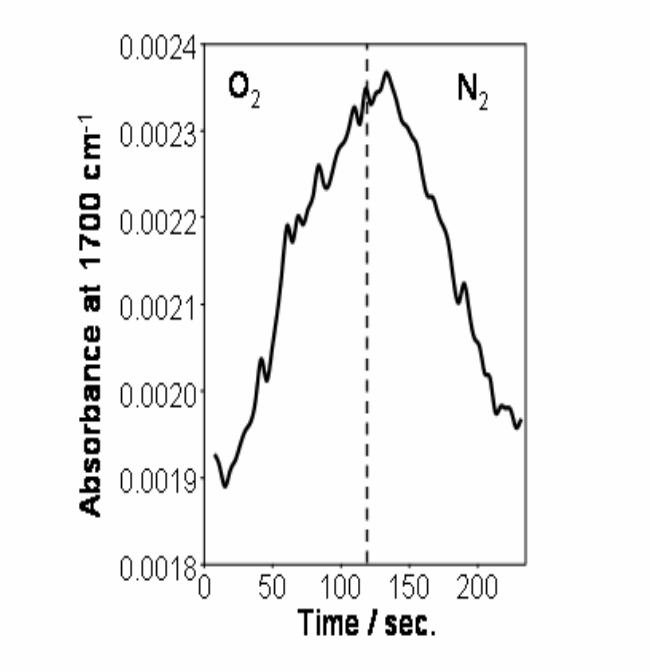

Figure 4-9: ATR-IR signal at 1700 cm^{-1} associated with oxalate as a function of time during a modulation experiment (T=232 seconds). In this experiment a solution of malonic acid (1.5×10^{-4} mol/l) was flowed over the TiO_2 sample during illumination. The stimulation parameter was the dissolved gas, which was O_2 during the first half period and N_2 during the second half period. The vertical line indicates the time at which the dissolved gas was changed from O_2 to N_2.

In this experiment the dissolved gas was modulated between N_2 and O_2. The coverage of oxalate is clearly modulated showing an increase in oxygen and a decrease in nitrogen. The rates of the various reaction steps can be influenced by the dissolved oxygen mainly in two ways. Oxygen acts as an acceptor for the electron of the photo-generated electron-hole pair. The resulting reactive species can directly attack adsorbed molecules, as is suggested by the $^{18}O_2$ experiments (Figure 4-7). The acceptance of the electron furthermore leads to an increased life-time of the photo-generated hole, and therefore to an increased reaction rate.

4.4.5 Mineralization of Succinic acid

Figure 4-10 shows several ATR-IR spectra related to the mineralization of succinic acid over TiO_2. Trace (a) shows a spectrum of succinic acid adsorbed on TiO_2 in the dark. The two subsequent spectra (b) and (c) were recorded while flowing succinic acid over the TiO_2 film during illumination. The next spectrum (d) represents the difference between two spectra recorded at the very beginning of illumination. Finally, the two top traces (e) and (f) represent the spectra of adsorbed malonate and oxalate on TiO_2 for comparison.

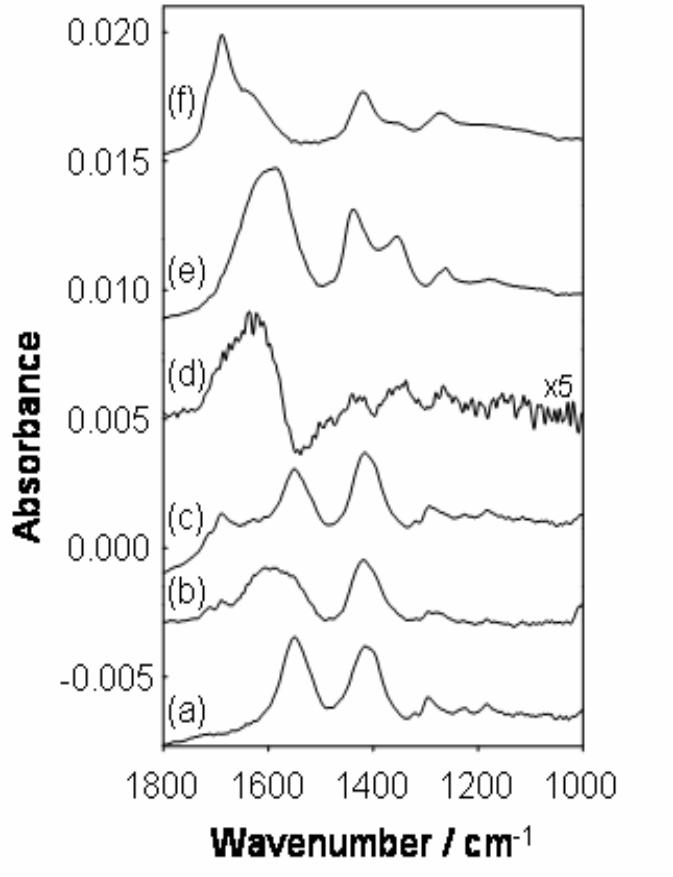

Figure 4-10: ATR-IR spectra related to succinic acid mineralization. Spectrum (a) was obtained while flowing succinic acid (1.5×10^{-4} mol/l) over the sample in the dark (for 30 min). Spectra (b) and (c) were measured during illumination, spectrum (b) 11 min and spectrum (c) 37 min after turning the light on. Spectrum (d) represents the spectral differences observed during the first 83 seconds of illumination. Spectra (e) and (f) are the spectra of adsorbed malonate and oxalate for comparison.

The spectrum of succinic acid adsorbed in the dark from water is characterized by two strong bands at 1550 and 1417 cm^{-1}, which can be assigned to antisymmetric and symmetric COO^- stretching vibrations, respectively. This shows that the molecule exists as succinate on the TiO_2 surface. The spectrum is significantly different from the one of malonate on TiO_2. The latter shows two distinct bands for the symmetric and two bands for the antisymmetric COO^- stretching vibrations, whereas the succinate spectrum is characterized by only one band for the symmetric and one for the antisymmeteric COO^- stretching vibrations. This indicates that the two carboxylate groups in the succinate are equivalent. Based on the energy difference Δ between the two carboxylate stretching modes an adsorption geometry can be proposed [41]. Because Δ is smaller for the adsorbed succinate than for the succinate in solution chelating and/or bridging coordination of both COO groups is indicated.

Upon illumination a broad band centered around 1600 cm^{-1} is growing in fast (Fig. 10, spectrum (b)) and becomes weaker again later on (Figure 4-10, spectrum (c)). Simultaneously, two signals are steadily growing in at 1708 and 1690 cm^{-1}, which can be assigned to oxalate. Note that the oxalate bands reveal a different kinetics from the band at 1600 cm^{-1}. The difference spectrum in Figure 4-10 (spectrum (d)) was recorded at the very beginning of illumination. In this spectrum the two most prominent bands of succinate appear negative, due to the disappearance of succinate from the surface. Positive bands are also observed associated with species appearing on the surface upon illumination. Comparison with the two spectra shown on top in Figure 4-10 reveals that these positive bands belong to malonate and oxalate. From the kinetics of appearance and disappearance of these bands, as discussed above, it can be concluded that succinate is transformed to malonate and then to oxalate. Hence, it seems that one dominant pathway for the photocatalytic mineralization of aliphatic dicarboxylic acids on TiO_2 is the consecutive shortening of the hydrocarbon chain by formal CH_2 elimination. Each of these formal steps is initiated by a photo-Kolbe reaction, which results in the elimination of CO_2, and subsequent steps that lead from the carbon-centered radical to a carboxylate.

4.5 Conclusion

Attenuated total reflection infrared (ATR-IR) spectroscopy in combination with modulation excitation spectroscopy (MES) and isotope labeling was used to study the mineralization of malonic acid over P25 TiO_2 photocatalyst. The enhancement of sensitivity achieved by the phase-sensitive detection of periodically varying signals made the detection of dissolved CO_2 possible. From the relative signals of CO_2 and $^{13}CO_2$ observed during the mineralization of selectively labeled malonic acid it was determined that 50% of the adsorbed malonate is completely converted to CO_2 (via oxalate), whereas 50% of the C_2 intermediates generated after the first photo-Kolbe reaction are desorbing from the surface and washed away without being oxidized. Modulation experiments furthermore revealed the presence of carbonates on the TiO_2 surface during illumination. Experiments in the presence of labeled $^{18}O_2$ showed that the ^{18}O is incorporated into the adsorbed oxalate. On the other hand oxalate was also formed from malonate upon illumination in the absence of dissolved oxygen. This shows that at least two different pathways lead from the carbon-centered radical to the oxalate after the first photo-Kolbe reaction. These pathways are characterized by different oxygen

sources, dissolved oxygen and possibly oxygen from water. Dissolved oxygen furthermore influences the rates of the different reaction steps. It acts as an electron acceptor and accelerates the photocatalytic reactions by preventing electron-hole recombination.

References

1. Wang, R.; Hashimoto, K.; Chikuni, M.; Kojima, E.; Kitamura, A.; Shimohigashi, M.; Watanabe, T., Nature 1997, 388, 431.
2. Asahi, R.; Morikawa, T.; Ohwaki, T.; Aoki, K.; Taga, Y., Visible-light photocatalysis in nitrogen-doped titanium oxides. Science 2001, 293, 269-271.
3. Hoffmann, M. R.; Martin, S. T.; Choi, W. Y.; Bahnemann, D. W., Environmental applications of smiconductor photocatalysis. Chem. Rev. 1995, 95, 69-96.
4. Calza, P.; Pelizzetti, E.; Minero, C., The fate of organic nitrogen in photocatalysis: an overview. Journal of Applied Electrochemistry 2005, 35, (7), 665-673.
5. Carp, O.; Huisman, C. L.; Reller, A., Photoinduced reactivity of titanium dioxide. Progress in Solid State Chemistry 2004, 32, (1-2), 33-177.
6. Harrick, N. J., Internal reflection spectroscopy. Interscience Publishers: New York, 1967.
7. Tejedor-Tejedor, M. I.; Yost, E. C.; Anderson, M. A., Characterization of benzoic and phenolic complexes at the goethite/aqueous interface using cylindrical internal reflection Fourier transform infrared spectroscopy. Part 1. Methodology. Langmuir 1990, 6, 979.
8. Hug, S. J.; Sulzberger, B., In situ Fourier transform infrared spectroscopic evidence for the formation of several different surface complexes of oxalate on TiO2 in the aqueous phase. Langmuir 1994, 10, 3587.
9. Bürgi, T.; Wirz, R.; Baiker, A., In situ attenuated total reflection infrared spectroscopy: A sensitive tool for the investigation of reduction-oxidation processes on heterogeneous Pd metal catalysts. J. Phys. Chem. B 2003, 107, 6774-6781.
10. Bürgi, T.; Baiker, A., In situ infrared spectroscopy of catalytic solid-liquid interfaces using phase-sensitive detection: Enantioselective Hydrogenation of a pyrone over Pd/TiO2. J. Phys. Chem. B 2002, 106, 10649-10658.
11. Ebbesen, S. D.; Mojet, B. L.; Lefferts, L., CO Adsorption and Oxidation at the Catalyst-Water Interface: An Investigation by Attenuated Total Reflection Infrared Spectroscopy. Langmuir 2006, 22, (3), 1079 - 1085.
12. Mul, G.; Hamminga, G. M.; Moulijn, J. A., Operando ATR-FTIR analysis of liquid-phase catalytuc reactions: can heterogeneous catalysts be observed? Vib. Spectr. 2004, 34, 109-121.
13. Ortiz-Hernandez, I.; Williams, C., In situ investigation of solid-liquid catalytic interfaces by attenuated total reflection infrared spectroscopy. Langmuir 2003, 19, 2956-2962.

14. He, R.; Davafa, R. R.; Dumesic, J. A., In situ ATR-IR spectroscopic and reaction kinetics studies of water-gas shift and methanol reforming on Pt/Al2O3 catalysts in vapor and liquid phases. J. Phys. Chem. B 2005, 109, (7), 2810 - 2820.

15. Bürgi, T.; Baiker, A., Attenuated total reflection infrared spectroscopy of solid catalysts functionong in the presence of liquid-phase reactants. Advances in Catalysis 2006, 50, 228-283.

16. Ferri, D.; Mondelli, C.; Krumeich, F.; Baiker, A., Discrimination of active palladium sites in catalytic liquid-phase oxidation of benzyl alcohol. Journal of Physical Chemistry B 2006, 110, (46), 22982-22986.

17. Nakamura, R.; Imanishi, A.; Murakoshi, K.; Nakato, Y., In situ FTIR studies of primary intermediates of photocatalytic reactions on nanocrystalline TiO2 films in contact with aqueous solutions. J. Am. Chem. Soc. 2003, 125, 7443 - 7450.

18. Nakamura, R.; Nakato, Y., Primary Intermediates of oxygen photoevolution reaction on TiO2 (rutile) particles, revealed by in situ FTIR absorptionn and photoluminescence measurements. J. Am. Chem. Soc. 2004, 126, 1290 - 1298.

19. Warren, D. S.; McQuillan, A. J., Influence of water on phonon and UV-induced IR absorptions of TiO2 photocatalytic particles films. J. Phys. Chem. B 2004, 108, 19373 - 19379.

20. Kesselman-Truttmann, J. M.; Hug, S. J., Photodegradation of 4,4 '-bis(2-sulfostyryl)biphenyl (DSBP) on metal glides followed by in situ ATR-FTIR spectroscopy. Environ. Sci. Technol. 1999, 33, (18), 3171 - 3176.

21. Ekström, G. N.; McQuillan, A. J., In situ infrared spectroscopy of glyoxylic acid adsorptiopn and photocatalysis on TiO2 in aqueous solution. J. Phys. Chem. B 1999, 103, 10562.

22. Araujo, P. Z.; Mendive, C. B.; Rodenas, L. A. G.; Morando, P. J.; Regazzoni, A. E.; Blesa, M. A.; Bahnemann, D., FT-IR-ATR as a tool to probe photocatalytic interfaces. Colloids and Surf. A Physicochem. Eng. Aspects 2005, 265, 73 - 80.

23. Mendive, C. B.; Bahnemann, D. W.; Blesa, M. A., Microscopic characterization of the photocatalytic oxidation of oxalic acid adsorbed on TiO2 by FTIR-ATR. Catal. Today 2005, 101, 237 - 244.

24. Dolamic, I.; Bürgi, T., Photoassisted decomposition of malonic acid on TiO2 studied by in situ attenuated total reflection infrared spectroscopy. J. Phys. Chem. B 2006, 110, 14898-14904.

25. Mendive, C. B.; Bredow, T.; Blesa, M. A.; Bahnemann, D. W., ATR-FTIR measurements and quantum chemical calculations concerning the adsorption and photoreaction of oxalic acid on TiO2. Phys. Chem. Chem. Phys. 2006, 8, 3232-3247.

26. Baurecht, D.; Fringeli, U. P., Quantitative modulated excitation Fourier transform infrared spectroscopy. Rev. Sci. Instr. 2001, 72, (10), 3782-3792.

27. Gisler, A.; Bürgi, T.; Baiker, A., Epoxidation of cyclic allylic alcohols on titania-silica aerogels studied by attenuated total reflection infrared and modulation spectroscopy. J. Catal. 2004, 222, (2), 461-469.

28. Bürgi, T.; Bieri, M., Time-resolved in-situ ATR spectroscopy of 2-propanol oxidation over Pd/Al2O3: Evidence for 2-propoxide intermediate. J. Phys. Chem. B 2004, 108, (35), 13364-13369.

29. Urakawa, A.; Wirz, R.; Bürgi, T.; Baiker, A., An ATR-IR flow-through cell for concentration modulation excitation spectroscopy: diffusion experiments and simulation. J. Phys. Chem. B 2003, 107, 13061.

30. Hug, S.; Bahnemann, D., Infrared spectra of oxalate, malonate and succinate adsorbed on the aqueous surface of rutile, anantase and lepidocrocite measured with in sotu ATR-FTIR. J. El. Spectr. Rel. Phenom. 2006, 150, 208 - 219.

31. Sakata, T.; Kawai, T.; Hashimoto, K., Heterogeneous Photocatalytic Reactions of Organic Acids and Water. New Reaction Paths besides the Photo-Kolbe Reaction. J. Phys. Chem. 1984, 88, 2344-2350.

32. Kraeutler, B.; Bard, A. J., Photoelectrosynthesis of Ethane from Acetate Ion at an N-Type TiO2 Electrode - Photo-Kolbe Reaction. Journal of the American Chemical Society 1977, 99, (23), 7729-7731.

33. Falk, M.; Miller, A. G., Infrared spectrum of carbon dioxide in aqueous solution. Vib. Spectr. 1992, 4, 105-108.

34. Rotzinger, F. P.; Kesselman-Truttmann, J. M.; Hug, S.; Shklover, V.; Grätzel, M., Structure and Vibrational Spectrum of Formate and Acetate Adsorbed from Aqueous Solution onto the TiO2 Rutile (110) Surface. J. Phys. Chem. B 2004, 108, (16), 5004 - 5017.

35. Physical and Engineering Data. January 1978 ed.; Shell Internationale Petroleum Maatschappij BV: The Hague, 1978.

36. Gu, W.; Tripp, C. P., Reaction of Silanes in Supercritical CO2 with TiO2 and Al2O3. Langmuir 2006, 22, 5748-5752.

37. Davidov, A., Molecular Spectroscopy of Oxide Catalyst Surfaces. John Wiley: West Sussex, 2003.

38. Serpone, N.; Nakaoka, Y.; Nishino, J.; Nosaka, Y., In Photocatalytic purification and treatment of water and air, Ollis, D. F.; Al-Ekabi, H., Eds. Elsevier: Amsterdam, 1993.

39. Hattori, H., Heterogeneous Basic Catalysis. Chemical Reviews 1995, 95, (3), 537-558.

40. Sato, S., Hydrogen and oxygen isotope exchange reactions over illuminated and nonilluminated TiO2. J. Chem. Phys. 1987, 91, 2895-2897.

41. Deacon, G. B.; Phillips, R. J., Relationships between the carbon-oxygen stretching frequencies of carboxylato complexes and the type of carboxylate coordination. Coord. Chem. Rev. 1980, 33, 227.

5

Adsorption of Thiol-Protected Gold Nanoparticles on TiO_2 and Their Behavior under UV Light Irradiation

5.1 Abstract

A combination of in situ attenuated total reflection infrared (ATR-IR) spectroscopy, UV-vis spectroscopy and transmission electron microscopy was used to study the adsorption of thiol-protected gold nanoparticcles on TiO_2 films and the behaviour of the resulting composite films upon UV irradiation. The gold nanoparticles were covered by charged thiols (N-acetyl-L-cysteine and L-glutathione) and had a mean core diameter of about 1 nm. The TiO_2 film was prepared by deposition of a slurry of TiO_2 nanoparticle with a particles size of 21 nm. The combination of the two spectroscopic techniques showed that the adsorption of the gold nanoparticles onto the TiO_2 films is significantly limited by intra film diffusion. Upon illumination the IR spectra revealed the removal of the adsorbed thiolates and the appearance of sulfates. These species were also observed when illuminating N-acetyl-L-cysteine adsorbed on TiO_2, i.e. in the absence of gold. In the latter case oxalate was observed in large quantity on the TiO_2 surface, in contrast to the illumination of the N-acetyl-L-cysteine-protected gold particles. This indicates a different pathway for the decomposition of the adsorbed thiol when adsorbed on the gold or directly on the TiO_2 surface. In situ UV-vis spectroscopy also shows the formation of larger particles upon illumination, which is confirmed by transmission electron microscopy.

5.2 Introduction

Materials composed of gold nanoparticles and a semi-conducting support such as TiO_2 are considered for various applications for example in surface patterning,[1] catalysis,[2-4] photocatalysis[5] and photovoltaic cells.[6] In the latter case the excitation of the semiconductor-metal nanocomposite by (sun-) light induces electron transfer processes that may be used for solar energy conversion,[7] i.e. for the production of hydrogen by water splitting. Activity and selectivity of such materials and catalysts strongly depend on the size of the gold particles.[8]

Different methods were considered in the past to prepare Au-TiO_2 catalyst materials such as metal ion impregnation and deposition-precipitation followed by drying, calcination and reduction.[9] During such procedures the Au particles advantages. The uneven precursor-solution loading due to gravitational less or clusters are formed directly on the support. However, these methods have some diforces leads to polydispersity of the resulting metal particles. The necessary thermal treatment furthermore results in severe agglomeration problems and may even cause chemical modification of the support through ionic diffusion.[5]

Therefore alternative methods for catalyst preparation are highly desirable. A different route relates to the preparation of metallic Au^0 particles in solution and subsequent deposition on the TiO_2[5]. This allows the better control of size and size distribution of the particles. Very small particles can be prepared by methods that are based on passivating ligands such as phosphines[10] and thiols.[11] These ligands prevent the particles from agglomeration in solution. Once the gold particles are deposited on the TiO_2 the passivating ligands can be removed by calcination of the material. It was for example shown that calcination at 300 °C leads to the removal of thiols as evidenced by X-ray photoelectron spectroscopy (XPS).[4] Calcination was also shown to lead to a moderate increase in the average particles size from 3.4 to 4.6 nm. The resulting material was active in the epoxidation of propylene.

The release of thiolates from gold surfaces can be achieved not only by thermally breaking the S-Au bond. Reductive desorption of sulfur[12] and thiolate oxidation by I2 [13] and reactive oxygen species[14] was also shown. It was furthermore reported that photogenerated radicals can efficiently liberate alkanethiolate ligands in a solution of monolayer-protected gold nanoparticles.[15] The exposure of alkanethiolate self-assembled monolayers (SAM) on gold surfaces to UV light (254 nm) leads to the oxidation of the thiolate to the sulfonate,[16] which can be used to pattern SAMs. Similarly, oxidized sulphur species were reported after exposing a film of thiol-stabilized gold nanoparticles to UV-light. Such treatment leads to the coagulation of the gold particles, which enabled the convenient fabrication of gold structures on surfaces.[1] Thiolate removal from gold particles under UV irradiation was assigned to plasmon photoelectrochemistry, i.e. to charge separation and redox reactions.[17] Furthermore, TiO_2 itself is a photocatalyst, which can be used to mineralize organic compounds.[18]

The removal of thiolates from gold surfaces and nanoparticles by light is an important process for the preparation of tailored catalyst materials and for the fabrication of patterned surfaces. However, the occurring processes are not very well understood due to the lack of direct molecular level information from the respective interfaces during irradiation, which hinders the more rational design of (catalyst) materials. Here we use in situ UV-vis and attenuated total reflection infrared (ATR-IR)[19, 20] spectroscopy to study the adsorption of charged gold nanoparticles from aqueous solution on TiO_2 particle films and the processes occurring during subsequent irradiation.

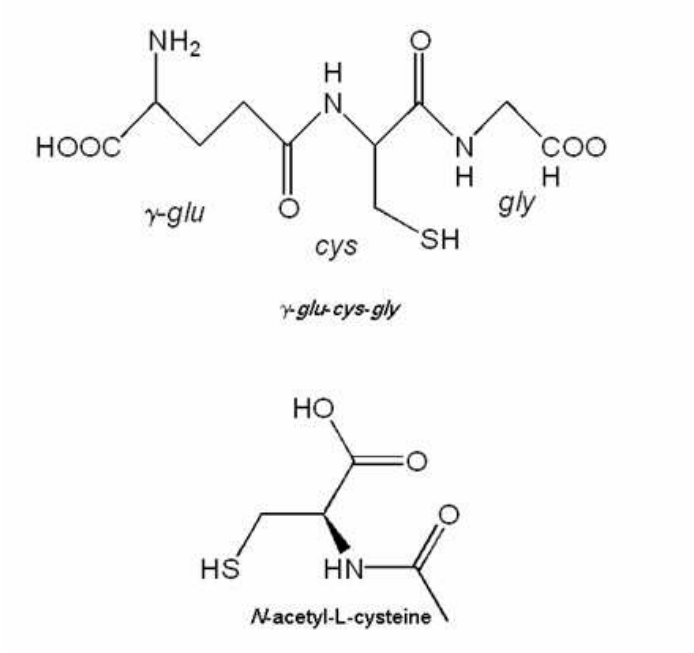

Scheme 5-1: Structure of N-acetyl-L-cysteine and L-glutathione.

5.3 Experimental Section

5.3.1 Materials

Degussa P25 TiO_2 with a surface area of 51 m^2 g^{-1}, average primary particle size of 21 nm and a tapped density of approximately 130 g/l was used. The preparation of the gold particles of about 1 nm core size used in this study was described in detail in previous reports.[21, 22] Briefly 1.01 mmol (400 mg) of tetrachloroauric acid and 4.06 mmol N-acetyl-L-cysteine (glutathione) were dissolved in 200 ml of 6:1 methanol:acetic acid, giving a red solution, which rapidly turned into a cloudy white suspension. After 15 minutes a freshly prepared aqueous $NaBH_4$ solution (70 ml, 2.13 mol/l) was slowly added under vigorous stirring. After 90 min of additional stirring, the resulting solution was filtered using 0.2 μm PTFE membranes (Millipore) to remove precipitates and subsequently evaporated under vacuum to near dryness. The nanoparticles were purified in two steps. The first one consisted in a series of precipitations with ethanol and filtration using 0.2 μm PTFE membranes. The removal of the remaining unreacted thiol or disulfide was finally completed by dialysis (Spectra/Por CE, molecular weight cut-off MWCO = 3'500). Particles were dissolved in 30 ml water and loaded into a membrane, which was then placed in a 2 L beaker of water and

slowly stirred. The water was changed every 10 hours over the course of 96 hours. The black solution was evaporated under vacuum at $T \leq 40°$ C to give a black powder.

(HCl 0.1 M Carlo Erba) was used to adjust the pH. N-Acetyl-L-cysteine (NAC, Scheme 5-1, Sigma-Aldrich > 99%) and glutathione (GSH, Scheme 5-1, Sigma-Aldrich > 99%) were used as received. All other reagents were analytical grade and used as received. Milli-Q water (18 MΩ cm) was used in all experiments.

5.3.2 Thin Film Preparation

A slurry was prepared from about 20 mg P25 TiO_2 and 25 ml water. After sonication (Ultrasonic cleaner, Branson 200) for 30 min TiO_2 thin-films were formed by dropping the slurry onto a Ge internal reflection element (IRE, 52 mm x 20mm x 1 mm; KOMLAS). The amount of slurry for one coating was typically about 0.5 ml. The solvent was allowed to evaporate, and the procedure was repeated several times, which allows one to adjust the film thickness. After drying for several minutes at 40°C in air, loose catalyst particles were removed by flowing water over the IRE. After drying in the air the film was ready for use. From the amount of deposited TiO_2 and its density an average film thickness was estimated. Films of about 4 μm and 70 μm thickness were prepared. Note that for dense TiO_2 films prepared by a sol-gel method UV light has a penetration depth of a few micrometers.[23] However, light incident on a powder can penetrate substantially deeper than that by diffuse reflection. Direct evidence that the UV light penetrates the TiO_2 films as used here stems from initial experiments with ZnSe internal reflection elements. We have noticed that the UV lamp induces a chemical reaction on the surface of the ZnSe, which results in a colour change from yellow to orange. (That is why Ge elements were used in this work.) This colour change was also observed with the TiO_2 film present, which shows that the UV light reaches the IRE surface through the TiO_2 film.

5.3.3 Methods

In situ ATR-IR spectra were recorded with two different flow-through cells. The first one was used for combined ATR-IR and UV-vis spectroscopy.[24] The second one was used for ATR-IR spectroscopy during UV irradiation.[25] The latter cell was made from a Teflon® piece, a fused silica plate (45 x 35 x 3 mm) with holes for in- and outlet (36 mm apart), and a flat

(1 mm) Viton® seal. The cell has a volume of 500 µl. The cell for combined ATR-IR and UV-vis spectroscopy was made of Teflon® with a volume of 77 µl and a gap between IRE and the surface of the cell of 250 µm. The ATR cell is equipped with a fused silica window (5 mm diameter and 3 mm thickness), which allows to record simultaneously UV-vis and ATR-IR spectra. The distance between inlet and outlet of the ATR cell is 36 mm and the window for UV-vis spectroscopy is positioned 10 mm from the outlet. A UV-vis probe was positioned in front of the window perpendicular to the IRE surface, such that the end of the probe was located approximately 4 mm above the catalyst layer. The probe (AVANTES) consists of six fibers that guide the light from a deuterium halogen source to the sample and one fiber that guides the reflected light to a UV-vis spectrometer (Avantes, 2.4 nm resolution) equipped with a 2024 pixel CCD detector array. Typical integration time for one spectrum was 100 ms.

For measurements the cell was mounted on an attachment for ATR measurements within the sample compartment of a Bruker Equinox-55 FTIR spectrometer equipped with narrow-band MCT detector. Spectra were recorded at 4 cm^{-1}. The nanoparticle solution was passed through the cell and over the TiO_2 film at a flow rate of 0.2 ml min^{-1} by means of a peristaltic pump (Ismatec, Reglo 100). Some experiments were performed in the absence of oxygen. For this nitrogen was bubbled through the water. Irradiation of the sample with UV light was carried out using a 75 W Xe arc lamp. The UV light from the source was guided to the cell via two fiber bundles. The light was passed through a 5 cm water filter to remove any infrared radiation. Schott UG 11 and BG 42 (50 x 50 x 1mm) broadband filters from ITOS were used to remove visible light (transmission below 380 nm). In order to check the influence of the visible light some experiments were performed with a GG 420 filter (ITOS) instead that blocks the light below 400 nm. An estimate based on the supplier specifications gave irradiance at the sample of slightly less than 2 mW cm^{-2}. For this estimate we considered the specified spectral irradiance of the arc lamp, the optical throughput of the lamp housing (rear window, beam condenser), the throughput through the fiber bundle, the transmittance of the optical filters, the reflection loss at the liquid filter and the cell window and the irradiated area (see supporting information for quantitative data). All experiments were performed at room temperature.

The adsorption of gold nanoparticles on the TiO_2 film was studied simultaneously by ATR-IR and UV-vis spectroscopy in the following way. After preparation of the TiO_2 film ($70\mu m$) the cell for simultaneous ATR-IR and UV-vis measurements was assembled and

mounted within the compartment of the FTIR spectrometer. Then water at pH 3 was flowed through the cell until the ATR-IR spectra were stable (about one hour). After that the flow was switched (at time T=0) to the nanoparticle solution (GSH-protected gold nanoparticles, 8 mg in 30 ml) and ATR-IR as well as UV-vis spectra were recorded simultaneously. Between the UV-vis measurements a shutter prevented extensive exposure of the catalyst to UV-light.

Samples for transmission electron microscopy (TEM) were collected by scratching the TiO_2 film off the internal reflection element after the experiment. TEM images were recorded with a Philips C200 electron microscope operated at 200 kV. The sample was dispersed in water and a drop was cast onto a carbon-coated copper grid.

5.4 Results and Discussion

5.4.1 Adsorption of Monolayer-protected Gold Nanoparticles on TiO_2

Figure 5-1 shows ATR-IR spectra that were recorded while flowing solutions of NAC-protected gold nanoparticles at pH 3 (spectrum (c)) and 5.5 (spectrum (b)) over a ca. $4\mu m$ thick TiO_2 film on a Ge internal reflection element. The spectra were recorded 30 min after starting the flow of nanoparticle solution. Clear signals are observed in the ATR-IR spectra, which can be assigned to NAC adsorbed on the nanoparticles.

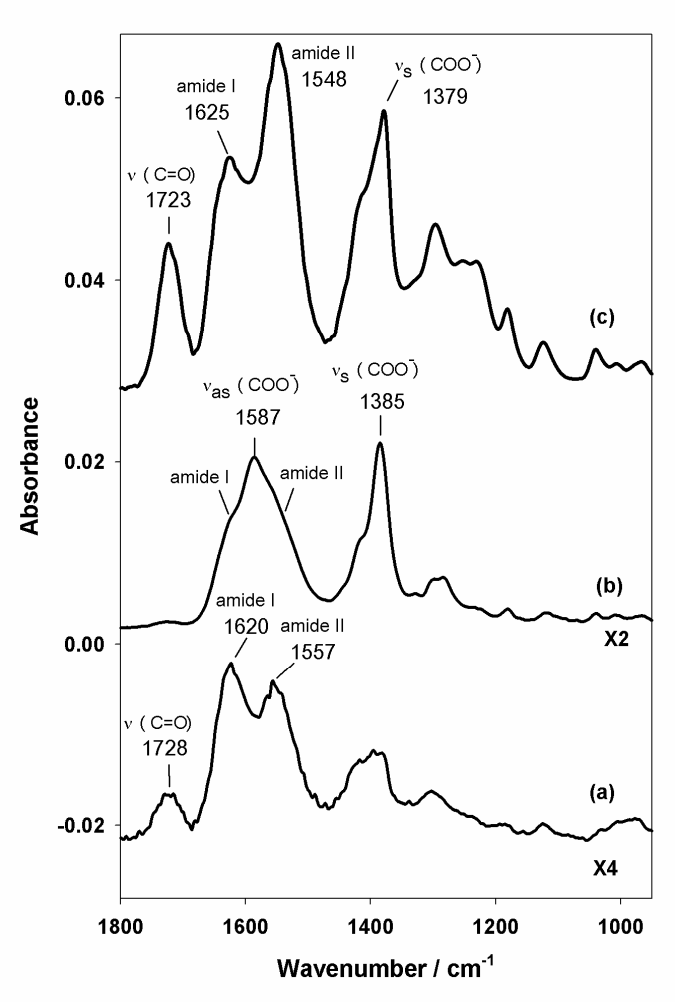

Figure 5-1: ATR-IR spectra of NAC-protected gold nanoparticles at pH 3 (c) and pH 5.5 (b) adsorbed on a TiO_2 film (4μm). For comparison a spectrum of NAC adsorbed on TiO_2 at pH 3 is also shown (a). The spectra were recorded one hour after starting adsorption from nanoparticle solution (1mg in 1ml). As the reference for the calculation of the absorbance spectra served the TiO_2 film before adsorption in the presence of water at the corresponding pH.

It should be noted that the solutions do not contain detectable amounts of free NAC, as was verified by ^{1}H NMR spectroscopy. The almost complete absence of a band above 1700 cm^{-1} in Figure 1 (b) indicates that at pH 5.5 the carboxylic acid group of NAC adsorbed on the gold particles is deprotonated. The pKa value of NAC is 3.2.[26] The most significant bands at 1587 and 1385 cm^{-1} can be assigned to vas(COO$^-$) and vs(COO$^-$) vibrational modes, respectively, of the deprotonated carboxylic acid group.[27] The shoulders on the former band can be assigned to amide I and amide II modes. At pH 3 (Figure 5-1 (c)) a significantly different spectrum was observed. Most evident is the appearance of a band at 1723 cm^{-1}, which shows that parts of the acid groups are now protonated. At the same time the

carboxylate band at 1379 cm^{-1} confirms the presence of deprotonated acid groups. Hence, at pH 3 both ionic forms coexist.

Figure 5-1 also reveals that at pH 3 the amount of adsorbed nanoparticles is considerably larger than at pH 5.5. Since the spectrum changes qualitatively with pH a relative quantification of the adsorbed amount of nanoparticles at the two pH values is difficult. Judging by the weak bands between 1000 and 1200 cm^{-1}, which do not shift with pH, and which do hardly change intensity upon changing pH in solution, about six times more nanoparticles are adsorbed at pH 3 than at pH 5.5. Upon flowing water at the corresponding pH over the sample the nanoparticles slowly desorb from the surface at pH 5.5, whereas almost no desorption is observed at pH 3 (see also later). This behavior indicates that the adsorption and binding to the surface is charge-driven. At both pH values the NAC covered gold nanoparticles are negatively charged, the average charge per particle being larger at pH 5.5, as evidenced by the ATR-IR spectra given in Figure 5-1. However, pH 5.5 is closer to the isoelectric point (IEP) of P25, which is in the range 6.4 – 7.0.[28, 29] Therefore the TiO_2 surface is far less charged at this pH, whereas at pH 3 it is strongly positively charged, which explains the stronger adsorption at the latter pH.

Figure 5-1 (a) also shows ATR-IR spectra of NAC (i.e. in the absence of nanoparticles) adsorbed on TiO_2 at pH 3. Significant differences between the spectra of adsorbed NAC and NAC-protected gold nanoparticles are observed. First of all the absolute intensity of the signals is about one order of magnitude larger for the particles. However, the spectra are also qualitatively different. Slight band shifts are observed in addition to important changes in relative intensity. For example the relative strength of the two intense bands at 1620 and 1557 cm^{-1} associated with amide I and amide II vibrations changes strongly. The intensity of the band at 1728 cm^{-1} furthermore indicates that the degree of deprotonation of NAC on TiO_2 is larger than the one for NAC on the gold particles at the same pH. Carboxylates have a strong affinity to TiO_2.[30] For NAC adsorbed on gold it was shown that the carboxylate interacts with the gold surface in addition to the thiol.[27] Vibrational circular dichroism (VCD) moreover indicated that this is also the case for the gold nanoparticles investigated here.[21] The qualitative differences in the NAC spectra may point towards a different conformation of the molecule in the two situations. When adsorbing the NAC-protected gold nanoparticles some NAC molecules are in direct contact with the TiO_2 surface. Whether these molecules interact via the carboxylate with the TiO_2 can not be answered based on the spectra.

Figure 5-2 shows a series of ATR-IR and UV-vis spectra that were recorded in situ while flowing a solution of L-glutathione (γ-glu-cys-gly, GSH) protected nanoparticles over a TiO_2 film (ca. 70 μm) at pH 3.

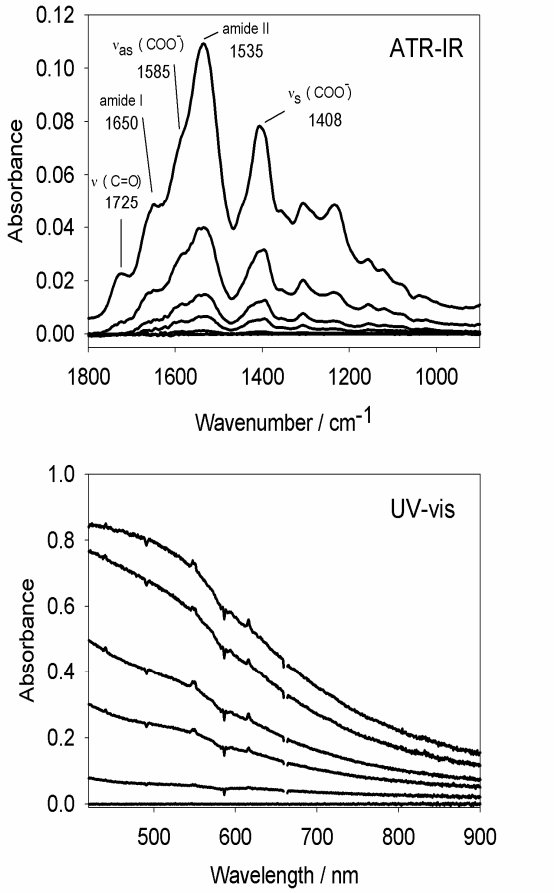

Figure 5-2: ATR-IR and UV-vis spectra recorded while flowing a solution (8 mg in 30 ml water) of GSH-protected gold nanoparticles over a TiO_2 film (70 μm) at pH 3. The TiO_2 film before adsorption in the presence of water at pH 3 served as the reference condition for calculation of the absorbance spectra. Spectra were recorded 0, 12, 19, 27, 47 and 89 minutes after starting the flow of nanoparticles.

At this pH GSH in solution is partially negatively charged[31] similar to NAC. Furthermore it has been shown that the adsorption of GSH on gold favors deprotonation of the carboxylic acid group at the gly part of the molecule.[32] The most significant bands in the spectrum can be assigned to the C=O stretching mode of protonated acid groups (COOH) at 1725 cm^{-1}, to the amide I and amide II modes at 1650 and 1535 cm^{-1} and to the antisymmetric and symmetric carboxylate vibrations at 1585 (shoulder) and 1408 cm^{-1}. In agreement with the ATR-IR spectra the UV-vis spectra indicate the adsorption of the nanoparticles on the TiO_2 film. There is no sign of a plasmon band in the UV-vis spectra, which confirms that the

particles diameter is equal to or smaller than 2 nm,[33] in agreement with transmission electron microscopy. The optical absorption spectrum of such small particles is characterized by a strongly increasing signal towards shorter wavelengths.

Figure 5-5 shows the ATR-IR signal at 1550 cm^{-1} and the UV-vis signal at 450 nm as a function of time for an experiment where GSH-protected gold nanoparticles were adsorbed on a thick TiO_2 film ($70\mu m$). The two signals were recorded simultaneously and in situ. Obviously the shape of the two curves is significantly different, which is due to the different sampling geometry for the two techniques.

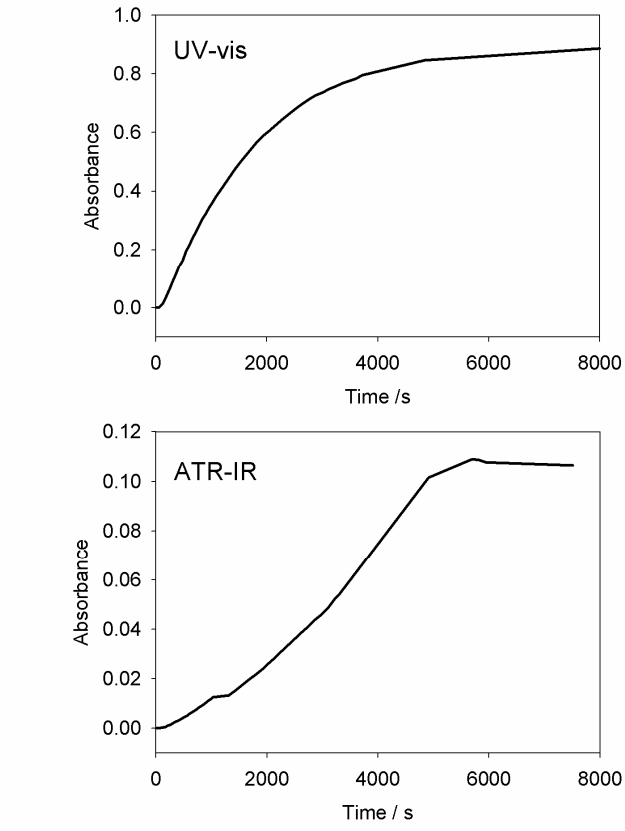

Figure 5-3: ATR-IR signal at 1536 cm^{-1} and UV-vis signal at 550 nm as a function of time that were recorded while flowing a solution (8 mg in 30 ml water) of GSH-protected gold nanoparticles over a TiO_2 film (70 μm) at pH 3 (see experiment shown in Figure 5-2). Note that in between UV-vis measurements the sample was in the dark.

In the UV-vis experiment the sample is probed perpendicular to the film and therefore an average over the whole film between the IRE/film interface and the film/solution interface is obtained. In contrast, ATR-IR only probes the volume the closest to the IRE. An estimate of the penetration depth dp at 1500 cm^{-1} [19] based on the effective refractive index of the wet

TiO_2 film yields a value of $0.52\mu m$. To estimate the effective refractive index of the film the refractive index of water (1.33) and anatase (2.49) and a void fraction of 0.5 were assumed.[34]

Figure 5-3 shows that it takes about two hours until the signals are stable. The combined information obtained from the two techniques reveals that mass transport through the thick film (70 μm) plays an important role. This leads to a gradient of adsorbed particles perpendicular to the IRE surface within the film. For example, after 2000 seconds more than 60 % of a full coverage is achieved on average over the whole film (see UV-vis), whereas on the part the closest to the IRE only about 20% of a full coverage is achieved (see ATR-IR). Adsorption on the outer part of the film is therefore fast, similar as was observed for the thin film by ATR-IR, whereas adsorption on the inner part of the film is limited by intra-film mass-transport of the nanoparticles. In this context it is important to note that upon formation of the film agglomeration of the TiO_2 particles leads to a porous network with pores of about 10 nm, as can be judged from inspection of TEM images of the dried powder (see supporting information). The size of the pores is therefore only a few times larger than the size of the nanoparticles itself (gold core plus protection layer). The mass transport within the TiO_2 film is likely quite complex. The diffusion of the particles through the porous film depends on the charge of both partners (particle and film), besides other factors like porosity of the film. However, upon adsorption of the particles on the outer surface of the film the surface charge changes locally, which changes the effective diffusion constant. In fact the latter becomes dependent on time and space within the film

5.4.2 Illumination of the Adsorbed Gold Nanoparticles

Figure 5-4 and Figure 5-5 show two series of ATR-IR spectra recorded while flowing water over the sample during UV illumination at pH 3 (Figure 4) and pH 5.5 (Figure 5).

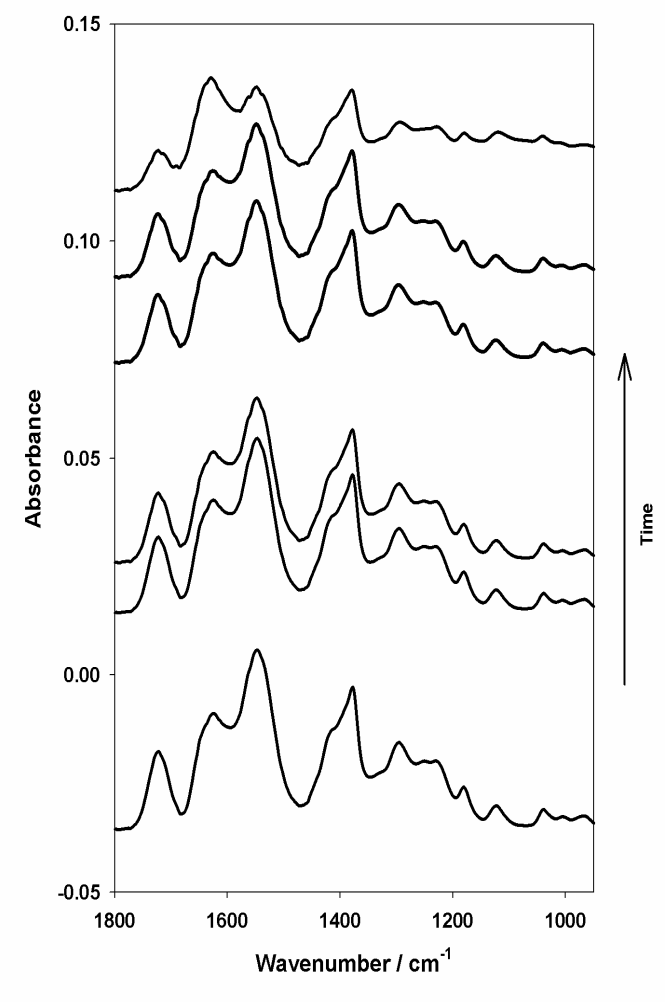

Figure 5-4: ATR-IR spectra of NAC-protected gold nanoparticles adsorbed on a TiO_2 film (4µm). The bottom spectrum was recorded at the end of adsorption. The following two spectra were recorded during flowing water in the dark and the three top spectra during UV-illumination. Water at pH 3 was flowed over the sample during illumination. Before illumination the nanoparticles were adsorbed at pH 3 for 2 hours. The last spectrum (top) was recorded 95 minutes after starting the illumination.

Before these experiments a solution of NAC-protected gold nanoparticles was flowed over the TiO_2 film for 25 minutes followed by a flow of water for 45 min. Clearly the signals associated with NAC adsorbed on the gold nanoparticles decrease with time upon illumination.

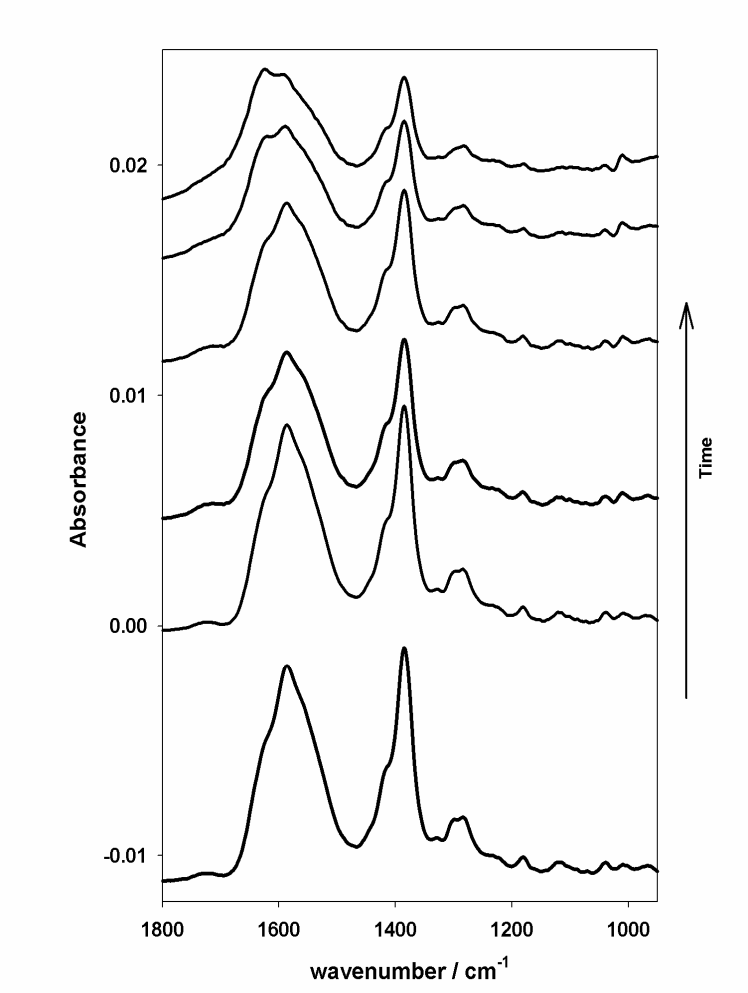

Figure 5-5: ATR-IR spectra of NAC-protected gold nanoparticles adsorbed on a TiO_2 film (4µm). The bottom spectrum was recorded at the end of adsorption. The following two spectra were recorded during flowing water in the dark and the three top spectra during UV-illumination. Water at pH 5.5 was flowed over the sample during illumination. Before illumination the nanoparticles were adsorbed at pH 5.5 for 2 hours. The last spectrum (top) was recorded 95 minutes after starting the illumination.

Figure 5-6 shows the ATR-IR signals at 1546 (a) and 1585 cm^{-1} (b) as a function of time corresponding to the experiments shown in Figure 5-4 and Figure 5-5. The dashed vertical line indicates the start of the illumination. Clearly, at pH 5.5 some desorption of NAC-protected nanoparticles is observed in the dark, whereas at pH 3 desorption during water flow is insignificant. Upon illumination the NAC bands decrease. Interestingly, at pH 3 the decrease of the signal is relatively slow during the first 1000 seconds of illumination, but after that initial period the rate increases.

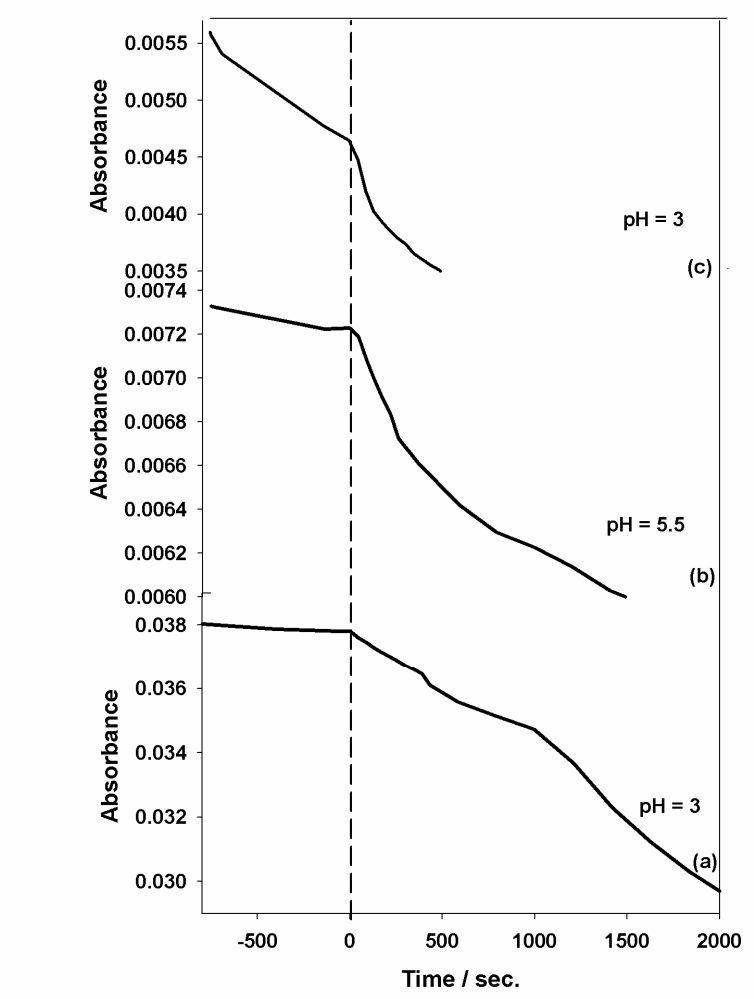

Figure 5-6: ATR-IR signals at 1546 (a) and 1585 cm-1 (b) as a function of time corresponding to the experiment described in Figure 5-4 and Figure 5-5. The ATR-IR signal at 1552 cm^{-1} of NAC adsorbed on TiO_2 at pH 3 as a function of time is also shown for comparison (c).

Figure 5-6 also shows the signal at 1552 cm^{-1} of NAC adsorbed on TiO_2 at pH 3 as a function of time (trace (c)). In this experiment NAC was adsorbed first before flowing water over the sample. Obviously, in the dark NAC desorbs from the TiO_2 surface at much higher rate than the NAC-protected gold nanoparticles (compare with Figure 5-6 trace (a)). The stronger adsorption of the nanoparticles compared to NAC could be due to the stronger electrostatic and van der Waals interaction or due to multiple interactions between particle and TiO_2 via carboxylate groups.

When turning on the UV-light NAC is removed fast. The relative decrease for NAC is larger than the one for the NAC-protected gold nanoparticles, even when taking into account desorption in the dark. In the case of NAC the signals decrease by about 15% within 500

seconds, whereas for the NAC-protected gold particles a decrease of only 6.6% is observed under the same conditions. The different relative rates point towards different light-induced processes in the two situations. This is confirmed by Figure 5-7 (top and middle), showing difference spectra recorded during irradiation of NAC and NAC-protected gold nanoparticles, respectively, on TiO_2. These spectra reveal the species formed during irradiation.

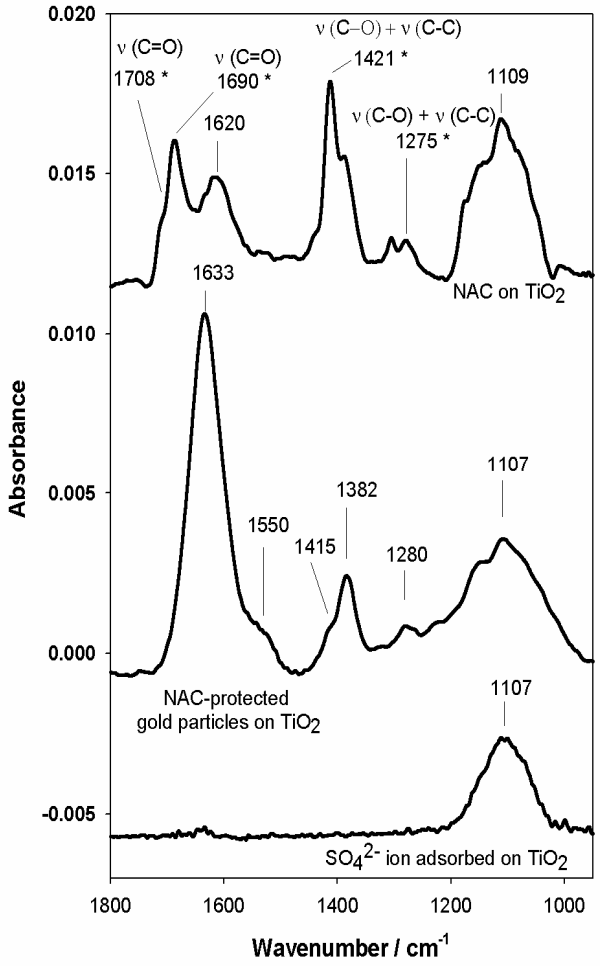

Figure 5-7: ATR-IR difference spectra corresponding to illumination experiments of the NAC-protected gold particles on TiO_2 (middle spectrum) and of NAC on TiO_2 (top spectrum) at pH 3. The difference spectra correspond to the last spectrum recorded during illumination from which the spectrum recorded before starting illumination was subtracted, in such a way that the NAC signals vanish. The spectra thus highlight the species that are formed upon illumination. Bands labeled with an asterisk are associated with oxalate species. The bottom spectrum was obtained after flowing a solution of H_2SO_4 (1 mM) over a calcined Au/TiO_2 catalyst.

Obviously the two spectra in Figure 5-7 are rather different. The middle spectrum (NAC-protected gold nanoparticles) is dominated by a band at 1633 cm^{-1}. Part of this band may originate from incompensation of water. When NAC or NAC-protected gold

nanoparticles leave the TiO_2 surface the amount of water probed by the evanescent field is increasing, which results in a water signal in the difference spectrum. The broad band centered around 1100 cm^{-1} can be assigned to oxidized sulfur species such as sulfate. Indeed, adsorption of sulfate on Au/TiO_2 resulted in a similar broad signal at 1100 cm^{-1}, as can be seen in Figure 5-7, bottom. It should be noted that this band did not appear in experiments where the sample was irradiated by visible light only (see supporting information). In the absence of oxygen this band was also missing (see supporting information). The origin of the other bands observed at 1280 cm^{-1}, 1382 cm^{-1} (shoulder at 1415 cm^{-1}) and about 1550 cm^{-1} is less clear. The latter band could be due to amide and/or carboxylate vibrations. Upon illumination of NAC on TiO_2 (top spectrum in (Figure 5-7) the broad sulfate signal at 1100 cm^{-1} is also observed. The most important difference with respect to the corresponding spectrum of NAC-protected gold nanoparticles (Figure 5-7) are the characteristic signals associated with oxalate species ($^{-}OOC\text{-}COO^{-}$) at 1690 cm^{-1} (with a shoulder at 1708 cm^{-1}), 1421 cm^{-1} and 1275 cm^{-1}.[30] In addition, the band at 1620 cm^{-1} can be assigned to a carboxylate vibration of a newly formed species. Oxalate species on TiO_2 have been observed previously, for example during photocatalytic mineralization of malonic and succinic acid,[25, 35] and the photoassisted reaction of glyoxylic acid on TiO_2.[36] Oxalate seems to be an ubiquitous species during irradiation of TiO_2 in the presence of carboxylic acids and its observation on the TiO_2 surface upon irradiation of adsorbed NAC is therefore not too surprising. On the other hand there is no sign of oxalate in the corresponding spectrum for the NAC-stabilized gold nanoparticles. This shows different reaction pathways for NAC in the two cases.

It is known that the photo-excited electron can be transferred from TiO_2 to adsorbed metal particles.[37] Alternatively, it has been shown that photo-excitation of gold particles can lead to an inverse flow of electrons, i.e. from the gold particle to the TiO_2.[6] In contrast to the bulk metal, gold nanoparticles have shown to be photoluminescent. Small gold nanoparticles show increased photochemical activity because of their high surface to volume ratio and their particular electronic properties.[38] The thiolate on the gold may thus act as an electron donor to the gold particle and therefore be oxidized. Upon irradiation the observed oxidized sulfur species could directly be formed on the gold particles similarly to what is noticed for thiols adsorbed on gold surfaces upon UV exposure.[16] Our experiments show that the UV part of the light is responsible for the deep oxidation of the sulfur in the presence of dissolved oxygen although the gold particles can be excited by visible light as well. On the other hand, the same

species are also apparent on the TiO_2 surface upon irradiation of NAC in the absence of the gold particles, which is ascribed to the action of the TiO_2 photocatalyst. The observation of sulfate species in both cases tempts one to assign their formation to the same process, i.e. the action of the TiO_2 photocatalyst. However, we think that this is not the case since this would imply desorption of the thiol from the gold particle prior to reaction on the TiO_2, which is rather unlikely. Possibly, the oxidation of the thiols directly takes place on the gold particles similar as was reported for the oxidation of self-assembled monolayers on gold surfaces.[16] The desorption of these compounds leads to partly naked gold particles.

Figure 5-8 shows difference spectra recorded at the beginning and at the end of illumination highlighting the species that are formed.

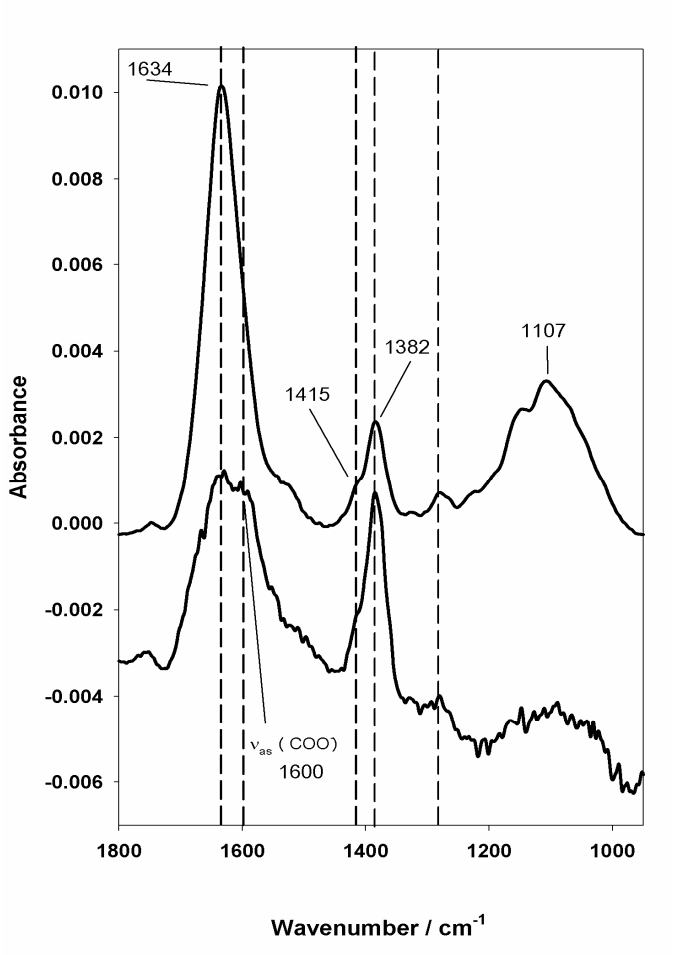

Figure 5-8: ATR-IR difference spectra corresponding to an experiment where NAC-protected gold particles on TiO_2 were illuminated at pH 3. The bottom spectrum corresponds to a difference spectrum recorded during the first 1000 seconds of illumination (see Figure 5-6). The top spectrum was recorded at the end of illumination.

The spectra are clearly different at the beginning of irradiation with relative strong bands at 1415 and 1382 cm^{-1} and relatively weak sulfate bands (1100 cm^{-1}). This indicates that the first bands are associated with less oxidized species, which are subsequently further oxidized to sulfates. Furthermore a band at around 1600 cm^{-1} is observed at the beginning of irradiation that is possibly associated with a carboxylate group of a newly formed species. We propose that the oxidation of the sulfur is proceeding via different pathways in the two cases, i.e. directly on the gold particles in the case of the NAC-protected gold particles, similar as found for self-assembled monolayers of thiols on gold, and on the TiO_2 via photo-oxidation in the case of NAC. The absence of oxalate signals in the experiments conducted with the NAC-protected gold nanoparticles indicates that the formation of the oxalate is a process that takes place on the TiO_2 surface and not in solution and/or on the gold particles. Upon illumination of TiO_2 radicals (hydroxyl, $O_2^{-}\cdot$) are formed, which can react with dissolved species or species adsorbed on the gold nanoparticles. The absence of oxalate in the case of NAC-protected gold nanoparticles indicates that the formation of oxalate is not directly mediated by such radicals. It should be noted that when adsorbing NAC onto a gold – TiO_2 catalyst oxalate is observed under irradiation.

5.4.3 Effect of Illumination on Gold Particle Size

When illuminating the gold nanoparticles adsorbed on the TiO_2 film a color change was observed. Before UV exposure the film was brownish, whereas after exposure its appearance was violet, which indicates a change in the metal core of the particles. Note that this color change was not observed when exposing the sample to visible light only or to UV light in the absence of oxygen. Indeed, in situ UV-vis spectroscopy revealed the development of a surface plasmon band at around 540 nm with time upon exposure to UV light in the presence of oxygen (see Figure 5-9), which indicates the presence of gold particles larger than about 3 nm.

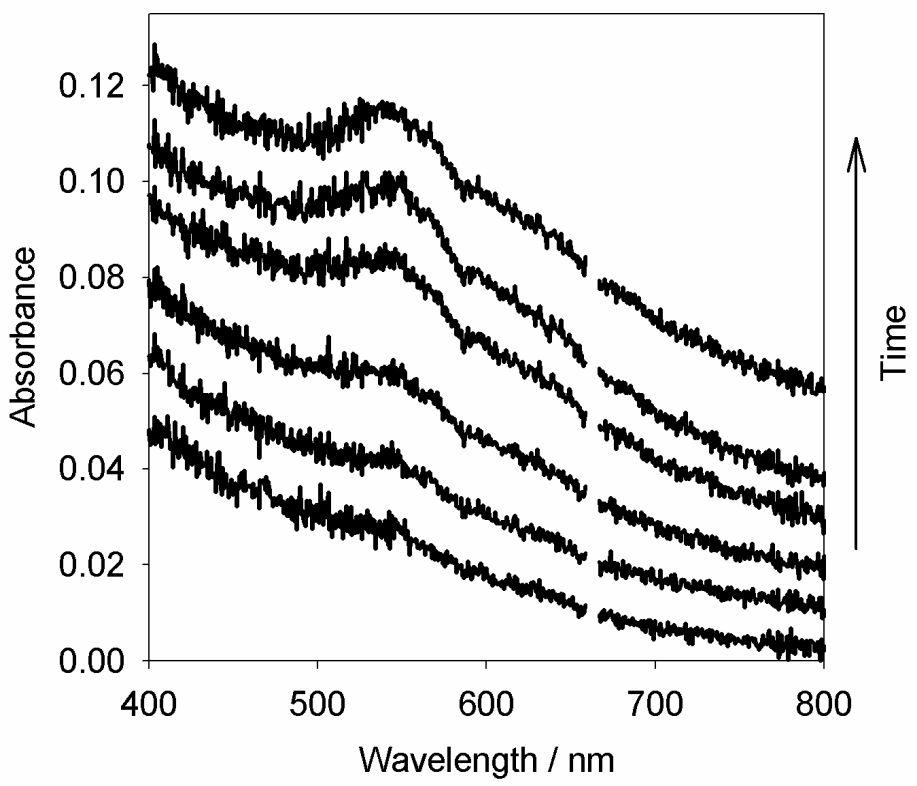

Figure 5-9 UV-vis spectra recorded while illuminating GSH-protected gold nanoparticles adsorbed on a TiO_2 film. The spectra were recorded (from bottom to top) 30, 40, 60, 90, 120 and 150 min after starting the illumination. During illumination water at pH 3 was flowed over the sample. The spectra are offset for clarity. Note that the UV-vis source of the spectrometer was used to illuminate the sample and that in between measurements the sample was illuminated.

This was confirmed by transmission electron microscopy (TEM) of the unexposed and exposed sample as shown in Figure 5-10.

The TEM of the sample after adsorption of NAC-protected gold nanoparticles reveals well-dispersed and very small gold nanoparticles on the TiO_2. The particles are on the order of 1 nm in diameter and distributed evenly over the whole surface. After UV-illumination the particles are considerably larger (5 nm).

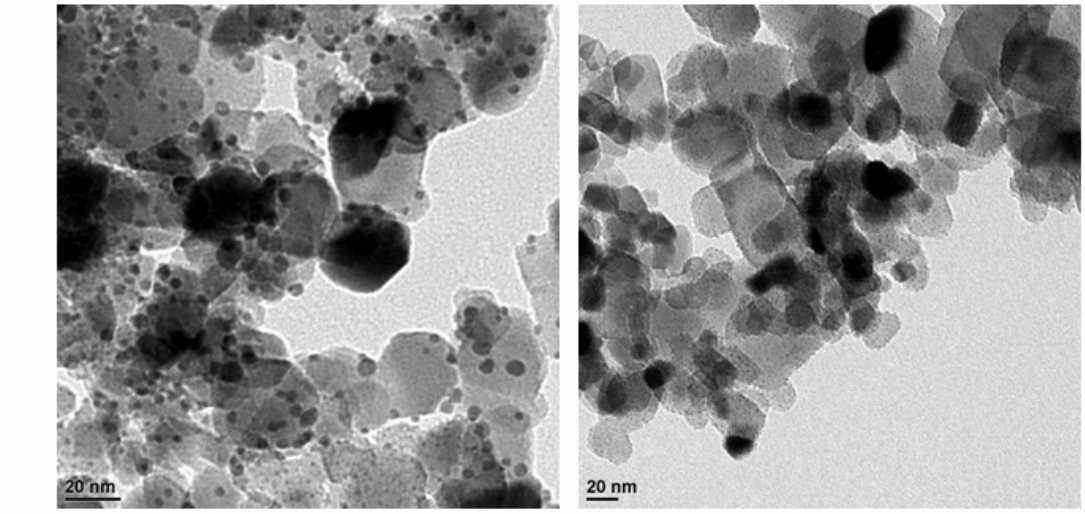

Figure 5-10: Transmission electron microscopy (TEM) images of NAC-protected gold nanoparticles on TiO_2 before (right) and after (left) 100 minutes of UV illumination.

The increase of the mean particle size upon illumination shows that the NAC-protected gold nanoparticles are mobile on the TiO_2 surface at room temperature under our conditions. The increase in particle size has to do with the (partial) removal of the NAC protection layer by the UV exposure thus enabling contact between gold cores. Note that with an intact NAC protection layer the gold nanoparticles can be dried and redispersed without sintering. The particles in the TEM images do not seem to be agglomerates of individual smaller particles. This indicates that the smaller particles melt together to form larger particles at room temperature (Scheme 5-2). Both the removal of the protection layer and the mobility of the particles on the support likely depend on the nature of the passivating molecules. The latter should be considered as an important parameter for the tailoring of supported gold catalysts prepared by the method applied here. Interestingly, in a recent report it was proposed, based on transmission electron microscopy, that gold nanoparticles linked to the TiO_2 through 3-mercaptopropionic acid (MPA) were immobile under UV irradiation.[5] Furthermore, it was proposed that the MPA withstands the photoreactions, although no direct molecular level information was provided. The apparent different behavior of MPA and NAC protected gold nanoparticles on TiO_2 may be due to the different chemical nature of the passivating molecule and the different conditions for the preparation of the material.

The different species observed at the very beginning of irradiation of NAC-protected gold nanoparticles and at the end (Figure 5-8) may be related to the finding that at the beginning the rate of disappearance of the NAC signals is slow and accelerates afterwards

(see Figure 5-6 (a)). One may speculate that this change has to do with the reaction of the NAC molecules on the gold particles that are in direct contact with the TiO_2 surface. Once these are consumed the better contact between gold and TiO_2 leads to a higher electron transfer rate, which furthermore accelerates NAC decomposition. Alternatively, it has been shown recently that the rate of charge transfer between TiO_2 and gold particle increases with the size of the latter.[39] Therefore, in our case the charge transfer should be initially slow for the small particles. Once the particle size has increased (see later) the electron transfer rate increases as well, thus accelerating NAC decomposition.

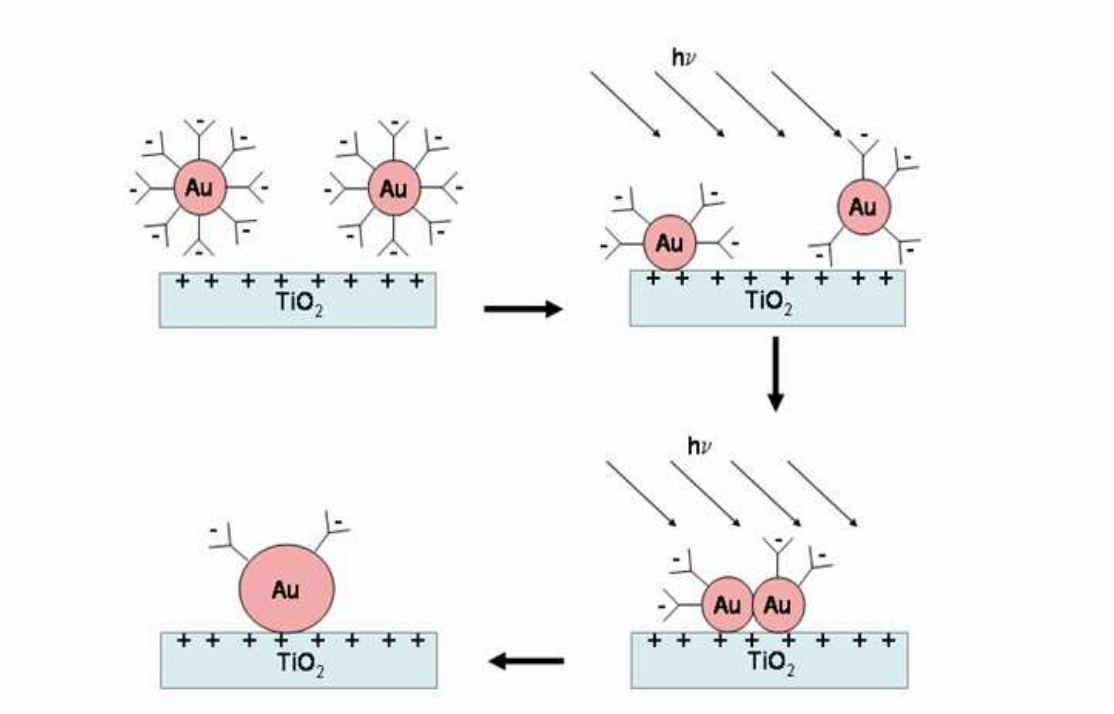

Scheme 5-2: Pictorial view of the processes occurring upon illumination of passivated gold particles adsorbed on TiO_2

5.5 Conclusion

The combination of attenuated total reflection infrared (ATR-IR) and UV-vis spectroscopy allows one to study mass transport within porous films supported on internal reflection elements due to the different sampling geometry of the two techniques. This combination revealed that the adsorption of gold nanoparticles covered by thiols onto porous films of TiO_2 is significantly limited by mass transport within the film. Upon illumination the adsorbed thiolates on the gold nanoparticles are partly removed and oxidized sulfur species

such as sulfates are observed on the surface. The latter species are also observed when illuminating N-acetyl-L-cysteine directly adsorbed on TiO_2, i.e. in the absence of gold particles. However, the mechanism of N-acetyl-L-cysteine decomposition seems to be different in the two cases, because in the latter situation a large amount of oxalate is observed on the TiO_2 surface, which is not the case for the gold nanoparticles. The partial removal of the thiolate protection layer leads to agglomeration of small particles and the formation of larger ones, which can be followed in situ through UV-vis spectroscopy by the development of a surface plasmon resonance band. This is also confirmed by TEM measurements. This finding shows that the protected particles are mobile on the TiO_2 surface at room temperature and in water, despite the presence of multiple carboxylate groups. For the synthesis of tailored catalysts it might be advantageous to prepare materials with even smaller gold particles than the ones obtained in this work. This requires the reduction of particle mobility during removal of the thiolate layer for example by using other thiols or by lowering the temperature during illumination.

References

1. Sun, S. Q.; Mendes, P.; Critchley, K.; Diegoli, S.; Hanwell, M.; Evans, S. D.; Leggett, G. J.; Preece, J. A.; Richardson, T. H., Fabrication of gold micro- and nanostructures by photolithographic exposure of thiol-stabilized gold nanoparticles. *Nano Lett.* **2006,** 6, (3), 345-350.
2. Haruta, M.; Kobayashi, T.; Sano, H.; Yamada, N., Novel Gold Catalysts for the Oxidation of Carbon-Monoxide at a Temperature Far Below 0-Degrees-C. *Chem. Lett.* **1987**, (2), 405-408.
3. Haruta, M.; Yamada, N.; Kobayashi, T.; Iijima, S., Gold Catalysts Prepared by Coprecipitation for Low-Temperature Oxidation of Hydrogen and of Carbon-Monoxide. *J. Catal.* **1989,** 115, (2), 301-309.
4. Chou, J.; McFarland, E. W., Direct propylene epoxidation on chemically reduced Au nanoparticles supported on titania. *Chem. Commun.* **2004**, (14), 1648-1649.
5. Li, J.; Zeng, H. C., Preparation of monodisperse Au/TiO_2 nanocatalysts via self-assembly. *Chem. Mat.* **2006,** 18, (18), 4270-4277.
6. Tian, Y.; Tatsuma, T., Mechanisms and applications of plasmon-induced charge separation at TiO_2 films loaded with gold nanoparticles. *J. Am. Chem. Soc.* **2005,** 127, (20), 7632-7637.
7. Kamat, P. V., Meeting the clean energy demand: Nanostructure architectures for solar energy conversion. *J. Phys. Chem. C* **2007,** 111, (7), 2834-2860.
8. Valden, M.; Lai, X.; Goodman, D. W., Onset of catalytic activity of gold clusters on titania with the appearance of nonmetallic properties. *Science* **1998,** 281, (5383), 1647-1650.
9. Stiles, A. B.; Koch, T. A., *Catalyst Manufacture*. 2nd Edition ed.; Dekker: New York, 1995.

10. Schmid, G., Large Clusters and Colloids - Metals in the Embryonic State. *Chem. Rev.* **1992,** 92, (8), 1709-1727.
11. Brust, M.; Walker, M.; Bethell, D.; Schiffrin, D. J.; Whyman, R., *J. Chem. Soc. Chem. Commun.* **1994**, 801.
12. Tada, H.; Soejima, T.; Ito, S.; Kobayashi, H., Photoinduced desorption of sulfur from gold nanoparticles loaded on metal oxide surfaces. *J. Am. Chem. Soc.* **2004,** 126, (49), 15952-15953.
13. Dasog, M.; Scott, R. W. J., Understanding the oxidative stability of gold monolayer-protected clusters in the presence of halide ions under ambient conditions. *Langmuir* **2007,** 23, (6), 3381-3387.
14. Sandhyarani, N.; Pradeep, T., Oxidation of alkanethiol monolayers on gold cluster surfaces. *Chem. Phys. Lett.* **2001,** 338, (1), 33-36.
15. Kell, A. J.; Alizadeh, A.; Yang, L.; Workentin, M. S., Monolayer-protected gold nanoparticle coalescence induced by photogenerated radicals. *Langmuir* **2005,** 21, (21), 9741-9746.
16. Brewer, N. J.; Rawsterne, R. E.; Kothari, S.; Leggett, G. J., Oxidation of self-assembled monolayers by UV light with a wavelength of 254 nm. *J. Am. Chem. Soc.* **2001,** 123, (17), 4089-4090.
17. Tian, Y.; Notsu, H.; Tatsuma, T., Visible-light-induced patterning of Au- and Ag-TiO_2 nanocomposite film surfaces on the basis of plasmon photoelectrochemistry. *Photochem. & Photobio. Sci.* **2005,** 4, (8), 598-601.
18. Linsebigler, A. L.; Lu, G.; Yates, J. T., Photocatalysis on TiO_2 surfaces: Principles, mechanisms, and selectrd results. *Chem. Rev.* **1995,** 95, 735 -758.
19. Harrick, N. J., *Internal reflection spectroscopy*. Interscience Publishers: New York, 1967.
20. Bürgi, T.; Baiker, A., Attenuated total reflection infrared spectroscopy of solid catalysts functionong in the presence of liquid-phase reactants. *Advances in Catalysis* **2006,** 50, 228-283.
21. Gautier, C.; Bürgi, T., Vibrational circular dichroism of N-acetyl-L-cysteine protected gold nanoparticles. *J. Chem. Soc. Chem. Commun.* **2005**, 5393-5395.
22. Gautier, C.; Bürgi, T., Chiral N-isobutyryl-cysteine protected gold nanoparticles: preparation, size selection and optical activity in the UV-vis and infrared. *J. Am. Chem. Soc.* **2006,** 128, 11079-11087.
23. Danion, A.; Disdier, J.; Guillard, C.; Abdelmalek, F.; Jaffrezic-Renault, N., Characterization and study of a single TiO_2-coated optical fiber reactor. *Int. J. Appl. Electromagnetics and Mechanics* **2006,** 23, (3-4), 187-201.
24. Bürgi, T., Combined in situ attenuated total reflection infrared and UV-Vis spectroscopic study of alcohol oxidation over Pd/Al2O3. *J. Catal.* **2005,** 229, 55-63.
25. Dolamic, I.; Bürgi, T., Photoassisted decomposition of malonic acid on TiO2 studied by in situ attenuated total reflection infrared spectroscopy. *J. Phys. Chem. B* **2006,** 110, 14898-14904.
26. Juch, R.; Birrenbach, G.; Pflugshaupt, C. 1995, Vol. United States Patents.
27. Bieri, M.; Bürgi, T., Adsorption kinetics, orientation and self-assembling of N-acetyl-L-cysteine on gold: A combined ATR-IR, PM-IRRAS and QCM study. *J. Phys. Chem. B* **2005,** 109, 22476-22485.
28. Dionysiou, D. D.; Suidan, M. T.; Bekou, E.; Baudin, I.; Laine, J. M., Effect of ionic strength and hydrogen peroxide on the photocatalytic degradation of 4-chlorobenzoic acid in water. *Appl. Catal. B-Environmental* **2000,** 26, (3), 153-171.
29. Gumy, D.; Morais, C.; Bowen, P.; Pulgarin, C.; Giraldo, S.; Hajdu, R.; Kiwi, J., Catalytic activity of commercial of TiO_2 powders for the abatement of the bacteria (E-

coli) under solar simulated light: Influence of the isoelectric point. *Appl. Catal. B-Environmental* **2006,** 63, (1-2), 76-84.

30. Hug, S.; Bahnemann, D., Infrared spectra of oxalate, malonate and succinate adsorbed on the aqueous surface of rutile, anantase and lepidocrocite measured with in sotu TR-FTIR. *J. El. Spectr. Rel. Phenom.* **2006,** 150, 208 - 219.
31. Rabenstein, D. L., pKa of glutathione. *J. Am. Chem. Soc.* **1973,** 95, 2797.
32. Bieri, M.; Bürgi, T., L-glutathione chemisorption on gold and acid/base induced structural changes: a PM-IRRAS and time-resolved in situ ATR-IR spectroscopic study. *Langmuir* **2005,** 21, (4), 1354-1363.
33. Alvarez, M. M.; Khoury, J. T.; Schaaff, T. G.; Shafigullin, M. N.; Vezmar, I.; Whetten, R. L., Optical absorption spectra of nanocrystal gold molecules. *J. Phys. Chem. B* **1997,** 101, (19), 3706-3712.
34. Braun, M. M.; Pilon, L., *Thin Solid Films* **2006,** 496, 505.
35. Dolamic, I.; Bürgi, T., Photocatalysis of dicarboxylic acids over TiO_2: An in situ ATR-IR study. *J. Catal.* **2007,** 248, (2), 268-276.
36. Ekström, G. N.; McQuillan, A. J., In situ infrared spectroscopy of glyoxylic acid adsorptiopn and photocatalysis on TiO_2 in aqueous solution. *J. Phys. Chem. B* **1999,** 103, 10562.
37. Subramanian, V.; Wolf, E. E.; Kamat, P. V., Catalysis with TiO_2/gold n anocomposites. Effect of metal particle size on the Fermi level equilibration. *J. Am. Chem. Soc.* **2004,** 126, (15), 4943-4950.
38. Schmid, G., *Nanoparticles: From Theory to Applications*. Wiley-VCH Verlag GmbH: Weinheim, 2004.
39. Kim, J.; Lee, D., Size-controlled interparticle charge transfer between TiO_2 and quantized capacitors. *J. Am. Chem. Soc.* **2007,** 129, 7706-7707.

6

An in Situ ATR-IR Study of Amino acid Adsorption and Photocatalytic Decomposition over TiO_2 Thin Films

6.1 Introduction

The interest in the study of nanostructured materials has been increasing in the last years, stimulated by interesting chemical and physical properties that these materials exhibit. Furthermore, the recent scientific progress was catalyzed by the powerful characterization techniques available today.

Metal oxide TiO_2 nanoparticles found extensive applications in many fields such as medicine, biology and environmental chemistry. An important aspect is the interaction of TiO_2 thin films with molecules at different interfaces. Adsorption of biomolecules onto TiO_2 thin films were extensively studied before[1-3]. Understanding of adsorption processes of proteins and amino acids are of essential importance to get a better insight into the photodecomposition of microorganisms and proteins in polluted waters.

Proteins and peptides are polymers of amino acids. The latter contain acid (-COOH) and amino (-NH_2) functional groups with various side chains on the α-carbon. Therefore adsorption and decomposition are expected to depend on the molecular structures of the amino acids. Hidaka and coworkers reported photocatalytic decomposition of several amino acids and formation of NH_4^+, NO_3^-, and CO_2 as final products[4, 5].

Here we studied by in situ attenuated total reflection infrared (ATR-IR) spectroscopy, the adsorption and photocatalytic decomposition of several amino acids, L-alanine, L-glutamic acid and L-asparagine in aqueous medium over TiO_2 thin films. It was shown that amino acids adsorb onto TiO_2 thin films prepared on a Ge internal reflection element (IRE) and undergo photocatalytic reaction upon UV irradiation.

6.2 Experimental

6.2.1 Catalyst and chemicals

Commercial Degussa P25 TiO_2 composed of 80% anatase and 20% rutile with surface area of 51 m^2/g and average particle size of 21 nm was used in the photocatalytic experiments. L-alanine (Sigma, 98%), L-asparagine (Fluka, 99.5%), L-asparagine -$^{15}N_2$ (ISOTEC 98% ^{15}N), L-glutamic acid (Fluka, 99.5%) and L-glutamic ^{15}N acid (Aldrich 98% ^{15}N) were used as received. Milli-Q water was used for all experiments. Scheme 6-1 shows the structure of the studied amino acids.

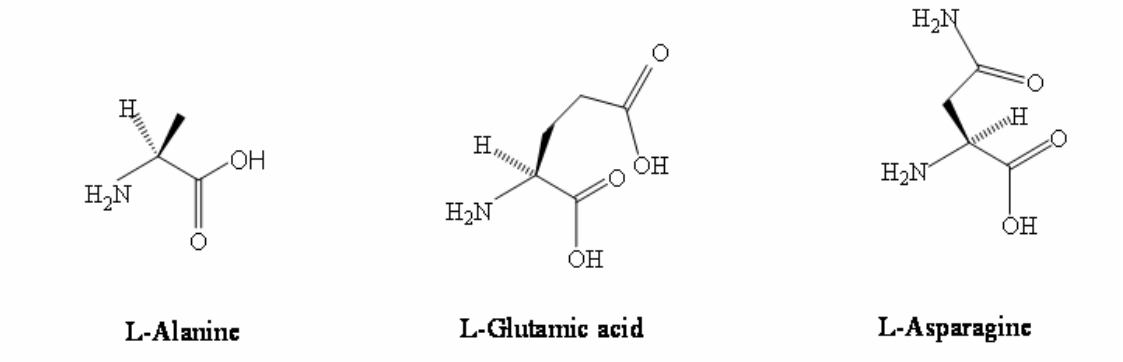

Scheme 6-1: Structure of studied amino acids

6.2.2 ATR-IR Spectroscopy

ATR spectra were recorded with a dedicated flow-through cell, made from a Teflon piece, a fused silica plate (45 mm X 35 mm X 3 mm) with holes for the inlet and outlet (36 mm apart), and a flat (1 mm) viton seal. TiO_2 thin films were formed by dropping an aqueous TiO_2 slurry onto a Ge internal reflection element (IRE) (52 mm X 20 mm X 1 mm; KOMLAS). The thin film preparation was performed as described before[6, 7]. The cell was mounted on an attachment for ATR measurements within the sample compartment of a Bruker Equinox-55 FTIR spectrometer equipped with a narrow-band MCT detector. Spectra were recorded at 4 cm^{-1}. The reactant was passed through the cell and over the catalyst at a flow rate of 0.2 mL/min by means of a peristaltic pump (Ismatec, Reglo 100) located in front of the cell. Solutions of amino acids (10^{-3} mol/L, pH about 3.5) were flowed over the TiO_2 film in the dark for 30 min in order to reach equilibrium. Irradiation of the sample with UV light was carried out using a 75 W Xe arc lamp. The UV light from the source is guided to the cell via two fiber bundles. The light was passed through a 5 cm water filter to remove any infrared radiation. A Schott UG 11 and BG 42 (50 mm X 50 mm X 1 mm) broadband filter from ITOS was used to remove visible light (transmission between 310 and 380 nm). An estimate based on the supplier specifications gave a power at the sample of slightly less than 2 mW/cm^2. All experiments were performed at room temperature.

6.3 Adsorption of amino acids onto TiO_2

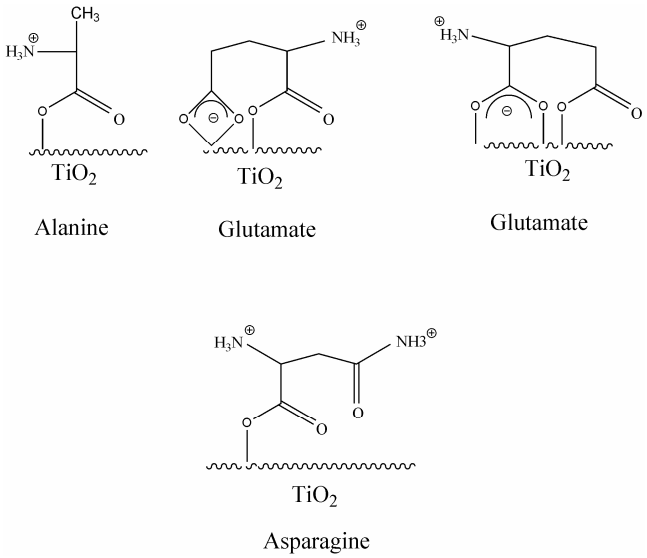

Scheme 6-2: Proposed adsorption modes of amino acids on TiO_2

6.3.1 L-Alanine

L-Alanine has an isoelectric point (pI) of 6 and pKa values of 2.35 and 9.87.[8]

Figure 6-1 shows ATR spectra of 0.1M L-alanine in the water solution (a) and 1mM alanine adsorbed on TiO_2 (b) both at pH= 3. The reference spectra are recorded in water over the bear Ge IRE (1mm) and over Ge IRE coated with TiO_2 thin film and water.

At pH= 3, the carboxyl group of alanine is deprotonated, which is confirmed by the absence of the band at 1733 cm^{-1} in the solution spectrum (see Figure 6-1 (a)) that is characteristic for the carbonyl stretching in the protonated carboxylic acid group of alanine. After flowing alanine through the cell and over the TiO_2 surface clear bands are observed in the ATR-IR spectrum (Figure 6-1 (b)) showing that alanine interacts with TiO_2 surface. The bands at 1608 cm^{-1} and 1416 cm^{-1} (Figure 6-1 (b)) are assigned to asymmetric and symmetric carboxylate stretching vibrations of adsorbed alanine. Upon adsorption the two carboxylate bands of adsorbed alanine shift slightly. The amino group of alanine is protonated at this pH as well. The broad band at 1517 cm^{-1} is assigned to the symmetric deformation mode of the NH_3^+. This band is very similar in shape and position for dissolved and adsorbed alanine. Several reports suggest that alanine interacts with TiO_2 via the carboxylate in a bridging form[6, 9]. Also, Nosaka at al. proposed an interaction of alanine with TiO_2 surface via acidic bridged OH groups on TiO_2[10]. From our experiments we propose an adsorption mode with

monodentate carboxylate for the L-alanine shown in Scheme 6-1. This assignment is based on the wavenumber difference Δ between the $\nu_{as}(COO^-)$ and $\nu_s(COO^-)$ modes of dissolved and adsorbed alanine.[11-13]

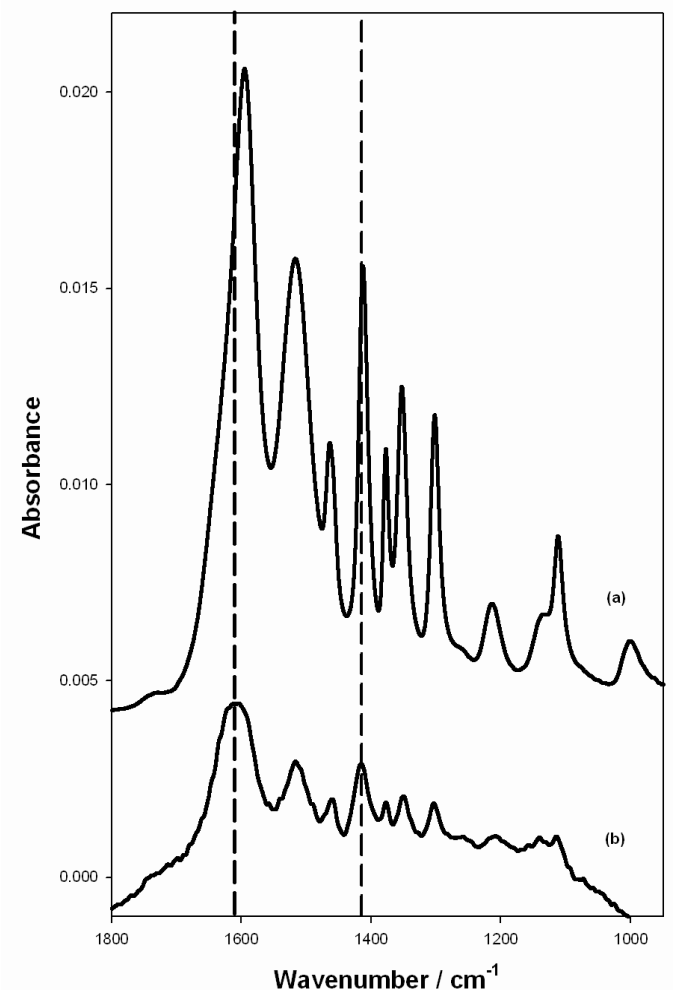

Figure 6-1: ATR-IR spectra of L-Alanine aqueous solutions over bare Ge IRE at concentration (0.1M) (a) and over TiO_2 film at (1mM) (b) both at pH=3

In the spectrum for adsorbed alanine wavenumber difference is $\Delta vas - vs = 197cm^{-1}$ and for dissolved L-alanine this difference in energy is $\Delta vas - s = 182cm^{-1}$, which is characteristic of monodentate adsorption. The observation that the symmetric deformation mode of the NH_3^+ is not affected by adsorption indicates that this functional group is not directly interacting with the surface.

6.3.2 L-Glutamic acid

Figure 6-2 shows (a) normal and (b) ^{15}N labeled L-glutamic acid in water at pH= 3.5. At this pH the distal carboxylic group is protonated which was confirmed by a band at 1717 cm^{-1} due to carbonyl stretching of the protonated carboxylic group. Glutamic acid has an isoelectric point (pI) of 3.15 with pKa values of 2.10, 4.3 and 9.478. The bands at 1600 and at 1407 cm^{-1} do not shift with labeling of the glutamic acid suggesting asymmetric and symmetric stretching of the $\alpha - COO^-$ group. Note that only the nitrogen atom of the amino group of glutamic acid is labeled. A broad shoulder at 1641 cm^{-1} appears in the spectrum for the labeled glutamic acid and a slight shift to lower wavenumbers of the band at 1518 cm^{-1} reveal the positions for asymmetric and symmetric deformation of the NH_3^+ group.

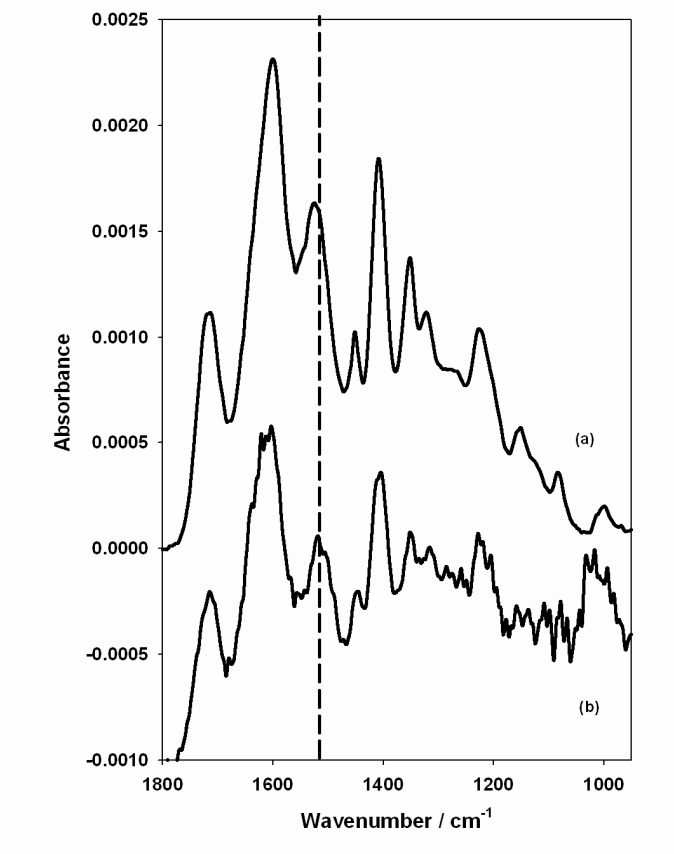

Figure 6-2: ATR-IR spectra of normal (a) and labeled (b) L-glutamic acid aqueous solutions over Ge IRE at pH=3.5

Figure 6-3 shows labeled and normal glutamic acid adsorbed on TiO_2 at pH= 3.5. The band at 1717 cm^{-1} (Figure 6-3) vanishes upon adsorption of glutamic acid on the TiO_2. This suggests deprotonation of the distal carboxylic acids group upon adsorption on TiO_2. As it

was proposed by McQuillan, the most intense bands at 1600 and 1553 cm^{-1} of adsorbed of L-glutamic acid on TiO_2 are assigned to the asymmetric carboxylate vibrations of glutamate[3]. Also the two bands at 1446 and 1407 cm^{-1} do not shift upon labeling and these bands can be assigned to the symmetric stretching modes of glutamate on TiO_2. Both carboxylate groups of glutamic acid are coordinated to TiO_2 and different adsorption modes are possible. Scheme 6-2 shows possible adsorption modes for glutamate on TiO_2.

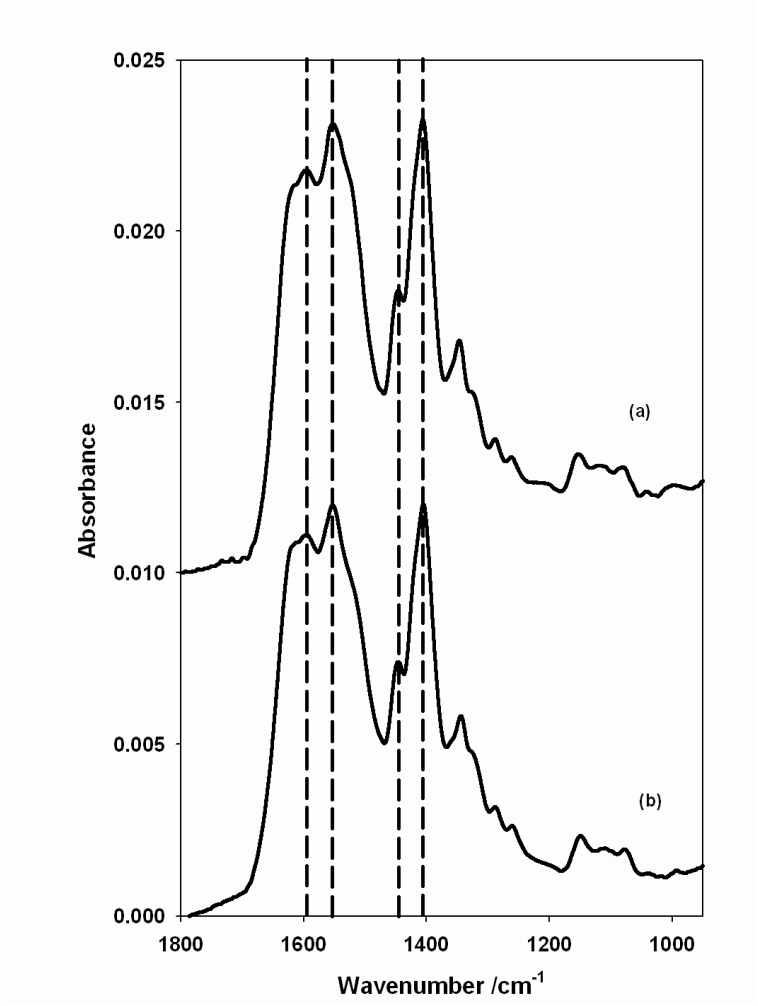

Figure 6-3: ATR-IR spectra of adsorbed normal (a) and labeled (b) L-glutamic acid onto TiO_2 thin film from aqueous solution at pH=3.5

6.3.3 L-Asparagine

Figure 6-4 shows infrared spectra of (a) L-asparagine and (b) L-$^{15}N_2$ asparagine dissolved in water over a Ge IRE at pH 3.5. The reference is water at the same pH on the respective IRE. The pKa values of L-asparagine (L-Asn) are 2.02 and 8.80[8]. The spectra show

that at this pH the carboxylic acid group of L-Asn is totally deprotonated since no band was observed above 1700 cm^{-1} that characterize the carbonyl stretching vibration of the protonated acid. Upon labeling significant shifts can be observed.

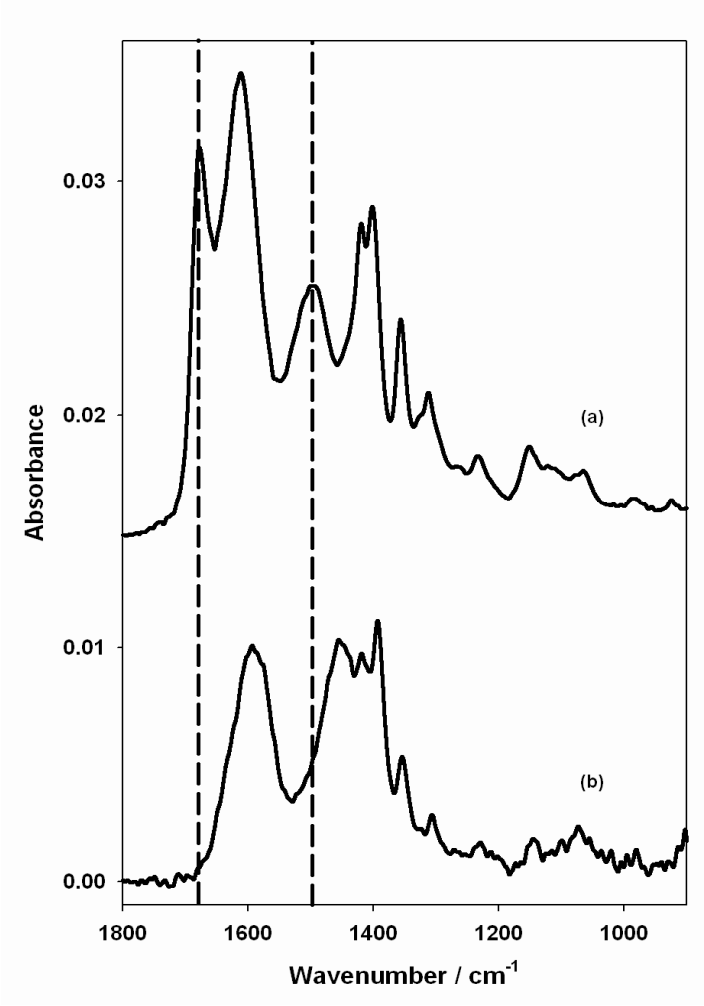

Figure 6-4: ATR-IR spectra of normal (a) and labeled (b) L-asparagine dissolved in water and recorded over Ge IRE at pH=3.5

For example the prominent amide band at 1678 cm^{-1} of unlabeled L-Asn shifts down upon labeling and merges with the broad feature around 1591 cm^{-1}. For the unlabeled L-Asn, spectrum (a), the large absorption band at 1612 cm^{-1} can be assigned to the antisymmetric carboxylate stretching and the sharp band at 1412 cm^{-1} to the symmetric stretching of the carboxylate. In the spectrum of the labeled L-Asn the band at 1591 cm^{-1} comprises the antisymmetric carboxylate stretching as well as the shifted amide band. The broad band at 1496 cm^{-1} in the spectrum (a) of unlabeled L-Asn shifts down upon labeling to 1457 cm^{-1} showing that nitrogen is involved in the corresponding vibration. This band may thus be

assigned to the symmetric deformation of the amino group. Note that both nitrogen atoms in L-Asn are labeled. Also the position of the band at 1403 cm^{-1}(unlabeled L-Asn) shifts down to 1393 cm-^{1} (labeled L-Asn). This band can be assigned to a NH_2 deformation of L-Asn. Bands at 1357 and 1313 cm^{-1} in the spectrum of unlabeled L-Asn are also shift down upon labeling and represent combination vibrations of C-N stretching and C-H deformation modes.

Figure 6-5 shows ATR-IR spectra of normal (a) and labeled (b) L-Asn on TiO_2 adsorbed from 1mM solution. After 40 minutes of flowing the amino acid over TiO_2 adsorption equilibrium is reached.

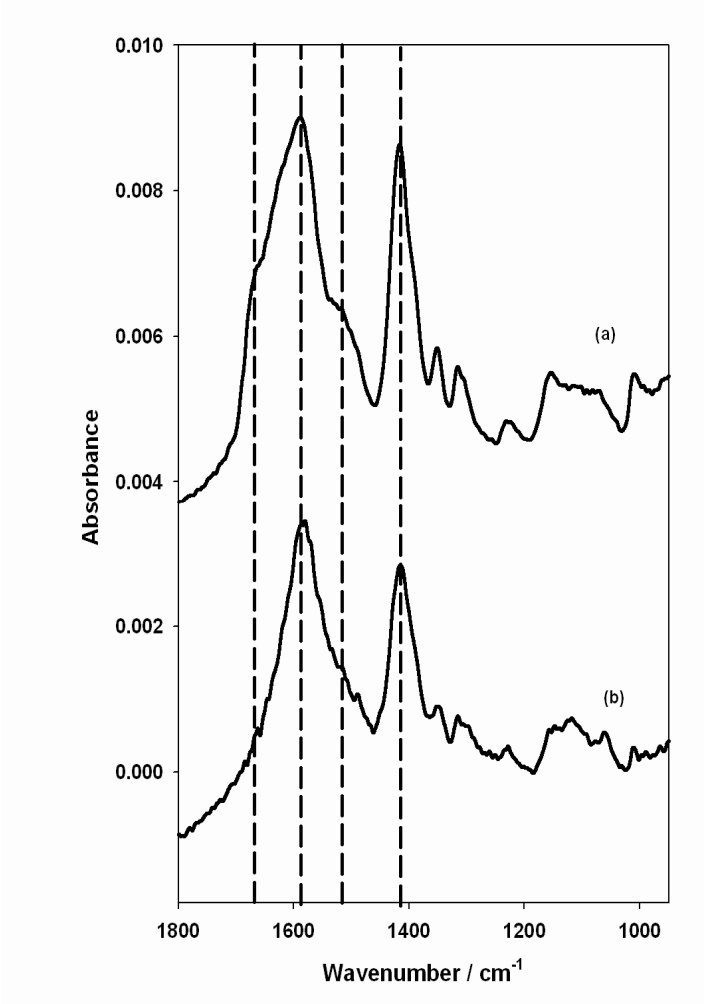

Figure 6-5: ATR-IR spectra of normal (a) and labeled (b) L-asparagine adsorbed onto TiO_2 thin film from aqueous solution (1mM) at pH=3.5

Note that at this concentration L-Asn was not detected in solution. The bands highest in intensity represent symmetric and asymmetric stretching of the carboxylate group of

L-Asn. The difference in the spectra of adsorbed and dissolved L-Asn suggests a specific interaction of the L-Asn with TiO_2. In this case the Δ value for the carboxylate of adsorbed L-Asn is 211 wavenumbers and for the dissolved L-Asn it is 192 wavenumbers. This suggests that L-Asn adsorbs to TiO_2 in monodentate form as is shown in Scheme 6-2. Again the bands associated with vibrations involving the nitrogen are shifting upon labeling.

6.4 Photocatalysis of amino acids

Figure 6-6 reveals the effect of UV illumination on the adsorbed amino acids as investigated by ATR-IR spectroscopy. First the amino acids were adsorbed in the dark on TiO_2 from water solution at a concentration of 1 mM at pH= 3.5. Note that at this concentration amino acids are not observed without TiO_2 film. The bottom spectra correspond to adsorbed (a) L-alanine, (b) L-asparagine, (c) L-glutamic acid on TiO_2 after adsorption in the dark. Upon UV illumination band characteristic for amino acids decay and new bands appear on the TiO_2 surface. The subsequent spectra were recorded in the dark and while flowing neat water over theTiO_2 film. This leads to desorption of the adsorbed amino acids, leaving behind on the TiO_2 surface the species that were formed during illumination. Previously pyruvic acid was determined as dominant species during L-alanine photodecomposition. Also acetic acid was detected as stable intermediate species during mineralization of L-alanine investigated by NMR.[14] However there is no clear sign of those species in our experiments. This discrepancy may arise from the fact that in the above mentioned report only dissolved species were analyzed, whereas in the present work, by using ATR-IR spectroscopy, special emphasis is given to adsorbed species. Acetic acid is known to adsorb only relatively weakly on TiO_2[15] and so does likely pyruvic acid.

A dominant species on TiO_2 observed during illumination of all three investigated amino acids is oxalate. We have shown before that the bands at 1708, 1690, 1421 and 1275 cm^{-1} are characteristic of the oxalate ($^-O_2C\text{-}CO_2^-$). The bands at 1421 and 1275 cm^{-1} are assigned to C-O + C-C and C-O + O-CO vibrations.

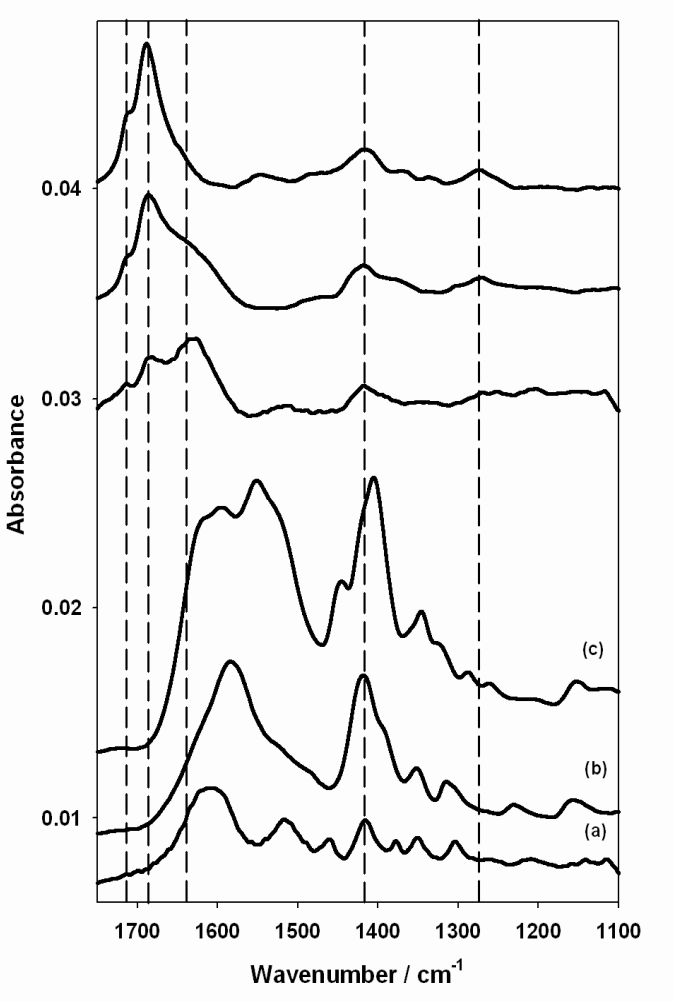

Figure 6-6: ATR-IR spectra of adsorbed (a) alanine, (b) aspartate and (c) glutamate on TiO_2 thin film from aqueous solution. All spectra were recorded at same pH=3.5 and same concentrations (1mM). Subsequent spectra represent new formed species after irradiation and washed with water in dark.

The two distinct vibrational bands in the spectrum around 1700 cm^{-1} correspond to the symmetric and antisymmetric C=O stretching vibration [16, 17]. We have shown before that oxalate hardly desorbs from TiO_2 and that it is readily decomposed upon UV illumination to two CO_2 molecules by consumption of two photogenerated holes. Therefore, oxalate can hardly be detected in solution and in particular not by 1H NMR. That is probably why in previous studies oxalate was not found, even though our experiments indicate that it is a mayor intermediate in the decomposition of amino acids.

Due to their complex structure amino acids are certainly not transformed completely to the oxalate. The fate of amino acids upon UV irradiation on TiO_2 is more complex. Some authors reported the presence of different species during mineralization like NH_4^+, NO_3^- and

CO_2[5]. A strong band that is observed especially in the mineralization of alanine at 1635 cm^{-1} can be assigned to the NH_4^+ ion on TiO_2 the surface (Figure 6-6). The same band is detected for the other two amino acids as well, although at lower intensity. The possible assignment of this band to NH_4^+ was confirmed by adsorption of NH_4Cl solution on TiO_2 (spectra not shown). We will show later that other species can be detected during amino acid decomposition by ATR-IR spectroscopy in combination with modulation excitation spectroscopy.

6.5 Conclusions

The adsorption of L-alanine, L-glutamic acid and L-asparagine on TiO_2 film from aqueous solution was studied by ATR-IR spectroscopy. ^{15}N isotopic labeling helped the assignment of the bands in the spectra. Photocatalysis of those amino acids over P25 TiO_2 is possible and it was followed in situ by ATR-IR. The content of adsorbed amino acids on the TiO_2 surface decreases upon UV illumination and oxalate was detected on TiO_2 surface. Oxalate was not observed before by studies mainly focusing on the dissolved species. Besides oxalate as dominant intermediate species on the surface during mineralization, ammonium was observed on the TiO_2 surface as well. The relative surface concentration of oxalate to ammonium was significantly different for the three investigated amino acids. This indicates that for different amino acids different reaction routes predominate.

References

(1) Roddick-Lanzilotta, A. D.; Connor, P. A.; McQuillan, A. J. Langmuir 1998, 14, 6479.

(2) Roddick-Lanzilotta, A. D.; McQuillan, A. J. Journal of Colloid and Interface Science 1999, 217, 194.

(3) Roddick-Lanzilotta, A. D.; McQuillan, A. J. Journal of Colloid and Interface Science 2000, 227, 48.

(4) Hidaka, H. Catalysis Letters, 60, 95.

(5) Hidaka, H.; Horikoshi, S.; Ajisaka, K.; Zhao, J.; Serpone, N. Journal Of Photochemistry And Photobiology A-Chemistry 1997, 108, 197.

(6) Carravetta, V. The journal of physical chemistry. B, Condensed matter, materials, surfaces, interfaces & biophysical, 110, 6160.

(7) Dolamic, I.; Bürgi, T. J. Phys. Chem. B 2006, 110, 14898.

(8) J. P. Greenslein and M. Winitz New York London, John Wiley and Sons, inc.

(9) Martra, G.; Horikoshi, S.; Anpo, M.; Coluccia, S.; Hidaka, H. Research on Chemical Intermediates 2002, 28, 359.

(10) Tran, T. H.; Nosaka, A. Y.; Nosaka, Y. Journal of Physical Chemistry B 2006, 110, 25525.

(11) Rotzinger, F. P.; Kesselman-Truttmann, J. M.; Hug, S.; Shklover, V.; Grätzel, M. J. Phys. Chem. B 2004, 108, 5004

(12) Ferri, D.; Bürgi, T.; Baiker, A. Helv. Chim. Acta 2002, 85, 3639.

(13) Dobson, K. D.; McQuillan, A. J. Spectrochim. Acta 1999, A 55, 1395.

(14) Matsushita, M.; Tran, T. H.; Nosaka, A. Y.; Nosaka, Y. Catalysis Today 2007, 120, 240.

(15) Rotzinger, F. The journal of physical chemistry. B, Condensed matter, materials, surfaces, interfaces & biophysical 2004, 108, 5004.

(16) Dolamic, I.; Burgi, T. Journal of Physical Chemistry B 2006, 110, 14898.

(17) Dolamic, I.; Burgi, T. Journal of Catalysis 2007, 248, 268.

7

Photocatalysis of Amino acids on TiO_2 Studied by in-Situ ATR-IR Spectroscopy

7.1 Abstract

The phototcatalysis of L-asparagine and L-glutamic acid over Au/TiO_2 and TiO_2 catalyst is investigated in situ by attenuated total reflection infrared (ATR-IR) spectroscopy in combination with modulation excitation spectroscopy. Oxalate is detected on the catalyst surface, which was not reported before by studies focusing on intermediates in solution. The ATR-IR spectra provide valuable information on the fate of the nitrogen. Ammonium is detected, in agreement with previous studies. Most importantly, strong signals of cyanide are observed, and this assignment is corroborated by ^{15}N labeling experiments. Cyanide was not reported before, to the best of our knowledge, for the photocatalysis of amino acids. Cyanide is formed in the presence and the absence of gold particles on the TiO_2 surface. The cyanide leads to leaching of gold via $[Au(CN)_2]^-$ species that are observed in solution by mass spectrometry. The finding that cyanide is formed in the photocatalysis of amino acid is relevant in view of the application of photocatalysis for purification of drinking water.

7.2 Introduction

Water purification is becoming an increasingly important subject due to human driven environmental pollution. Particularly, making available drinking water may become a mayor issue in forthcoming decades. An efficient and ecological way is the sun-light driven potocatalytic treatment of polluted water using semiconductor materials such as TiO_2. TiO_2 is a promising photocatalyst because it is chemically inert, has a strong oxidation power and is cheap. Organic molecules, i.e. pollutants containing C, H and O, can be mineralized completely to water and CO_2 over TiO_2.

An interesting application of photocatalysis by TiO_2-based materials is the elimination of microorganisms like bacteria, fungi and single-celled organisms. Abatement of these in a simple but efficient way is crucial for providing drinking water to a large fraction of today's world population. The microorganisms mentioned above are complex aggregates of different bio-molecules. In order to better understand their behavior under photocatalytic conditions it is beneficial to better understand the behavior of the individual constituents. Here we focus on the photocatalysis of amino acids over TiO_2-based materials. This has been the subject of several investigations.[1-6]

Particular interesting in these studies is the fate of the heteroatoms nitrogen and sulfur. We have shown recently that photocatalyis of cysteine derivatives leads to sulfate species.[7] The fate of the nitrogen has been studied for various amino acids for example by Hidaka and coworkers, who detected ammonia (NH_4^+) and nitrate (NO_3^-) chromatographically at ratios of 3-12 after eight hours reaction time in a batch reactor[5, 8].

Photo-excitation of an electron from the valence to the conduction band of TiO_2 leads to the generation of an electron-hole pair. In order to extend the lifetime of the electron – hole pair and to increase the efficiency of the process metal nanoparticles can be used, which act as an electron acceptor[7, 9]. Both the electron and the hole can migrate to the surface of the catalyst particle and induce chemical reactions. Photocatalysis by TiO_2 is largely an interface phenomenon. We therefore chose to study the catalytic solid-liquid interface in situ by a combination of attenuated total reflection infrared (ATR-IR) spectroscopy and modulation excitation spectroscopy (MES)[10-12]. The former technique allows one to measure vibrational spectra of the interface and the latter provides, among other things, an increased sensitivity. Using this combination of techniques we show here that on the catalyst surface oxalate is formed as an important intermediate. Oxalate was not reported before in studies focusing on the photocatalysis of amino acids probably because it does not desorb into the solution. More importantly we observe strong signals of cyanide (CN^-) in the spectra. Cyanide was not reported before for the photocatalysis of amino acids but of course this finding is relevant in view of the importance of photocatalysis to provide clean drinking water.

7.3 Experimental

7.3.1 Catalyst and chemicals

Commercial type Degussa P25 TiO_2 composed of 80% anatase and 20% rutile with surface area of 51 m^2/g and average particle size of 21 nm was used in the photocatalytic experiments. L-Asparagine (Fluka, 99.5%, L-Asn), L-asparagine -$^{15}N_2$ (ISOTEC 98% ^{15}N), L-glutamic acid (Fluka, 99.5%, L-Glu), L-glutamic ^{15}N acid (Aldrich 98% ^{15}N), KCN (Fluka, $\geq$98, 0%) and HCl (Carlo Erba, 37%) was used as received.

7.3.2 Preparation of the Au-TiO_2 active catalyst

N-acetyl-L-cysteine monolayer protected gold nanoparticles were prepared as reported previously [13] and were used for the preparation of the gold titanium dioxide catalysts Au-TiO_2. 20 mg of N-acetyl L-cysteine protected gold nanoparticles of 1-2 nm in core size diameter were dissolved in 500 ml of water. The pH of this solution is in the range of 6, which is close to isoelectric point (IEP) of P25 TiO_2.[14] The water solution of gold nanoparticles was adjusted by addition of 0.1M HCl to pH= 3.5 and 500 mg of TiO_2 powder was added to the solution. At this pH the surface of TiO_2 is positively charged which forces the adsorption of the gold particles. The slurry was stirred for two hours, filtered off and washed with water. The catalyst was then heated for 2 hours to 300° C in air. This liberates the N-acetyl-L-cysteine from the gold particle surface and leads to agglomeration. Figure 7-1 shows Transmission Electron Microscopy (TEM) of the Au-TiO_2 catalysts before and after annealing at 300° C. The size of gold nanoparticles after heating was 5 nm and the gold loading about 2.7 wt %. Besides this Au-TiO_2 catalyst TiO_2 was used for comparison in some experiments.

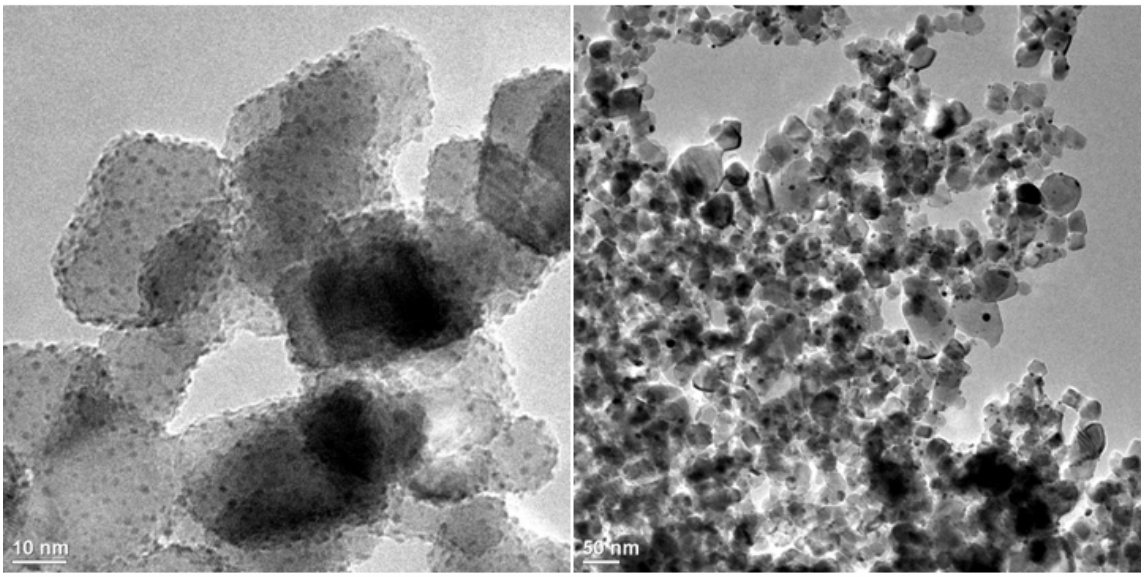

Figure 7-1: Transmission electron microscopy (TEM) images of NAC-protected gold nanoparticles on TiO_2 before (left) and after (right) two hours of annealing at 300°C.

Thin films of the catalyst were prepared by dissolving 25 mg of Au-TiO_2 catalyst in 25 mL of water (Milli-Q, 18 MΩcm). The slurry was sonicated (Branson 200 ultrasonic cleaner) for 30 minutes. The thin film was formed by dropping the slurry onto a Ge internal reflection element (IRE, 52mm x 20mm x 1 mm; KOMLAS). After solvent was evaporated at 30°C the procedure was repeated three times. After drying for several minutes at 30°C in air,

loose catalyst particles were removed by flowing water over the IRE. For every experiment a new catalyst film was prepared.

7.3.3 In situ spectroscopy

ATR spectra were recorded with a dedicated flow-through cell, made from a Teflon piece, a fused silica plate (45mm x 35mm x 3 mm) with holes for in- and outlet (36 mm apart), and a flat (1mm) viton seal. The cell was mounted on an attachment for ATR measurements within the sample compartment of a Bruker Equinox-55 FTIR spectrometer equipped with a narrow-band MCT detector. Spectra were recorded at 4 cm^{-1}. For irradiation of the sample UV light was provided by a 75 W Xenon arc lamp. The UV light from the source was guided to the ATR-IR cell via two fiber bundles. The light was passed through a 5 cm water filter to remove any infrared radiation. A Schott UG 11 and BG 42 (50mm x 50mm x 1 mm) broadband filter from ITOS was used to remove visible light (transmission between 270 and 380 nm). An estimate based on the supplier specifications gave a power at the sample of slightly less than 2 mW/cm^2. The experimental setup is schematically shown in Figure 7-2.

Electron spray mass spectrometry was used to identify dissolved species. These measurements were performed on a LCQ-IT, Finning® instrument equipped with ESI source.

7.3.4 Modulation excitation spectroscopy (MES) and data acquisition

The catalytic system was stimulated by periodically varying of UV light flux. The concentrations of all species in the system which are affected by this external parameter also change periodically. Phase sensitive detection and subsequent demodulation of the spectra separates the periodically varying from the static signals. By applying MES in combination with ATR-IR spectroscopy, the signal to noise ratio can be significantly improved, which assists in the detection of minor species occurring during reaction. During one modulation period (typically 150–235 s), 60 IR spectra were recorded at a sampling rate of 40 or 80 kHz (4–8 scans/s) using the rapid scan function of the FTIR spectrometer. Typically 20 scans per spectrum recorded in a single period were averaged. Two modulation periods were performed before data acquisition was started. The IR spectra were then averaged over five modulation periods. UV light modulation was achieved using an electronic shutter (Newport model 71445). The light flux was modulated (on-off) in the presence of aqueous amino acid solution over Au-TiO_2. Electrical signals generated by the FTIR spectrometer within the data

acquisition loop were used to switch the shutter in order to synchronize modulation and data acquisition. Before the modulation experiments, the amino acids solutions were flowed over Au-TiO_2 catalyst for 45 minutes in the dark. After 45 minutes adsorption equilibrium was reached. The time-resolved absorbance spectra $A=(\tilde{\nu},t)$ where transformed into phase-resolved spectra using a digital phase sensitive detection (PSD) according to:

$$A_k^{\phi_k^{PSD}}(\tilde{\nu}) = \frac{2}{T}\int_0^T A(\tilde{\nu},t)\ \sin\left(k\omega t + \phi_k^{PSD}\right)\ dt \qquad \text{Equation 7-1}$$

Where k= 1, 2, 3… determines the demodulation frequency (e.g., fundamental, first harmonic), T is the modulation period, $\tilde{\nu}$ denotes the wavenumber, ω the stimulation frequencies and ϕ_k^{PSD} is the demodulation phase angle. With a set of time resolved spectra $A(\tilde{\nu},t)$ the foregoing equation can be evaluated for different demodulation phase angles, ϕ_k^{PSD} resulting in a series of phase-resolved spectra $A_k^{\phi_k^{PSD}}$. Modulation experiments are applicable only when the system response is reversible. More information about technique can be fined elsewhere [15, 16].

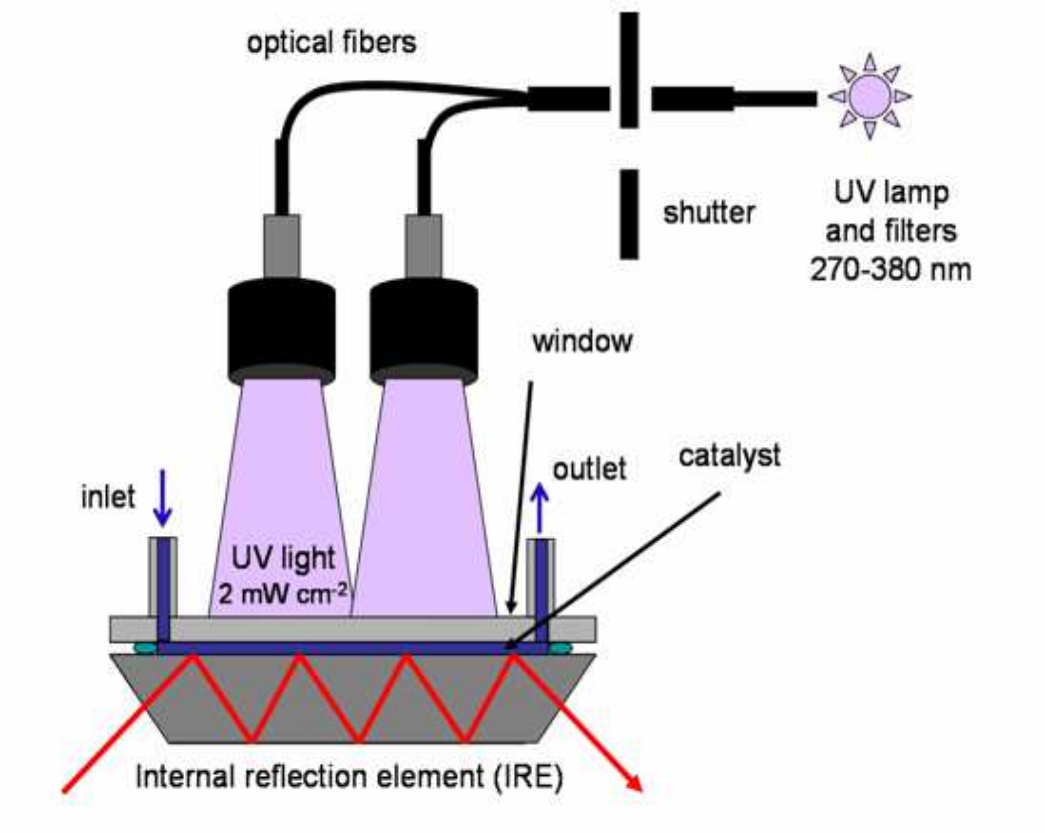

Figure 7-2: Schematic setup for in situ ATR-IR spectroscopy of photocatalytic reactions in a small volume flow-through cell.

7.4 Results and discussion

7.4.1 Intermediate species during amino acid mineralization over TiO_2 and Au-TiO_2

ATR-IR spectroscopy in combination with modulation spectroscopy shows that during photocatalytic mineralization of amino acids over TiO_2 and Au-TiO_2 film several different processes can occur on the surface, which is likely related to the complex structure of these molecules. Intermediate species formed upon illumination strongly depend on the reaction conditions, like pH, concentration of dissolved oxygen and on the catalyst used. Amino acids can be transformed to oxalate, which is further mineralized to CO_2[17]. Figure 7-3 shows light modulation experiments under different conditions for the mineralization of L-Glu over Au-TiO_2. When oxygen is present in the experiments oxalate occurs on the surface (spectrum (c)) giving rise to the bands at 1709 and 1421 cm^{-1}.

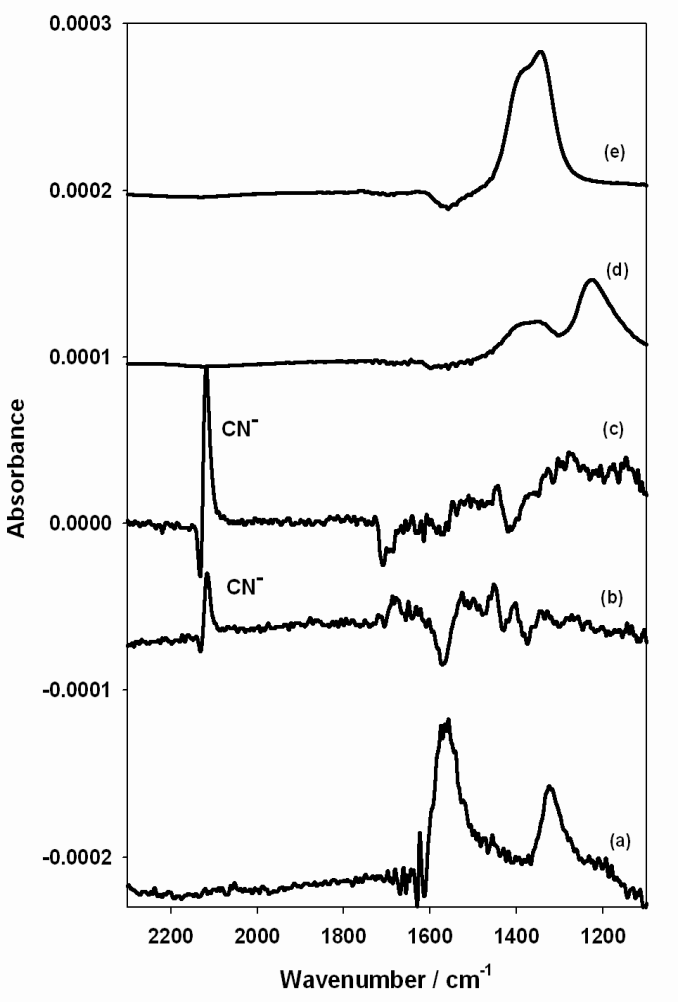

Figure 7-3: ATR spectra of (a) NH_4Cl (d) $NaNO_2$ (e) $NaNO_3$ adsorbed from aqueous solution on Au-TiO_2 and demodulated ATR-IR spectra of a light modulation experiment where solution of L-glu (1mM) were flowed over Au-TiO_2 saturated by N_2, spectrum (b) and O_2, spectrum (c).When oxygen is present in the experiments oxalate occurs on the surface (spectrum (c)).

In contrast, when the reactant solution was saturated by N_2 (spectrum (b)) oxalate species are suppressed. The dominant broad band at 1567 cm^{-1} in the spectrum indicates the presence of ammonium ions NH_4^+ on Au-TiO_2. As a comparison, spectrum (a) was recorded while exposing the Au-TiO_2 catalyst to aqueous NH_4Cl solution. This is in agreement with a previous report showing that the nitrogen of the amino acids are photoconverted predominantly into NH_4^+ and into NO_3^- ions[5]. In this work the fate of the nitrogen atom(s) of some amino acids was analyzed using chromatographic methods after about 8 hours of illumination. NH_4^+/NO_3^- ratios of 3-12 were found. Our experiments indicate the presence of NH_4^+ but no clear sign of NO_3^- (nor NO_2^-) was found (see spectra (d) and (e) for comparison). It should be noted however, that the conditions in the report mentioned above and applied

here are different, most importantly the residence time. In our flow-through system the reactant solution is in contact with the catalyst film for some seconds only, whereas eight hours of irradiation in a batch system was used in ref [5]. This might indicate that the formation of oxidized species like NO_3^- is a relatively slow process. A study on the photocatalysis of polyvinylpyrrolidone polymer over TiO_2 showed that NH_4^+ is formed immediately, whereas NO_3^- was achieved only after about 30 minutes of irradiation[8]. The most prominent feature in the demodulated ATR-IR spectra both in the presence and absence of dissolved oxygen is a bipolar band at 2133 and 2119 cm^{-1}, which will be discussed in detail in the following.

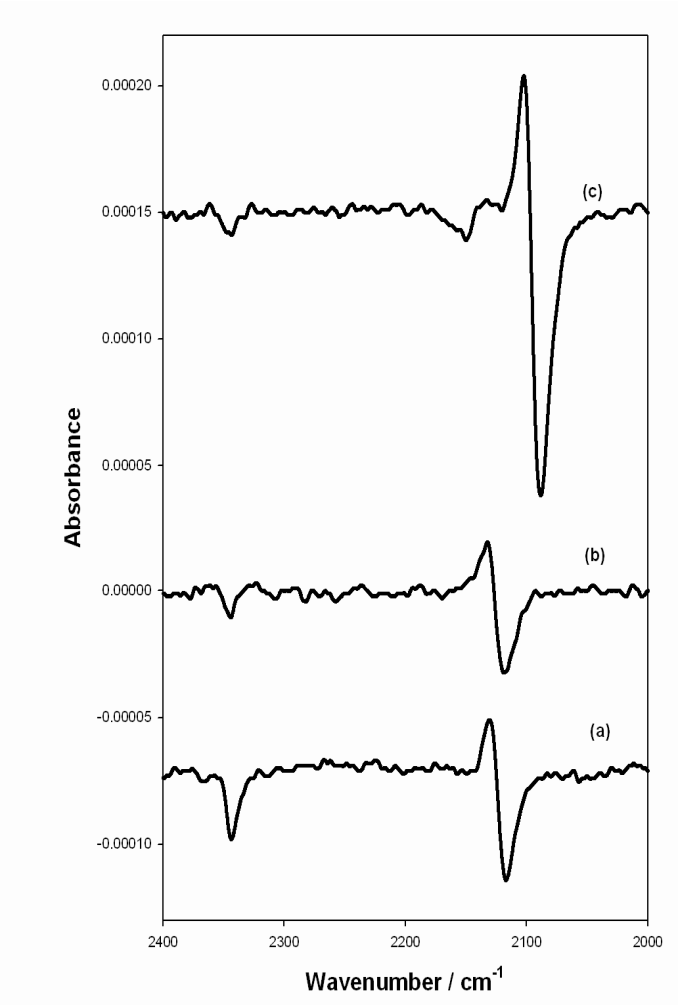

Figure 7-4: ATR demodulated spectra of light modulation experiments where aqueous solution of (a) L-Glu acid (b) L-Asn and (c) $^{15}N_2$-labeled L-Asn (1mM) were flowed over the Au-TiO_2.

Figure 7-4 shows demodulated spectra of light modulation experiments. In the experiments, solutions of L-Glu (a), L-Asn (b) and ^{15}N–labelled L-Asn (c), respectively, at pH = 3.5 were flowed through the ATR-IR cell and over Au-TiO_2 film.

The two most prominent bands in spectra (a) and (b) are observed at 2133 and 2119 cm^{-1} and will be shown in the following to belong to cyanide CN^- ions adsorbed on the gold nanoparticles. To understand the bipolar nature of the signal (positive, negative) one has to recall that demodulated spectra can be understood as difference spectra between two states. In this case the two states correspond to light-on and light-off situations. The low energy component at 2119 cm^{-1} is formed during decomposition of the amino acids upon illumination and corresponds to cyanide adsorbed on the gold surface under these conditions. The high energy component at 2133 cm^{-1} belongs to the same species on the gold but in the dark. Spectrum (c) shows the same species from the experiment where labeled L-Asn was used. Note that all nitrogen atoms are labelled (^{15}N) in L-Asn. The shifts due to the labeling are consistent with CN^-.

The band observed at 2343 cm^{-1} in all experiments is due to dissolved CO_2, which stems from the mineralization of the amino acid. Also, when the CN^- bands shift to lower wavenumbers upon labeling a new band becomes evident in the spectrum at 2157 cm^{-1}. The band may be assigned to CO adsorbed on Ti-OH groups. This band position is in good agreement with previous reports.[18] The characteristic band for the Ti^{4+}-CO, which is around 2200 cm^{-1}, is not observed in our experiments.[19]

To corroborate the identification of the CN^- ions and to learn more about its interaction with the Au-TiO_2 catalyst an aqueous KCN solution ($1.5x10^{-4}$M) was flowed over the sample. The ATR-IR spectra of this experiment are shown in Figure 7-5.

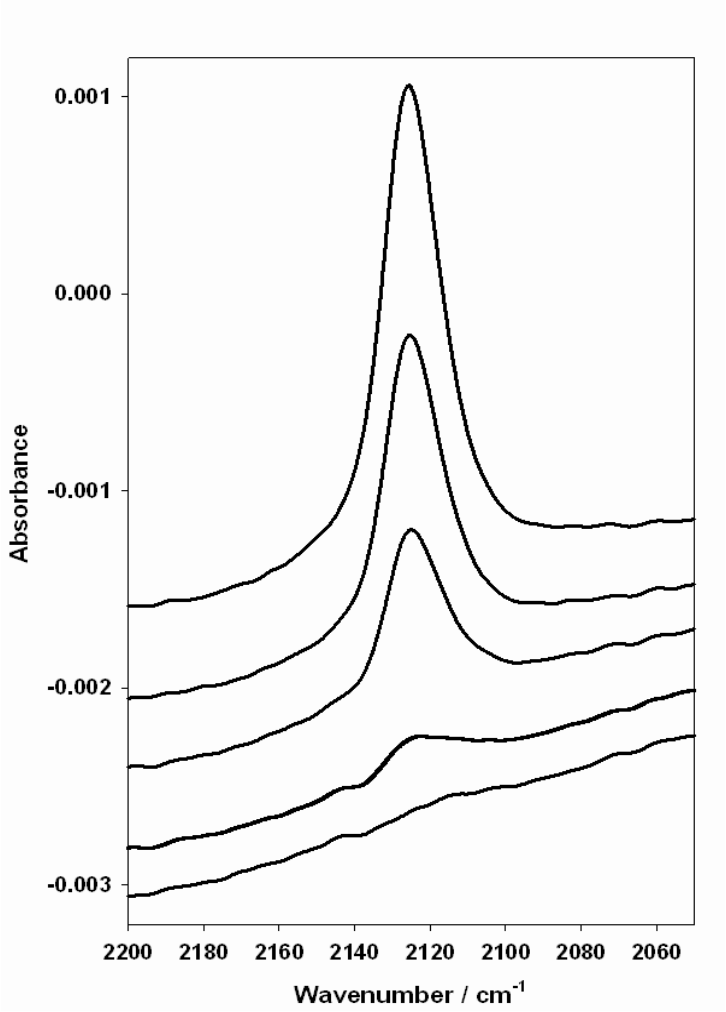

Figure 7-5: ATR spectra recorded while flowing KCN aqueous solution ($1.5x10^{-4}$M) over Au-TiO_2 film. The spectra were recorded at 0, 34, 68, 117, 175 seconds from top to bottom, after starting the flow of solution over the film.

Right after starting the flow a band centered at 2125 cm^{-1} becomes evident associated with CN^- adsorbed on gold, in good agreement with the bands observed in the demodulated spectra. However, immediately after that the intensity of the band decreases and completely disappears within around 3 minutes. This behavior indicates very fast adsorption of CN^- followed by oxidation of the gold to $[Au(CN)_2]^-$ and leaching of gold from the TiO_2 surface. Gold cyanidation, i.e. the extraction of gold with cyanide, is a well known process, which is for example used in gold mining. Indeed, ESI-MS analysis showed the presence of $[Au(CN)_2]^-$ after admitting KCN to Au-TiO_2 catalyst.

Figure 7-6 shows the signals at 2133 and 2119 $cm^{-1}$of CN^- as function of time during the light modulation experiment of L-Glu.

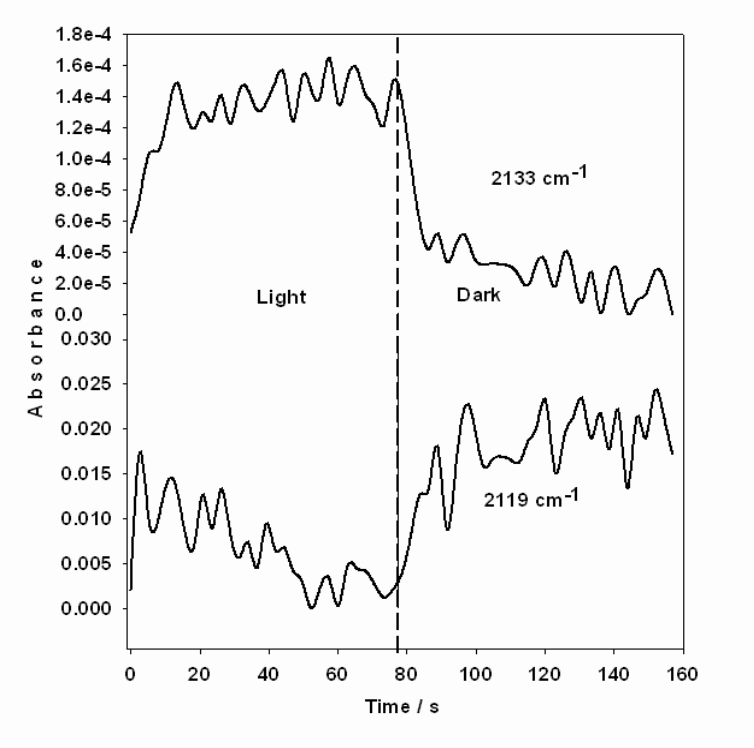

Figure 7-6: ATR signals as a function of time for a light modulation experiments with modulation period T=157s. At t= 0 the UV light was switched on and light was switched off at =78.5 s. The ATR signals were average over five modulation periods.

With the light on, the intensity of the band at 2119 cm^{-1} decrease and it increase fast when switching the light off again. At the same time the band at 2133 cm^{-1} grows. We ascribe this behavior of the CN^- stretching frequency in the light modulation to different electronic structure of the catalyst during illumination and in the dark. During illumination photogenerated electrons and holes diffuse to the surface of the TiO_2 particles. Electrons can react with Ti sites according to $e^- + Ti(IV)\text{-}O\text{-}H \rightarrow Ti(III)\text{-}O\text{-}H^-$. When illuminating the Au-TiO_2 catalyst the excited electrons from the valence band are accepted by gold nanoparticles due to their high electron affinity and are not (or at least less) trapped at the Ti(IV) sites. Due to the tendency to accept electrons during illumination the potential of the gold particles shifts negative and this affects the vibrational frequency of CN^- species adsorbed on the metal surface.[20] From the shift the potential change can be estimated to around 0.5 V.[20]

Figure 7-6 also shows that the bands at 2133 and 2119 cm^{-1} show different kinetics of appearance and disappearances. In the dark and during illumination the properties of the gold particles are different due to the different potential. When the gold particles are electron rich the potential is negative and the coverage of the adsorbed CN^- increases. When the gold

particles become neutral, the coverage of adsorbed CN^- species decrease upon oxidation of gold nanoparticles. The time-resolved spectra show that CN^- species are present on the surface during both experimental states, i.e. in the dark and in the light (spectra not shown).

The presence of the CN^- species on the Au-TiO_2 catalyst, as spectroscopically observed, may imply leaching of the gold nanoparticles from the TiO_2 and formation of $[Au(CN)_2]^-$ complexes in the solution. Figure 7-7 shows the ESI-MS spectrum of the cell effluent gathered for a photocatalytic experiment where L-Asn was decomposed over Au-TiO_2.

During that experiment L-Asn was adsorbed in the dark on Au-TiO_2 catalyst. Reaching adsorption equilibrium the UV light was switched on and a sample was colleted at the ATR cell outlet for 10 minutes. The ions at 131 and 167 m/z are assigned as $[L\text{-}Asn - H]^-$ and $[L\text{-}Asn - H + 2H_2O]^-$, respectively, corresponding to unreacted L-Asn. The ion at 249.27 m/z is assigned as $[Au(CN)_2]^-$ can be related to the process of gold leaching during degradation of amino acid over Au-TiO_2.

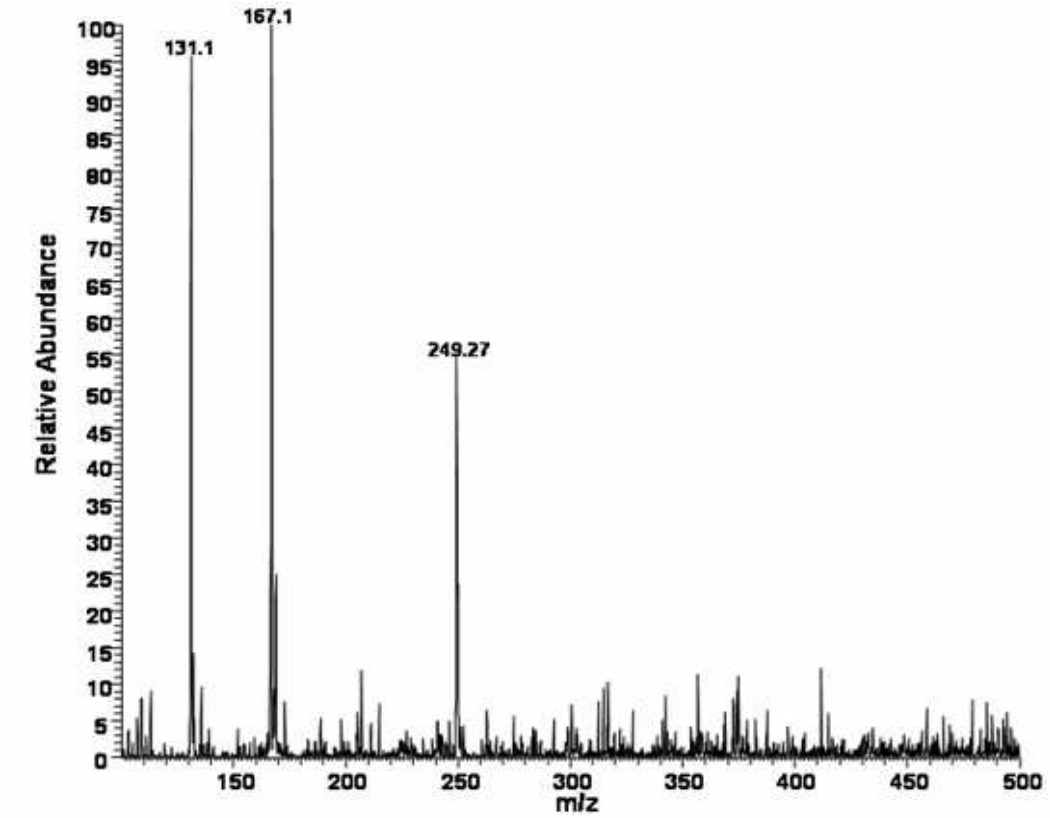

Figure 7-7: ESI-MS spectrum of L-Asparagine gathered after photodecomposition over Au-TiO_2 film in flow-through cell.

Figure 7-8 shows demodulated spectra of light modulation experiments. In the experiment solution of L-Asn was flowed over bare TiO_2 (spectrum (b)) and Au-TiO_2 catalyst (spectrum (a)). From spectrum (b) it is clear that CN^- species are formed on the TiO_2 surface as well.

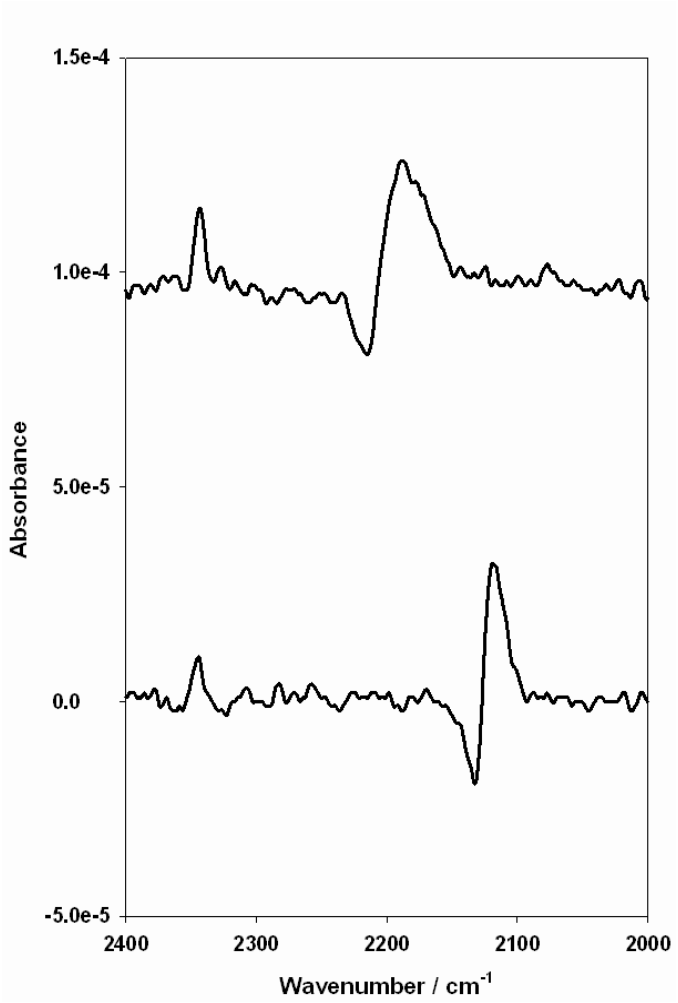

Figure 7-8: ATR demodulated spectra of light modulation experiments where L-asn aqueous solution was flowed over Au-TiO_2 spectrum (a) and over bare TiO_2 film spectrum (b)

The bands at 2216 and 2187 cm^{-1} can be assigned to CN^- adsorbed on TiO_2. Also in both spectra dissolved carbon dioxide is observed.[12] Figure 7-9 shows the time dependence of the two signals at 2216 and 2187 cm^{-1} on TiO_2 during the experimental course. When the system is illuminated the band at 2216 cm^{-1} is formed very fast on the surface reaching the maximum in 65 seconds. After that the signal is decreasing still during illumination reaching a minimum after 92 seconds. This behavior of the band somehow implies that CN^- intermediates are formed on TiO_2 catalyst and destroyed during irradiation as well.

The band at 2187 cm^{-1} develops in intensity when the light is off. We assign the two bands to CN^- adsorbed on different sites on the TiO_2 surface. By comparison of the spectra in Figure 7-8 it can be concluded that on the Au-TiO_2 the CN^- adsorbs on the gold, since no sign of CN^- on TiO_2 is evident. This reveals the much larger affinity of CN^- for gold than for TiO_2.

Our experiments do not give an indication on the further fate of CN^- under photocatalytic conditions. However, Bard and coworkers showed that cyanide is slowly oxidize to cyanate and the latter seems to be rater resistant towards further oxidation.[21, 22]

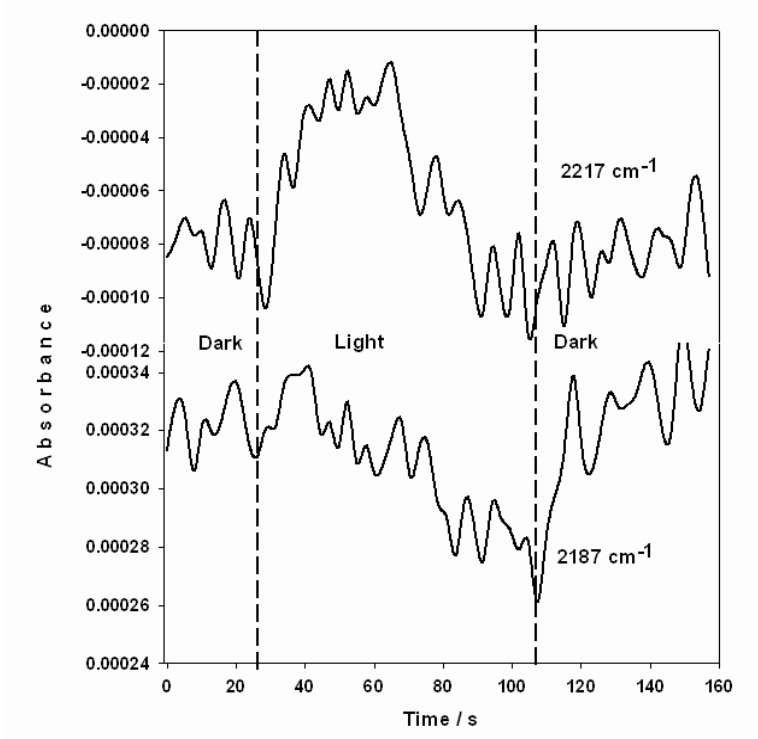

Figure 7-9: Time dependence of two ATR signals during light modulation experiments with modulation period T=157 s. At t= 26.1 s light was switched on and at t=104.6 s switched off. The ATR signals were averaged over five modulation periods.

7.5 Conclusions

Our in situ ATR-IR experiments show that in the presence of oxygen in solution oxalate species can be observed on the TiO_2 surface during the photocatalytic mineralization of amino acids over Au-TiO_2 and TiO_2. The experiments furthermore shed some light on the fate of the nitrogen atom. Ammonium and particularly cyanide were observed. The latter species was not reported before for the photocatalysis of amino acids. This finding is relevant in view of the application of photocatalysis for purification of (drinking) water. Moreover, in

the case of the Au-TiO_2 the cyanide leads to the leaching of gold in the form of $[Au(CN)_2]^-$, which can be detected in solution.

References

1. Hidaka, H., Photodecomposition of amino acids and photocurrent generation on TiO_2/OTE electrodes prepared by pulse laser deposition. *Catalysis Letters* 60, **2004** (1-2), 95-98.
2. Ikeda, S., Photocatalytic activity of transition-metal-loaded titanium(IV) oxide powders suspended in aqueous solutions: Correlation with electron-hole recombination kinetics. *Physical chemistry chemical physics* 3, **2001** (2), 267-273.
3. Strehle, M., A Raman spectroscopic study of the adsorption of fibronectin and fibrinogen on titanium dioxide nanoparticles. *Physical chemistry chemical physics* 6, **2004** (22), 5232-5236.
4. Takahara, Y., Photooxidation of organic compounds in a solution containing hydrogen peroxide and TiO2 particles under visible light. *Journal of applied electrochemistry* 35, (7), **2005** 793-797.
5. Hidaka, H.; Horikoshi, S.; Ajisaka, K.; Zhao, J.; Serpone, N., Fate of amino acids upon exposure to aqueous titania irradiated with UV-A and UV-B radiation - Photocatalyzed formation of NH_3, NO_3^- and CO_2. *Journal Of Photochemistry And Photobiology A-Chemistry* **1997,** 108, (2-3), 197-205.
6. Martra, G.; Horikoshi, S.; Anpo, M.; Coluccia, S.; Hidaka, H., FTIR study of adsorption and photodegradation of L-alpha-alanine on TiO_2 powder. *Research on Chemical Intermediates* **2002,** 28, (4), 359-371.
7. Adsorption of Thiol-Protected Gold Nanoparticles on TiO_2 and Their Behavior under UV Light Irradiation. *Journal of physical chemistry. C* **2008,** 112, (15), 5816-5824.
8. Horikoshi, S., Photocatalyzed degradation of polymers in aqueous semiconductor suspensions V. Photomineralization of lactam ring-pendant polyvinylpyrrolidone at titania/water interfaces. *Journal of photochemistry and photobiology. A, Chemistry* **2001,** 138, (1), 69-77.
9. Dawson, A., Semiconductor-metal nanocomposites. Photoinduced fusion and photocatalysis of gold-capped TiO2 (TiO2/Gold) nanoparticles. *Journal of Physical Chemistry B* **2001,** 105, (5), 960-966.
10. Baurecht, D., Quantitative modulated excitation Fourier transform infrared spectroscopy. *Review of scientific instruments* **2001,** 72, (10), 3782-3792.
11. Burgi, T.; Baiker, A., In situ infrared spectroscopy of catalytic solid-liquid interfaces using phase-sensitive detection: Enantioselective hydrogenation of a pyrone over Pd/TiO2. *Journal of Physical Chemistry B* **2002,** 106, (41), 10649-10658.
12. Dolamic, I.; Burgi, T., Photocatalysis of dicarboxylic acids over TiO2: An in situ ATR-IR study. *Journal Of Catalysis* **2007,** 248, (2), 268-276.
13. Gautier, C.; Bürgi, T., Vibrational circular dichroism of N-acetyl-L-cysteine protected old nanoparticles. *J. Chem. Soc. Chem. Commun.* **2005**, 5393-5395.

14. Gumy, D., Catalytic activity of commercial of TiO2 powders for the abatement of the bacteria (E-coli) under solar simulated light: Influence of the isoelectric point. *Applied catalysis. B, Environmental* 63, **2006** (1-2), 76-84.

15. Bürgi, T.; Baiker, A., In situ infrared spectroscopy of catalytic solid-liquid interfaces using phase-sensitive detection: Enantioselective Hydrogenation of a pyrone over Pd/TiO2. *J. Phys. Chem. B* **2002,** 106, 10649-10658.

16. Urakawa, A.; Wirz, R.; Bürgi, T.; Baiker, A., An ATR-IR flow-through cell for concentration modulation excitation spectroscopy: diffusion experiments and simulation. *J. Phys. Chem. B* **2003,** 107, 13061.

17. Dolamic, I., Bürgi T., Photocatalysis of dicarboxylic acids over TiO2: An in situ ATR-IR study. *Journal of catalysis* 248, (2) **2007**, 268-276.

18. Toledo-Antonio, J. A.; Capula, S.; Cortes-Jacome, M. A.; Angeles-Chavez, C.; Lopez-Salinas, E.; Ferrat, G.; Navarrete, J.; Escobar, J., Low-temperature FTIR study of CO adsorption on titania nanotubes. *Journal of Physical Chemistry C* **2007,** 111, (29), 10799-10805.

19. Hadjiivanov, K.; Lamotte, J.; Lavalley, J. C., FTIR study of low-temperature CO adsorption on pure and ammonia-precovered TiO2 (anatase). *Langmuir* **1997,** 13, (13), 3374-3381.

20. LeRille, A.; Tadjeddine, A.; Zheng, W. Q.; Peremans, A., Vibrational spectroscopy of a Au(hkl)-electrolyte interface by in situ visible-infrared difference frequency generation. *Chemical Physics Letters* **1997,** 271, (1-3), 95-100.

21. Frank, S., and Bard A.J., Heterogeneous Photocatalytic Oxidation of Cyanide Ion in Aqueous-Solutions at Tio2 Powder. *Journal of the American Chemical Society* **1977,** 99, (1), 303-304.

22. Frank, S., and Bard A.J. Heterogeneous Photocatalytic Oxidation of Cyanide and Sulfite in Aqueous-Solutions at Semiconductor Powders. *The Journal of physical chemistry* **1977,** 81, (15), 1484-1488.

Appendix

A

Supplementary Information of Chapter 5

A.1 ATR-IR Spectra

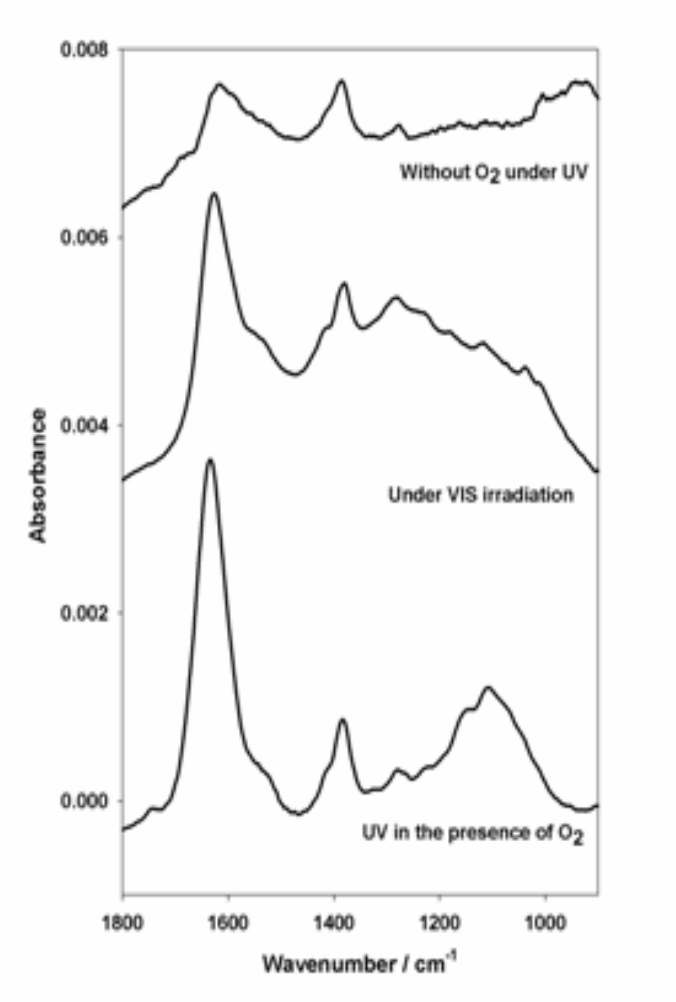

Figure A-A-1: ATR-IR spectra of newly formed species on TiO_2 after reaction under different conditions. Bottom: Species formed after UV irradiation of NAC protected gold nanoparticles on TiO_2. Top: Same experiment but in the absence of O_2. Middle: Newly formed species after reaction of NAC protected gold nanoparticles on TiO_2 under visible light illumination.

A.2 TEM-Micrograph

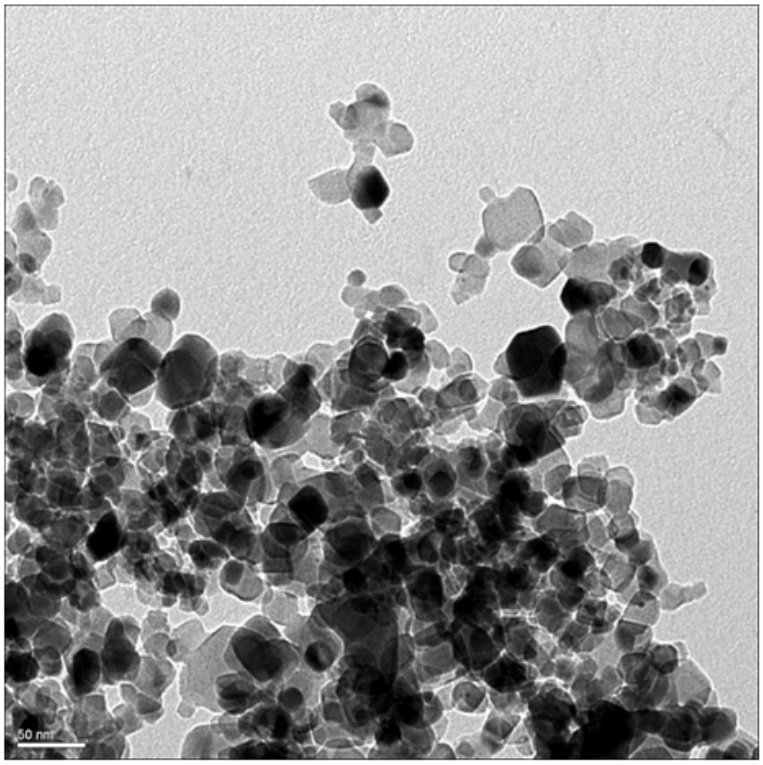

Figure A-2: TEM micrograph obtained after draying an aqueous slurry of TiO2 particles, which leads to their agglomeration

A.3 Estimate of the Irradiance at the Sample

According to the specifications of the supplier the 75 W Xe lamp has an irradiance of 6 mW m-2 nm-1. For the spectral range between 270 and 380 nm (110 nm) this yields

6 mW m-2 nm-1 x 110 nm = 660 mW m-2

-For the F/1 condenser a factor of 0.11 has to be applied, whereas the rear reflector increases the output by 60%.

660 mW x 0.11 x 1.6 = 116.16 mW

-The transmission through the bifurcated fiber bundle is 60%.

116.16 mW x 0.6 = 69.7 mW

-Reflection losses at all interfaces (liquid filter, optical filters, cell window, 10 interfaces, 5% loss per interface, 0.9510) are accounted for by a factor of 0.6.

69.7 mW x 0.6 = 41.8 mW

-Considering the transmission of the BG42 and UG11 filters between 270 and 380 nm result in a factor of 0.164

41.8 mW x 0.164 = 6.85 mW

-The area of the two spots from the bifurcated fiber bundle is about 3.5 cm2.

This results in a final irradiance at the sample of 6.85 mW / 3.5 cm2 = 1.96 mW cm-2.

Acknowledgement

This thesis is a result of four years of work and I would like to thank all people who helped and inspired me through this work.

I especially want to thank my supervisor Professor Thomas Bürgi for his guidance during my research and study at the University of Neuchâtel. His patience, enthusiasm and unfailing energy made this work possible, keeping me on the right track all the time. Also, I would like to thank Thomas for giving me the opportunity to attend several international conferences and for his confidence in me to present our laboratory at these events. I am very grateful for his support and trust.

Many thanks to Natallia Shalkevich, Julien Boudon, Dr. Cyrille Gautier, Dr. Marco Bieri, Dr. Silvia Angeloni-Suter, Dr. Chakravarty Devulapalli, Dr Qiaoling Li, and Dr. Satyabrata Si for many nice and funny moments we spend together.

I am grateful to Natallia and Julian for many TEM images they made for our group. Also thanks to Julian for creating the nice website of our group making our work and ourselves visible everywhere.

Great thank you goes to secretary staff of the Department of Chemistry and Microtechnology for solving administrative problems and André Floreano and Philippe Stauffer for help in technical problems.

Also I would like to thank the Swiss Science National Foundation (SSNF) for financial support.

Finally, thanks to my wife Ljiljana and our daughter Vasilija for their love, support and passion we shard during my PhD study.

List of Publications

Publications related to this thesis

- Photoassisted decomposition of malonic acid on TiO_2 studied by in situ attenuated total reflection infrared spectroscopy, Igor Dolamic and Thomas Bürgi, J. Phys. Chem. B 2006, 110 (30), 14898-904. (Chapter 3)
- Photocatalysis of dicarboxylic acids over TiO_2: An in situ ATR-IR study, Igor Dolamic and Thomas Bürgi, Journal of Catalysis, 2007, 248 (2) 268-276. (Chapter 4)
- Adsorption of thiol-protected gold nanoparticles on TiO_2 and their behavior under UV light irradiation, Igor Dolamic Cyrille Gautier, Julien Boudon, Natallia Shalkevich and Thomas Bürgi, J. Phys. Chem. C 2008 112 (15) 5816-24. (Chapter 5)
- Photocatalysis of amino acids on TiO_2 studied by in-situ ATR-IR spectroscopy, manuscript in preparation (Chapter 7)

Other publications

- Probing chiral nanoparticles and surfaces by infrared spectroscopy, Cyrille Gautier, Marco Bieri, Igor Dolamic, Julian Boudon, Silvia Angeloni and Thomas Bürgi, *Chimia* **2006** 60 (11) 777-78

Curriculum Vitae

Name	Igor Dolamic
Date of Birth	March 14, 1975
Place of Birth	Doboj, Bosnia and Herzegovina
Nationality	Bosnian

Education

Since 2004	Doctoral studies under the supervision of Prof. Thomas Bürgi at the Institute of Microtechnology, University of Neuchâtel, Switzerland
02/2003	Diploma in Biological and Food Engineering, University of Banja Luka, Bosnia and Herzegovina
06/1994	Secondary school 'Nikola Tesla, Teslic, Bosnia and Herzegovina, Technician of Electrical Engineering

Conferences/Workshops

09/2004	Workshop on Application of Special Techniques in FTIR ATR Spectroscopy, University of Vienna, Austria (Prof. U.P. Fringeli)
09/2006	4th EFCATS School on Catalysis, Catalyst Design-from Molecular to Industrial Level, St. Petersburg, Russia, Oral Presentation
10/2006	Swiss Chemical Society (SCS) Fall Meeting, Zurich, Switzerland, Poster Presentation
08/2007	Europacat VIII, Turku/Abo, Finland, Poster presentation
09/2007	Swiss Chemical society (SCS) Fall Meeting, Lausanne, Switzerland, Poster Presentation
02/2008	Photocatalysis and Solar Energy Conversion Solar '08 Oral Presentatio